TECHNISCHE UNIVERSITÄT MÜNCHEN
FAKULTÄT FÜR CHEMIE
LEHRSTUHL FÜR ORGANISCHE CHEMIE II

Structural and functional characterization of the ClpXP1/2 protease complex from *Listeria monocytogenes*

Dóra Balogh

Vollständiger Abdruck der von der Fakultät für Chemie der Technischen Universität München zur Erlangung des akademischen Grades eines

Doktors der Naturwissenschaften (Dr. rer. nat.)

genehmigten Dissertation.

Vorsitzender:		Prof. Dr. Matthias J. Feige
Prüfer der Dissertation:	1.	Prof. Dr. Stephan A. Sieber
	2.	Prof. Dr. Kathrin Lang

Die Dissertation wurde am 12.03.2020 bei der Technischen Universität München eingereicht und durch die Fakultät für Chemie am 20.04.2020 angenommen.

For Those Who Are Interested

Abstract

Caseinolytic proteases (Clp) are important for targeted protein degradation in bacteria and in organelles of eukaryotic cells. They also play a role in bacterial stress response and in virulence regulation. Most bacteria possess one *clpP* gene in their genomes but the highly stress tolerant pathogen *Listeria monocytogenes* has two isoforms (ClpP1 and ClpP2) that can form a hyperactive heterocomplex with unknown biological function. The Clp protease complex comprises a proteolytic subunit ClpP and a chaperone, for example ClpX. ClpP is a barrel-shaped tetradecamer composed of two stacked heptameric rings. When the hexameric ClpX ring binds to ClpP, a 6/7 symmetry mismatch arises on the binding surface. Because of the lack of structural data, the molecular basis of this symmetry mismatch has not been understood so far. In this thesis, the function of the ClpP1/2 heterocomplex and the structure of the ClpXP1/2 complex is examined.

To learn about the distinctive cleavage site specificities of ClpP1 and ClpP2, protein digests were analyzed by mass spectrometry. An inhibitor screening surprisingly revealed that the ClpP2 homocomplex is overactivated in the presence of tripeptide chloromethyl ketone inhibitors. In-depth kinetic studies showed that the reason for this is the enhanced affinity to ClpX upon partial inhibitor binding. The ClpP1/2 heterocomplex also displays stronger ClpX binding compared to the ClpP2 homocomplex, which explains its higher proteolytic activity.

This high affinity between ClpX and ClpP1/2 leads to the stabilization of the complex and allowed us to conduct cryo-electron microscopy studies. For the first time, we could successfully show the asymmetric interactions on the ClpX–ClpP2 interface and resolve the 6/7 symmetry mismatch. Furthermore, the dynamic changes in ClpXP1/2 upon complex formation were investigated by hydrogen/deuterium exchange mass spectrometry experiments.

Additionally, we identified ClpP1/2 as an intracellular thermometer due to the fact that it can build the highly active heterocomplex only at high temperatures. Phenotypic and proteomic analyses of Δ*clpP* mutants showed that the ClpPs are not only heat shock proteins, but are also involved in the regulation of oxidative stress.

Overall, this work contributes to the understanding of the function of bacterial ClpP heterocomplexes and provides the basis for further structural work on Clp protease complexes.

Zusammenfassung

Caseinolytische Proteasen (Clp) sind wichtig für gezielte Proteolyse in Bakterien und in Organellen von eukaryotischen Zellen. In bakterieller Stressantwort und in Virulenz spielen sie ebenfalls eine Rolle. Die meisten Bakterien besitzen ein *clpP*-Gen, aber das sehr stresstolerante Pathogen *Listeria monocytogenes* hat zwei Isoformen (ClpP1 und ClpP2), die einen hyperaktiven Heterokomplex mit unbekannter biologischer Funktion formen können. Der Clp-Proteasekomplex besteht aus der proteolytischen Untereinheit ClpP und aus einem Chaperon, zum Beispiel ClpX. ClpP ist ein faßförmiges Tetradekamer aufgebaut aus zwei gestapelten heptamerischen Ringen. Wenn der hexamerische ClpX-Ring auf ClpP bindet, entsteht eine 6/7-Asymmetrie an der Bindungsoberfläche. Die molekulare Grundlage der Asymmetrie ist mangels struktureller Daten nicht bekannt. In dieser Dissertation wird die Funktion des ClpP1/2-Heterokomplexes und die Struktur der ClpXP1/2-Komplex untersucht.

Um die unterscheidenden Schnittstellenspezifitäten von ClpP1 und ClpP2 kennen zu lernen, wurden verdaute Proteinsubstrate mittels Massenspektrometrie analysiert. Überraschenderweise offenbarte ein Inhibitorscreening eine Überaktivierung des ClpP2-Homokomplexes in Anwesenheit von Chlormethylketon-Inhibitoren. Detaillierte kinetische Studien zeigten, dass der Grund dafür die erhöhte Affinität zwischen ClpX und ClpP2 nach partieller Inhibitorbindung ist. Der ClpP1/2-Heterokomplex weist genauso eine höhere Affinität zu ClpX im Vergleich zu dem ClpP2-Homokomplex auf, was dessen erhöhte Proteaseaktivität erklärt.

Diese hohe Affinität zwischen ClpX und ClpP1/2 stabilisiert den Komplex und erlaubte es, kryoelektronenmikroskopische Studien durchzuführen. Wir konnten zum ersten Mal erfolgreich die Interaktionen auf der ClpX–ClpP-Bindungsoberfläche zeigen und die 6/7-Asymmetrie lösen. Außerdem wurden die dynamischen Änderungen in ClpXP1/2 nach Komplexbildung mit Wasserstoff/Deuterium-Austausch-Massenspektrometrie untersucht.

Aufgrund der Tatsache, dass der sehr aktive ClpP1/2-Heterokomplex nur bei höheren Temperaturen entsteht, haben wir ClpP1/2 als intrazelluläres Thermometer identifiziert. Phenotypische und proteomische Analysen der Δ*clpP*-Mutanten zeigten, dass die ClpP-Proteasen nicht nur Hitzeschockproteine sind, sondern auch in der Regulation von oxidativem Stress involviert sind.

Insgesamt trägt diese Dissertation zum Verständnis der Funktion von bakteriellen ClpP-Heterokomplexen bei und gibt die Grundlage für weitere strukturelle Arbeiten an den Clp-Proteasekomplexen.

Acknowledgements

I would like to thank my supervisor Prof. Stephan A. Sieber for his support and guidance throughout my PhD. I am very greatful that he allowed me to work on my own ideas and always encouraged me, even when the experiments were not working as we have expected. I would also like to thank my mentor Dr. Christoph Göbl for all his help.

My special thanks go to my collaboration partners Dr. Christos Gatsogiannis, Prof. Stefan Raunser and Dr. Felipe Merino. Without their amazing work and enthusiasm we would not have been able to obtain the first cryo-EM structure of ClpXP. I also thank Dr. Marcin Poręba and Prof. Marcin Drag for synthesizing ClpP substrates and inhibitors. I thank Prof. Thilo Fuchs and Dr. Jakob Schardt for their help with cloning in *Listeria*.

I consider myself very lucky that I could work in the Sieber group. I thank all the current members and alumni for the great atmosphere, for the fruitful scientific discussions and for all the fun we had together. Your support during difficult times even outside of the lab meant very much to me. I would like to thank the members of the ClpP subgroup (Maria Dahmen, Matthias Stahl, Markus Lakemeyer, Christian Fetzer, Mathias Hackl, Anja Fux, Konstantin Eckel, Patrick Allihn, Thomas Gronauer and Barbara Eyermann) for the great discussions. Special thanks to my first desk neighbour Jonas Drechsel for enduring my bad jokes for years, and for not complaining very much about the heat while I was freezing. I also thank my second neighbour Volker Kirsch for the fun atmosphere in the office and for all his help in data analysis and paperwork.

I would also like to thank Mona Wolff, Katja Bäuml and Katja Gliesche for their great technical assistance in the lab. I thank my interns Simon Giosele, Jonathan Schwach, Deniz Kobell, Simon Ullrich and Franziska Bemmann for their help with the experiments. I thank Christina Brumer for her valuable help in complicated administrative matters. I thank Stuart Ruddell, Dietrich Mostert, Christan Fetzer, Mathias Hackl, Thomas Gronauer and Patrick Allihn for correcting the manuscript.

My experience in research during my bachelor's and master's contributed greatly to my motivation to start my PhD studies. I thank Ervin Kovács and Patrick Schrepfer for teaching me how to do research and how not to despair after failures.

Finally, I am very thankful to my parents Erika Kovács and Péter Balogh for all their help throughout my life and for making excellent education possible for me. I also thank my brother Bálint and my sisters Zsófi, Judit and Annamari for supporting me all this time. My special thanks go to my husband Andreas Hölzl for his help with statistics and programming during my reseach. I am also deeply grateful for his constant support during my whole PhD, especially for the extremely much help during the last months.

Contents

Part I

Scientific background

1. Introduction

1.1. Regulated proteolysis

Regulation of the life cycle of proteins is crucial for the survival of cells in all domains of life. The transcription, translation, folding and turnover of proteins must therefore be strictly controlled and adjusted to adopt to environmental changes. Every organism needs protein degradation machineries to recycle damaged proteins and remove certain regulatory proteins. Dysfunctional protein degradation has been linked to aging, cancer, neurodegenerative and metabolic disorders.[1] In pathogenic bacteria, regulated proteolysis is not only important for viability but also for virulence.[2]

In prokaryotes, the ATP-dependent proteases ClpAP, ClpCP, ClpEP, ClpXP, FtsH, HslUV (ClpYQ) and Lon are responsible for the removal of proteins.[3–5] They belong to the AAA+ (**A**TPases **a**ssociated with diverse cellular **a**ctivities) protein superfamily. Lon and FtsH contain an ATPase and a protease domain on a single polypeptide chain, whereas the caseinolytic proteases (Clp) are built up of separate protease and ATPase proteins.[3]

1.1.1. The ClpXP protease

The proteolytic subunit of the Clp protease complexes is the serine protease ClpP. Two heptameric ClpP rings form a barrel-shaped tetradecamer (fig. 1a). The assembly of an active tetradecamer requires interactions through antiparallel β-sheets on the ring-ring interface and salt bridges through the Asp170/Arg171 oligomerization sensor.[6,7] Hydrophobic residues form pockets on the apical sides of the barrel, where the ATPases can dock (fig. 1a, b). The active sites (in most ClpPs the conserved Ser98-His123-Asp172 catalytic triad) can be found inside the barrel, protected from most cellular proteins (fig. 1a, c).[8] This architecture ensures that no unspecific proteolysis occurs in the cell. The conformations of the catalytic triad and of the Asp170/Arg171 residues are coupled to each other. The oligomerization sensor can only connect the two heptamers if the triad is correctly aligned.[7]

A number of pathogenic bacteria (e.g. *Listeria monocytogenes*,[9] *Mycobacterium tuberculosis*,[10] *Clostridium difficile*,[11] *Pseudomonas aeruginosa*,[12] *Chlamydia trachomatis*[13]) have two or three ClpP isoforms. The characterization of these isoforms and deciphering their individual physiological roles are still topic of ongoing research. In *L. monocytogenes*,[14] in *M. tuberculosis*[15] and in *C. trachomatis*[13] heterooligomer formation increases the proteolytic activity. Tetradecamer formation by two homoheptameric rings of different ClpP isomers has been shown in *L. monocytogenes*[14] and in *M. tuberculosis*[16]. Structural data for other species with two or more ClpP isoforms are missing to date.

Most of the hexameric Clp ATPases (ClpA, ClpC, ClpE, ClpX) bind to the protease ClpP through flexible loops,[17] while other members of the Clp ATPase family (ClpB and ClpL) act as free chaperones responsible for protein solubilization under stress.[18,19] Negative-stain electron

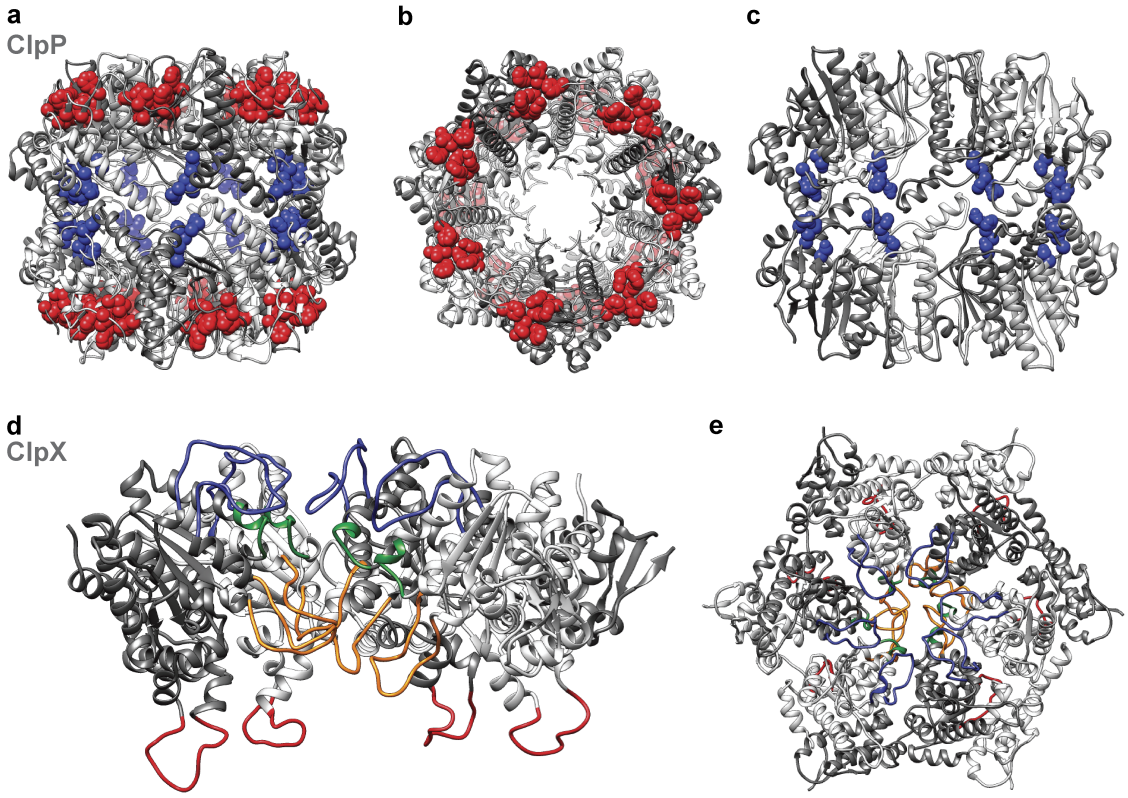

Figure 1 Structures of ClpP and ClpX. a–c Structure of *L. monocytogenes* ClpP2 (PDB-ID: 4JCT). **a** Side view of the tetradecamer. **b** Top view with the hydrophobic pockets (red shperes). **c** Inner side of the barrel with the catalytic triads (blue spheres). **d–e** Model of *L. monocytogenes* ClpX without the N-terminal zinc-binding domains. **e** Inner side of the pore. The pore-1 loops with the GYVG motif (green), pore-2 loops (orange), RKH loops (blue) and IGF loops (red) are highlighted. **d** Top view.

microscopy (EM) images have shown that the chaperones can bind to one or both ends of the ClpP barrel.[20] However, these low-resolution data could not show the binding between the heptameric ClpP and the hexameric chaperone rings on the molecular level thus the 6/7 asymmetry remains unexplained. Mutational studies revealed that two loops are required for binding: the IGF-loops on the side of the ring and the pore-2 loops inside the axial pore.[21,22]

The Clp ATPases recognize the substrates via short degradation sequences (degrons) and unfold them in an ATP-dependent manner before the polypeptide chain enters the degradation chamber of ClpP.[23] Clp chaperones also interact with adaptor proteins (such as MecA, McsB, SspB, ClpS) that modulate substrate recognition and chaperone function.[5] In ClpX, the N-terminal zinc-binding domain and the RKH loop are involved in substrate recognition.[24,25] The pore-1 loop is involved in substrate gripping and translocation.[25,26] ClpX can recognize N- and C-terminal, as well as internal degradation tags.[27,28] One of the physiologically most important degrons ist the SsrA tag, which is *trans*-translationally attached to ribosome-stalled proteins via a transfer messenger RNA (tmRNA).[29] The adaptor protein SspB aids the recruitment of SsrA-tagged proteins for degradation by ClpXP.[30]

1.1.2. Modulation of ClpP function

As ClpP is an essential protein in some bacteria (e.g. *M. tuberculosis*, *Corynebacterium glutamicum*, *Streptomyces lividans*) and is also required for virulence factor regulation, it is a

promising target for antibacterial research.[31] There are two strategies to manipulate ClpP function, namely overactivating and inhibiting ClpP. Acyldepsipeptides (ADEPs) are antibiotics that enable ClpP to digest proteins without a chaperone partner, which leads to uncontrolled protein degradation and consequently to cell death.[32] ADEPs also interfere with ClpX and ClpC binding thus inhibiting the degradation of physiological substrates.[33] The inhibition or deletion of ClpP in *S. aureus* and in *L. monocytogenes* is not lethal for the bacteria but it leads to decreased virulence factor production.[34–37] β-Lactones and phenyl esters are potent covalent ClpP inhibitors, but their use as antivirulence drugs is hindered by their hydrolytic instability.[34,38] General serine protease inhibitors such as boronates and fluorophosphates are also active against ClpP, but in case of these increasing the specificity against other serine proteases is an important goal for further development.[39,40]

In eukaryotes, ClpP is located in the mitochondrial matrix where it is required for protein homeostasis and for the mitochondrial unfolded protein response.[41] Mutations in the human *clpP* gene have been associated with Perrault syndrom, a rare disease that causes deafness and reduced female fertility.[42] ClpP can be upregulated in numerous primary and metastatic cancers.[43] Acute myeloid leukemia cells with abnormal ClpP levels were shown to be killed with a β-lactone inhibitor, which was not toxic for normal hematopoietic cells.[44] ClpP has also been linked to Parkinson's disease, because α-synuclein decreases the activity of ClpP, which results in mitochondrial dysfunction and cell death.[45] Therefore, activating or stabilizing human ClpP could be a therapeutic strategy in Parkinson's disease.

1.2. *Listeria monocytogenes*

L. monocytogenes is a food-borne pathogen that causes listeriosis, a disease with a high mortality rate of 20–30%.[46] It is especially dangerous for the elderly, for pregnant women and their unborn babies as well as for immunocompromised patients. Severe forms of listerosis involve sepsis, meningitis and fetal infection because *L. monocytogenes* can cross the blood-brain barrier and the fetoplacental barrier.[47,48] *L. monocytogenes* is an exceptionally stress tolerant bacterium: it can grow under low and high temperatures (−0.4 to 45 °C), at high salt concentrations and under acidic conditions.[49] For this reason it is very challenging for the food processing industry to eliminate *L. monocytogenes* and prevent its growth during food storage. Over the last twenty years, the number of reported listeriosis outbreaks has been growing worldwide.[50]

After ingestion of *L. monocytogenes*, it can cross the intestinal epithelium and spread to the liver, spleen and brain through the blood and the lymphatic system. It can be internalized by phagocytes or bind to the surface of nonphagocytic cells and initiate receptor-mediated endocytosis with the help of the proteins internalin A and B. Afterwards, the toxins listeriolysin O (LLO) and two phospholipases (PlcA, PlcB) open up the vacuole enabling the bacterium to enter the cytosol.[48] In the cytosol, *L. monocytogenes* can hijack human actin to actively move from cell to cell. The actin assembly-inducing protein (ActA) mediates the polymerization of actin, and builds so-called actin comet tails from short actin filaments.[51] *L. monocytogenes* can

grow intracellularly, and the production of LLO outside of the lysosome causes malformation of the other organelles.[48]

1.2.1. Regulation of protein expression in *L. monocytogenes*

A fast response to environmental changes is crucial for *L. monocytogenes*, as it must be able to switch from a saphrophyte to an intracellular pathogen.[52,53] Even inside the host cell there are dramatic changes in the environment when the bacterium enters and leaves the acidic and oxidative lysosome. General and specific stress resonse pathways are activated at different stages of infection.[54]

There are two main heat shock response mechanisms in *L. monocytogenes*. The class I heat shock genes encode chaperones such as GroES, GroEL and DnaK. They are negatively regulated by the transcription factor HrcA.[55]

The alternative sigma factor σ^B positively controls the transcription of the class II general stress response genes.[56] These genes code for a variety of functions and they include heat, osmotic and acidic stress genes, as well as bile acid and antibiotic resistance genes. Many virulence factors are directly or indirectly controlled by σ^B. PrfA (listeriolysin positive regulatory protein) is a σ^B-controlled protein, which is the transcriptional regulator of the following virulence factors: listeriolysin O, ActA, internalins InlA, InlB and InlC, phospholipases PlcA and PlcB, the metalloprotease Mpl.[57]

The class III heat shock proteins are AAA+ chaperones and proteases (ClpB, ClpC, ClpE, ClpP1, ClpP2) and they are under the control of the temperature-sensitive repressor CtsR.[58]

There are further stress response genes that are independent of HrcA, σ^B and CtsR, and their regulation is not known. The chaperone ClpX and the protease FtsH belong to this group.[58]

Furthermore, the SOS response is activated if DNA damage occurs, for example after H_2O_2 or UV exposure.[59] The activator RecA binds to single-stranded DNA (ssDNA) and induces the autoproteolysis of LexA, the transcriptional repressor of the SOS regulon. In *L. monocytogenes* there are 29 LexA-controlled genes, most of them are DNA polymerases required for DNA repair.[60]

1.2.2. Genetic, transcriptomic and proteomic analyses of *Listeria monocytogenes* under stress

Researchers have conducted a large number of genetic, transcriptomic and proteomic studies in *L. monocytogenes* in order to gain a global understanding of its adaptation to different stresses.

Early proteomic studies revealed the induction of GroEL, DNaK, DnaN and Flp (ferritin) after heat stress.[61–63] Van der Veen et al.[60] looked at whole-genome expression profiles at different time points after exposing the cells to 42 °C. They found that not only heat shock genes, but also the class II stress response and the SOS response were upregulated, while cell division was downregulated. They also identified 28 genes that are important for growth at high

temperatures in a genome-wide random insertion screen.[64] Many of these genes were also induced after heat shock, suggesting that heat shock and growth at high temperature are similarly regulated.

The effects of oxidative stress on the proteome have been less thoroughly investigated. In a recent study using transcriptome sequencing, only a few genes were found to be dysregulated. Among these, periredoxin and its transcription regulator *orhA* and *orhB*, the bile acid resistance genes *bilEA* and the superoxide dismutase *sodA* were upregulated.[65]

Chatterjee at al.[54] analysed the gene expression patterns of *L. monocytogenes* during intracellular growth in murine macrophages. The data suggest that the bacteria are under sugar starvation inside the host cell, since sugar metabolism was suppressed and hexose uptake along with alternative carbon source metabolism pathways were upregulated. The class I and III heat shock proteins were strongly induced and some class II stress response and SOS response genes were also upregulated. As expected, the PrfA-dependent virulence factors were upregulated. Furthermore, cell division was negatively regulated. Consequently, intracellular growth is very stressful for the bacteria.

Transcriptomic and proteomic studies under other stress conditions (osmotic, acidic, alkaline and low-temperature) also showed that not only the specific stress responses but also the above mentioned general stress response pathways are activated.[66–70] This explains the cross-protective stress response phenomenon, which has been observed for *L. monocytogenes*. After exposure to sub-lethal stress, the bacteria develop a phenotype that exhibits increased resistance against the same and different stressors.[66,67]

1.2.3. ClpP1/2 in *Listeria monocytogenes*

The transcriptome and proteome analyses of *L. monocytogenes* mentioned in section 1.2.2 have shown that the class III heat shock proteins (Clp proteases) are crucial for general stress adaptation and virulence.

Unlike most of the bacteria, *L. monocytogenes* has two different *clpP* genes. It is well established, that ClpP2 is required for virulence, and it is upregulated intracellularly and under heat, acid and oxidative stress.[14,36,54] The cellular function of ClpP1 has not been investigated in detail. Transcriptome analyses have shown that it is similarly regulated like ClpP2 and it is also repressed by CtsR, although the two genes are not on the same operon.[14,71] In vitro experiments revealed that ClpP1 alone is an inactive heptamer but it can form a hyperactive heterocomplex with ClpP2 (fig. 2a). ClpP1 has an asparagine in its catalytic triad (Ser-His-Asn) instead of aspartate, and it is misaligned in ClpP1 heptamers.[7] However, it takes up an active conformation after binding to ClpP2 (fig. 2b).[14]

ClpP activation upon heterooligomerization has also been observed for *M. tuberculosis* ClpP1/2, but only in the presence of synthetic peptide activators.[15] The physiological role of the ClpP1/2 heterocomplex formation in bacteria is not yet understood.

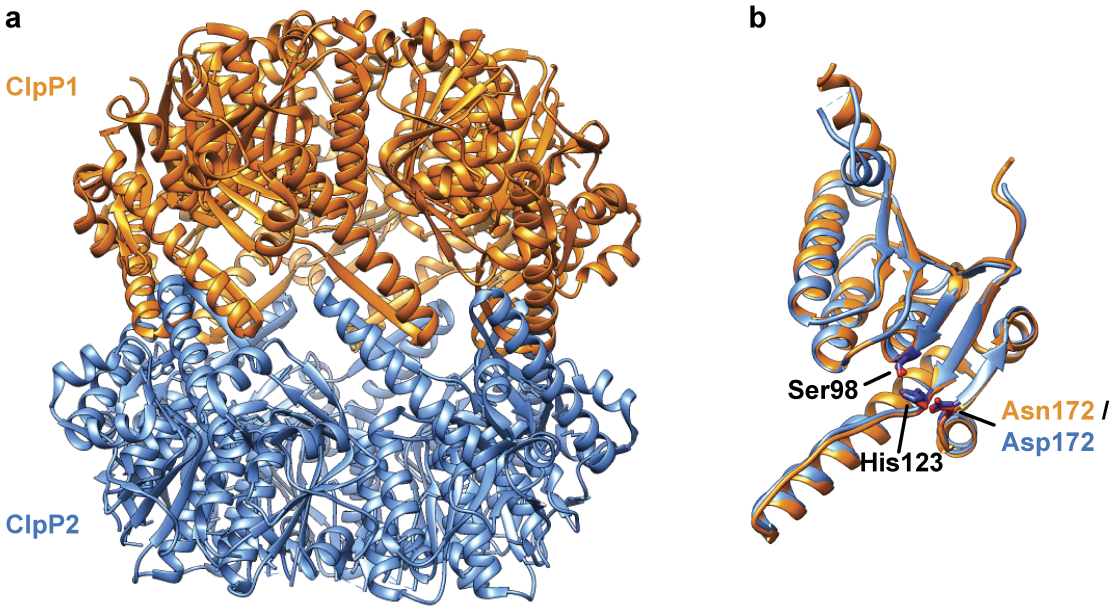

Figure 2 Structure of the ClpP1/2 heterocomplex. **a** Tetradecameric structure of *L. monocytogenes* ClpP1/2 (PDB-ID: 4RYF). ClpP1 is shown in orange, ClpP2 is shown in blue. **b** Structural alignment of the ClpP1 and ClpP2 monomers from the heterocomplex. The residues of the catalytic triad are depicted in stick representation.

2. Aim of this thesis

ClpP is a highly conserved protein but only a few organisms possess more than one isoform. One goal of this work was to bring to light the differential functions of ClpP1 and ClpP2 in *L. monocytogenes*. Firstly, in vitro studies were conducted to uncover the differences and similarities in their substrate specificities. Subsequently, known ClpP inhibitors and tailor-made ClpP1 and ClpP2 inhibitors were tested in order to further analyse the catalytic mechanisms. The cellular functions of both ClpP isomers were investigated with integrated proteomic experiments. The role of temperature in the modulation of ClpP1/2 formation and activity was studied in detail.

The second goal was to obtain a high-resolution structure of ClpXP, because the interactions between ClpP and Clp ATPases could only be investigated by indirect methods so far. Due to the low affinity and asymmetry of these complexes gaining atomic structures was very challenging. Nevertheless, unveiling the unique 6/7 symmetry mismatch is essential to understand the mechanism of this universal protein degradation machinery.

Part II

Research

3. Insights into ClpXP proteolysis: heterooligomerization and partial deactivation enhance chaperone affinity and substrate turnover in *Listeria monocytogenes*

Published in *Chemical Science*, **2017**, 8, pp 1592-1600
by Dóra Balogh*, Maria Dahmen*, Matthias Stahl, Marcin Poręba, Malte Gersch, Marcin Drag and Stephan A. Sieber.

*equal contribution

DOI: 10.1039/c6sc03438a

Author contributions

Stephan A. Sieber and Marcin Drag designed the study. Marcin Poręba synthesized the fluorogenic peptide library and the CMK inhibitors. Maria Dahmen and Malte Gersch performed the peptidase screenings. Dóra Balogh determined the proteolytic cleavage specificity and performed biochemical assays with inhibitors. Maria Dahmen and Dóra Balogh measured the apparent ClpX-ClpP affinity. Dóra Balogh, Maria Dahmen and Matthias Stahl analyzed the data. Dóra Balogh prepared the figures. Dóra Balogh and Stephan A. Sieber wrote the manuscript. All authors discussed the results.

3.1. Introduction

ATP-dependent proteolysis represents an important mechanism for removal of misfolded or ribosome-stalled proteins under stress conditions. In prokaryotes AAA+ chaperones (such as ClpX, ClpA and ClpC) recognize and unfold substrate proteins by ATP consumption and direct the linear peptide chain into a proteolytic barrel of caseinolytic protease P (ClpP).[23,72–74] ClpP is a transient tetradecameric serine hydrolase composed of two heptameric rings that are stacked face-to-face. Each subunit carries an active Ser-His-Asp catalytic triad that is essential for activity.[20,75] ClpP by itself lacks proteolytic activity but is able to digest small peptides that diffuse into the barrel via axial pores.[76,77] The first specific inhibitors reported for ClpP include the β-lactones, which exhibit an irreversible mode of action and, depending on their chemical structure, can cause either retention of the tetradecameric state or deoligomerization of ClpP.[78,79] More detailed insights into inhibitor-mediated complex disassembly were provided through a new generation of covalent phenyl esters and relevant modeling studies. These studies suggested that steric clash of the inhibitor within the active site triad triggers a rearrangement at the heptamer interface, causing dissociation of the ClpP tetradecamer into two heptameric rings.[38] Recently, the first reversible ClpP inhibitors were reported, which distort the active site catalytic triad through structural rearrangements.[80] However, this inactive state

of the ClpP peptidase could be reversed through formation of the ClpXP complex, highlighting the power of conformational control within this dynamic system. ClpXP interaction is mainly mediated by ClpX-loops which bind into hydrophobic clefts located at the ClpP axial surface.[22]

Interestingly, some bacterial strains such as *Mycobacterium tuberculosis* and *Listeria monocytogenes* encode two ClpP isoforms (ClpP1 and ClpP2).[7,9,14,15,81] While *L. monocytogenes* ClpP2 (ClpP2) resembles related enzymes in other bacteria such as *Escherichia coli* and *Staphylococcus aureus*, ClpP1 shares only 44% sequence identity with *E. coli* ClpP, forms predominantly inactive heptamers, lacks a conserved N-terminal chaperone binding motif and exhibits a truncated catalytic triad in which Asp172 is replaced by an Asn residue.[7] Mutational studies and in-depth X-ray crystallographic analysis revealed that this Asn residue is responsible for a conformational selection of the inactive heptameric state.[7] Accordingly, mutation of this Asn to an Asp induced tetradecamer formation and increased catalytic activity of ClpP1.[7]

Negative stain EM images of mixed ClpP1 and ClpP2 indicated the formation of heterocomplexes composed of two homoheptameric rings.[9] Importantly, it was found that ClpP1 is only active when complexed with ClpP2, which forces ClpP1 into an active conformational state.[7] The molecular reason for this surprising finding could be explained by a crystal structure of the ClpP1/2 heterocomplex.[14] All active sites within the heterocomplex, including Asn of ClpP1, were aligned in an active conformation, which demonstrated that heterocomplex formation regulates ClpP1 activity. While the heterocomplex was less active in peptidase assays, a 10-fold increase in proteolytic activity over the homocomplex was observed when in the presence of ClpX. From a functional perspective, this implies that the cell produces a hyperactive enzyme during stress conditions, when misfolded proteins must be removed efficiently. Indeed, quantitative real-time PCR showed increased *clpP1* and *clpP2* expression under heat stress.[14] So far, no systematic analysis of ClpP1 and ClpP2 peptidolytic and proteolytic cleavage specificities has been performed, leaving their role in substrate recognition unresolved. Structural studies and β-lactone inhibitor screenings showed subtle differences in the P1 binding pockets and revealed a preference of ClpP2 for medium to long aliphatic and aromatic side chains. ClpP1, on the other hand, did not bind inhibitors specifically and only bound the natural product vibralactone.[7,9]

Interestingly, ClpP1 and ClpP2 from *M. tuberculosis* (MtClpP1 and MtClpP2) also assemble into a similar heterocomplex.[15,16,81] However, many mechanistic and functional differences compared to the *L. monocytogenes* heterocomplex have been reported. For example, MtClpP1 and MtClpP2 are both tetradecamers, which show only weak proteolytic activity on their own in the presence of chaperones.[15] Peptidolytic activity is only enabled through MtClpP1/2 heterocomplex formation and requires the presence of activating peptides.[15,16,33] Proteolytic substrate turnover is facilitated in association with the chaperones MtClpX or MtClpC1.[15,82] Moreover, peptide substrate screenings with MtClpP1 revealed a cleavage preference after Met, Leu, Phe and Ala residues, while MtClpP2 was largely inactive.[40] Although structural information remains elusive, mutational studies within the hydrophobic clefts of MtClpPs showed that chaperones only bind the heterocomplex via MtClpP2.[83] The stoichiometry of the

L. monocytogenes complexes remains unknown. However, as tetradecameric ClpP1(N172D) is inactive in proteolysis assays with ClpX, the ClpP1/2 heterocomplex does not seem to bind ClpX via the ClpP1 ring.[14]

Here, we utilize peptide libraries to identify ClpP1 and ClpP2 cleavage specificities. While these preferences were largely abrogated in the proteolytic complexes, both isoforms retained a certain degree of individual specificity in protein digests. Biochemical analyses were used to dissect the multiple steps of proteolysis and revealed that the elevated activity of the heterocomplex stems from a 7-fold increased binding affinity for the ClpX chaperone. Surprisingly, stimulation of proteolysis was also observed when a customized chloromethylketone-based (CMK) inhibitor partially modified the active sites of homotetradecameric ClpP2. A closer mechanistic inspection of this inhibition mode revealed an increased affinity for the chaperone ClpX to be the fundamental activation principle.

3.2. Results and discussion

3.2.1. ClpP1 and ClpP2 exhibit cleavage site specificity in peptidase screenings

A structural overlay of ClpP1 and ClpP2 revealed subtle differences in their S1 pockets.[14] Specifically, ClpP1 exhibited a smaller and more defined cleft, restricting accessibility to smaller substrate side chains, while ClpP2 resembles ClpPs from other organisms, e.g. *E. coli*, and provides access to larger substituents.[84] In light of this divergence, we tested a previously established synthetic library of 172 fluorogenic 7-amino-4-carbamoylmethylcoumarin (ACC)-tagged peptide substrates containing various natural and unnatural amino acid substituents at the P1, P2 and P3 sites (fig. 3a).[85] Cys was omitted from the substrate library since this amino acid is susceptible to oxidation under synthesis conditions, storage and its use in kinetic assays. The library was screened against ClpP2, wild type ClpP1/2 as well as the active site mutants ClpP1/2(S98A) and ClpP1(S98A)/2 in order to unravel cleavage preferences of the individual heterocomplexes (fig. 3b). Interestingly, in the mutated heterocomplexes, ClpP1 favored small Leu and Met residues while ClpP2 was capable of cleaving substrates containing a large 2-aminooctanoic acid (2-Aoc) group at the P1 position. This overall specificity reflects the available space within the S1 pockets and corresponds well with previous data in which β-lactone inhibitors with large, hydrophobic chains effectively inhibited ClpP2, but not ClpP1.[7] A cleavage preference for 2-Aoc was also previously shown for *S. aureus* SaClpP, which shares 78% sequence identity with ClpP2, suggesting an evolutionarily conserved function of these highly homologous ClpPs.[85] Similarly, ClpP1/2 preferred 2-Aoc-containing substrates, as a result of the increased peptidolytic activity of ClpP2 in the heterocomplex and its influence on the cleavage pattern.

Comparison of P2 and P3 libraries revealed a less stringent specificity and identified some additional preferences and similarities of cleavage sites (fig. 3b). For example, homoarginine (hArg) was well tolerated at the P2 position and 3,4-dichlorophenylalanine at the P3 position by both ClpP variants. D-amino acids were not processed, suggesting a high degree of stereo-

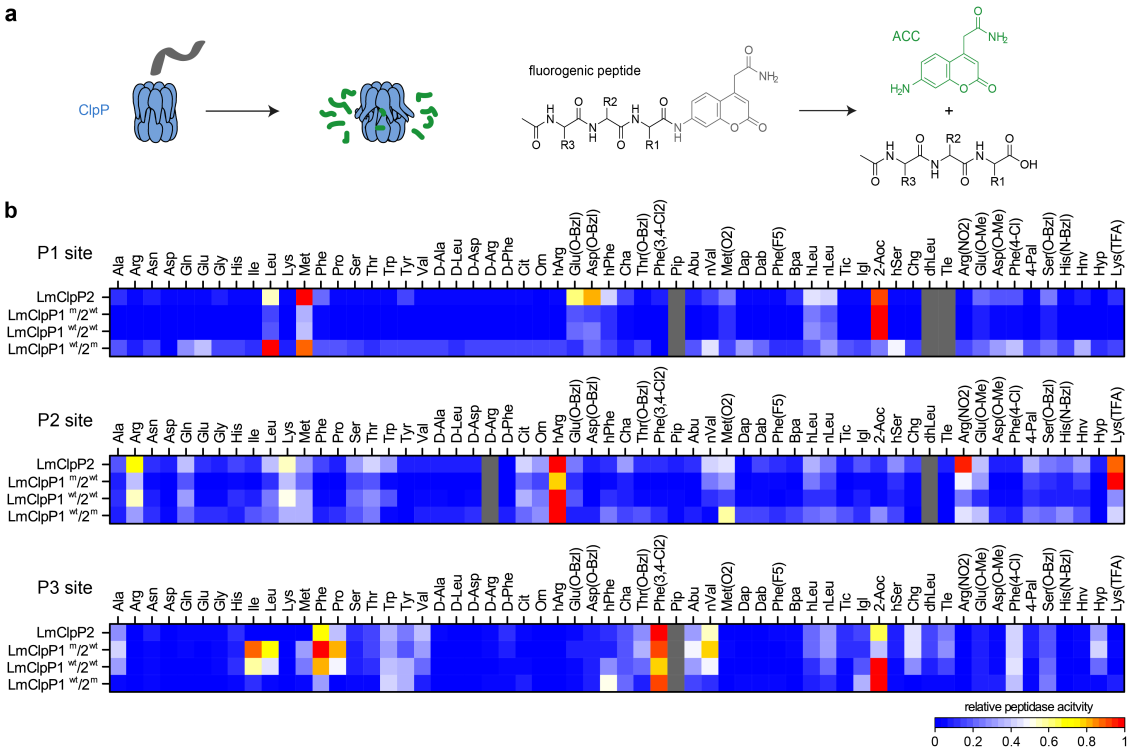

Figure 3 Peptide library screenings a Principle of ClpP peptidase assay: after cleavage of an ACC-tagged tripeptide by ClpP an increase in fluorescence is measured. (General structure of the P1 library: Ac-Ala-hArg-Xaa-ACC, P2 library: Ac-Ala-Xaa-Leu-ACC, P3 library: Ac-Xaa-hArg-Leu-ACC.) **b** Cleavage specificity of ClpP variants (wt: wild type, m: S98A active site mutant) in peptidase assays represented as a heatmap. Each row is normalized to the lowest (0) and to the highest (1) activity. Substrates in gray and peptides containing Cys could not be obtained. Please refer to table 1 for the nomenclature of non-natural amino acids. Peptidase activities were measured in triplicates.

chemical discrimination by ClpP. For example, Leu at the P1 position was readily turned over in its L-configuration, but the corresponding D-stereoisomer could not be processed by any of the constructs. As the substrate specificity extends beyond the scope of natural amino acids, it is possible that chaperone-independent hydrolysis of peptidic, cellular metabolites could be an additional function of ClpP1/2.

3.2.2. Cleavage specificity in protease assays

Having identified substrate preferences of ClpP1 and ClpP2 at the peptide level, we investigated if this specificity holds true for cleavage of proteins as well. Therefore, two cognate *L. monocytogenes* ClpP substrate proteins, serine hydroxymethyltransferase (GlyA) and nicotinate phosphoribosyltransferase (PncB), were fused to a ClpX SsrA recognition tag and the purified recombinant proteins were subjected to ClpXP protease assays (fig. 4a). SsrA-tagged green fluorescent protein (GFP), RNA polymerase sigma factor (EcRpoS) and NAD-specific glutamate dehydrogenase (SaGudB), substrates previously used in EcClpXP and SaClpXP protease assays,[85] were also included to broaden the substrate scope of the study. We tested each of the four ClpP2, ClpP1/2, ClpP1/2(S98A) and ClpP1(S98A)/2 constructs and analyzed protein digests via high-resolution tandem mass-spectrometry (MS/MS) coupled to a nano-HPLC using established procedures.[85] Peptide fragments were sequenced and analyzed via the Protein|Clpper software (www.oc2.ch.tum.de). The algorithm calculates $\log_2$ scores S by

Table 1 Names and abbreviations of non-natural amino acids used in the peptidase substrate library screening.

Abbreviation	Name
D-Ala	D-alanine
D-Leu	D-leucine
D-Asp	D-aspartic acid
D-Arg	D-arginine
D-Phe	D-phenylalanine
Cit	citrulline
Orn	ornithine
hArg	homoarginine
Glu(O-Bzl)	glutamic acid 4-benzyl ester
Asp(O-Bzl)	aspartic acid 4-benzyl ester
hPhe	homophenylalanine
Cha	cyclohexylalanine
Thr(O-Bzl)	*O*-benzylthreonine
Phe(3,4-Cl2)	3,4-dichlorophenylalanine
Pip	piperidine-2-carboxylic acid
Abu	2-aminobutanoic acid
nVal	norvaline
Met(O2)	methionine sulfone
Dap	2,3-diaminopropionic acid
Dab	2,4-diaminobutyric acid
Phe(F5)	pentafluorophenylalanine
Bpa	*p*-benzoylphenylalanine
hLeu	homoleucine
nLeu	norleucine
Tic	1,2,3,4-tetrahydroisoquinoline-3-carboxylic acid
Igl	2-indanylglycine
2-Aoc	2-aminooctanoic acid
hSer	homoserine
Chg	cyclohexylglycine
dhLeu	dehydroleucine
Tle	*tert*-leucine
Arg(NO2)	N_ω-nitroarginine
Glu(O-Me)	glutamic acid γ-methyl ester
Asp(O-Me)	aspartic acid γ-methyl ester
Phe(4-Cl)	*p*-chlorophenylalanine
4-Pal	4-pyridylalanine
Ser(O-Bzl)	*O*-benzylserine
His(N-Bzl)	*N*(im)-benzylhistidine
Hnv	β-hydroxynorvaline
Hyp	4-hydroxyproline
Lys(TFA)	*N*-6-trifluoroacetyllysine

dividing the occurrence of an amino acid A at cleavage site position P by the natural occurrence of this amino acid in the respective protein. Thus, $\log_2(S)$ values larger than 0 indicate that the respective residue is enriched at a given position, whereas $\log_2(S)$ values smaller than 0 reflect depletion.[85]

Overall, a sufficient sequence coverage comprising 4668 unique peptides and 11 508 peptide-

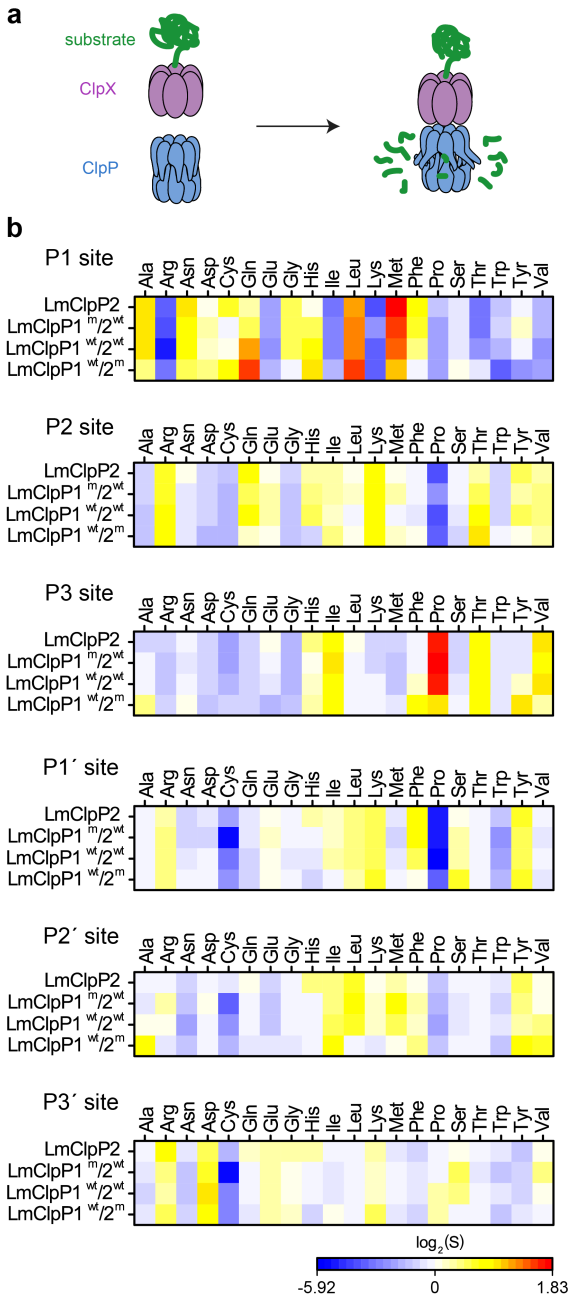

Figure 4 Cleavage specificity in a protease assay a Principle of ClpP protease assay: SsrA-tagged substrate proteins are digested by the ClpXP complex and the produced peptides are analyzed by MS/MS. **b** Cleavage specificity of ClpP variants (wt: wild type, m: S98A active site mutant) in protease assays represented as a heatmap. ClpXP digests of substrate proteins were analyzed by Protein|Clpper.[85] $\mathrm{Log}_2(S) > 0$ means that cleavage occured more often than expected from the amino acid composition of the substrate proteins, $\log_2(S) < 0$ represents less frequent cleavage than random cleavage. Data represent two independent experiments with five different substrate proteins.

to-spectrum matches were obtained, which led to the analysis of 22 925 cleavage reactions (3221 for ClpP2, 4647 for ClpP1/2, 8618 for ClpP1/2(S98A) and 6439 for ClpP1/2(S98A)) (fig. 4b). Although less pronounced compared to the peptidase data, a distinct cleavage pattern was observed at the P1 site with a preference for Leu and Met by both ClpP isoforms, which matches previous ClpXP analyses.[40,85] Strikingly, a difference in specificity was observed for ClpP1, which also preferred cleavage after Gln. This preference was less prominent in the peptidase assays and is unique to this proteolytic complex amidst other ClpXPs investigated so

far. In contrast to the peptide substrate library screening, only a few amino acids (Arg, Lys, Trp for all enzymes and Ile and Thr for Clp2) were strongly depleted in the protease screening. In addition, Protein|Clpper analysis of the digests showed much lower overall specificity at the P2, P3 and prime sites than at the P1 site. Nevertheless, Pro appears to be a crucial cleavage blocker if present at P2 or P1' sites, which is likely attributable to its rigidity and locking the protein backbone in a kinked conformation. However, Pro at P3 increases the probability of being processed in the case of ClpP2.

3.2.3. Identification of ClpP1/ClpP2 peptidase and protease inhibitors

Previously reported β-lactones[78] did not inhibit ClpP1, thus failing to lend any insights into the heterocomplex mechanism.[7] However, with the peptide screening data in hand, we were able to design customized ClpP inhibitors in order to analyze the role of each isomers in more detail. A tripeptide scaffold with a C-terminal chloromethyl ketone (CMK) group was used to irreversibly bind the active site. Although peptide-CMK inhibitors are less selective and exhibit limited cell-permeability for in situ applications, the main advantages of these compounds are their stability upon enzyme active site binding as well as their customizability. We thus synthesized two inhibitors that incorporated the best residues from the P1, P2 and P3 library screening. Hence, 2-Aoc and Leu were selected for P1, while P2 and P3 sites contained hArg and 3,4-dichlorophenylalanine, respectively, yielding **Leu-CMK** and **Aoc-CMK** inhibitors (fig. 5a). The synthesis of these compounds was performed in a similar manner as described by Kato et al.[86] In brief, Ac-Phe(3,4-Cl_2)-hArg-COOH dipeptide was synthesized on 2-chlorotrityl chloride resin and coupled with NH_2-Leu-CMK (or NH_2-2-Aoc-CMK). In addition, we included **E2** and **D3** in our study as representative β-lactone inhibitors, as well as **AV170**, a recently introduced ClpP inhibitor with an electrophilic phenyl ester moiety (fig. 5a).[38]

The peptidolytic activity of ClpP2, ClpP1/2, ClpP1/2(S98A), ClpP1(S98A)/2 and ClpP1-(N172D) was measured by the hydrolysis of Ac-Ala-hArg-Leu-ACC, a substrate that showed optimal turnover by both isomers. Inhibitors were used in three concentrations, 100, 10 and 1 μM to estimate their potency (fig. 5b, fig. 6). As all complexes deviate in their peptidolytic rates, substrate turnover in the absence of inhibitor was normalized to 100% activity. **AV170** and both CMK inhibitors were the most effective against ClpP2, followed by **D3** and **E2**. A similar profile was observed for heterooligomeric ClpP1/2 and ClpP1(S98A)/2, suggesting that inhibition of ClpP2 alone is sufficient to affect the overall complex activity. In contrast, the inhibition pattern for ClpP1 in ClpP1/2(S98A) and ClpP1N172D) complexes were quite different. Here, only the CMKs showed any inhibitory effect, and **Leu-CMK** exhibited significantly higher potency compared to the 2-Aoc analog. **Leu-CMK** completely abolished ClpP1 activity in the heterocomplex at 1 μM, reflecting its preference for small residues at the P1 site. With the first potent ClpP1 inhibitors in hand, we commenced with mechanistic studies of ClpXP proteolysis.

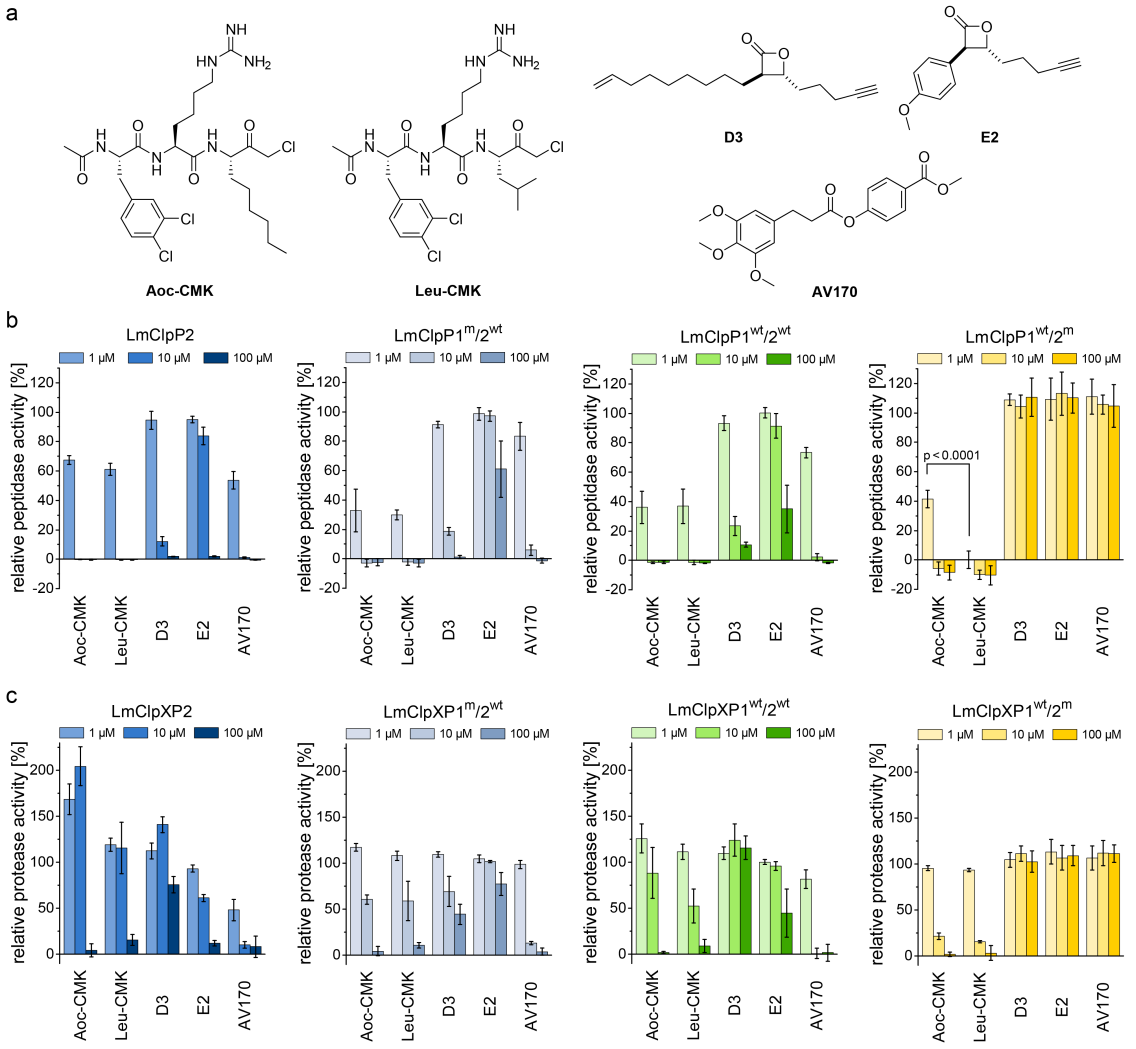

Figure 5 Screening of ClpP inhibitors. **a** Structures of the inhibitors used in this study. **b** Peptidase assay (1 µM ClpP and 200 µM Ac-Ala-hArg-Leu-ACC substrate). **c** Protease assay (0.2 µM $ClpP_{14}$, 0.4 µM $ClpX_6$ and 0.4 µM eGFP-SsrA). Three different inhibitor concentrations were tested. Data are normalized to the DMSO control as 100%. Datasets represent at least two independent experiments which were measured in triplicate (mean ± standard deviation). *p*-Value was determined by Student's *t*-test.

3.2.4. Partial inhibition of homooligomeric ClpP2 stimulates proteolysis

ClpP2, ClpP1/2, ClpP1/2(S98A) and ClpP1(S98A)/2 were reconstituted with ClpX and proteolysis of GFP-SsrA was monitored by a decrease in fluorescence signal according to previously established protocols.[87] Inhibitors were added at three concentrations (100, 10 and 1 µM) to estimate their effects on enzymatic activity. Phenyl ester **AV170** turned out to be the most effective inhibitor against each complex, except ClpP1/2(S98A), highlighting the restricted binding site preferences of the ClpP1 isoform (fig. 5c). Similarly, none of the β-lactones were able to inhibit ClpP1, although the newly designed CMKs showed pronounced effects on both isoforms. The compounds reduced proteolysis of all three heterocomplex constructs in a concentration-dependent manner, but, surprisingly, **Aoc-CMK** enhanced GFP degradation by the ClpXP2 homocomplex. A similar, but less pronounced, proteolytic stimulation of ClpXP2 was observed with aliphatic β-lactone **D3**. To investigate this unexpected finding in more detail, proteolytic assays with all complexes were performed at incremental inhibitor concentration

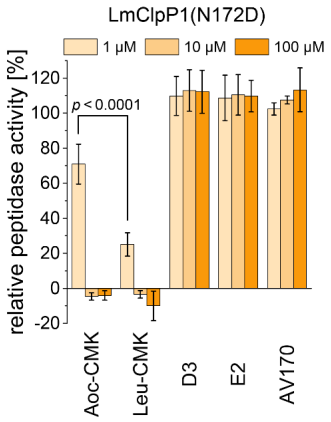

Figure 6 Peptidase assays of ClpP1(N172D). 1 µM ClpP1(N172D) and 200 µM Ac-Ala-hArg-Leu-ACC substrate were used. Three different inhibitor concentrations were tested. Data are normalized to DMSO control as 100%. The dataset represents two independent experiments which were measured in triplicate (mean ± standard deviation). *p*-value was determined by Student's *t*-test.

steps (fig. 7a). Interestingly, 5 µM **Aoc-CMK** resulted in the strongest activation of ClpXP2 proteolysis (162%) while higher concentrations decreased, and finally abolished, complex activity at 50 µM. Intact protein MS analysis of the most activated species revealed 20% ClpXP2 complex occupancy of the inhibitor. This suggests that incomplete inhibitor binding to the ClpP2 tetradecamer stimulates proteolysis in association with ClpX, but not peptidolysis, when in the absence of chaperone (see results above). The degree of modification reached 52% at 100 µM, which was sufficient to fully abolish proteolytic activity (fig. 7a). As CMKs are general ClpP inhibitors, we tested the effect of partial **Aoc-CMK** activation with the *S. aureus* SaClpXP system and obtained 26% stimulation, highlighting that this intriguing phenomenon is less pronounced in other homologs and may thus be a specific feature of ClpP2 (fig. 8).

Importantly, partial binding alone cannot explain the proteolytic enhancement since aromatic lactone **E2** inhibited ClpXP2 without significant activation, while **D3** showed 41% activation (fig. 7b). In addition, all three heterocomplex constructs revealed only marginal to no enhancement of turnover with **Aoc-CMK**, suggesting that homotetradecameric ClpP2 is required to trigger this effect. Similarly, **Leu-CMK** stimulated ClpP2 to a much lesser extent than **Aoc-CMK**, highlighting that both the intrinsic reactivity as well as the compound structure are crucial for the activity. We thus commenced with in-depth analysis of the mechanistic requirements responsible for these effects.

3.2.5. Alkylation of ClpP2 triggers ClpX binding

It is known that ClpP1/2 heterooligomerization, in combination with ClpX chaperone binding, enhances proteolysis.[14] Strikingly, we observe here an additional activation mechanism, predominantly for the homocomplex, which raises the question of whether there is a common underlying mechanism. We set out to answer this question by studying the homo- and heterocomplexes with a suite of biochemical and analytical methods. For these studies, we selected **Aoc-CMK** as a suitable tool compound due to its strong stimulatory effect and irreversible mode of alkylation.

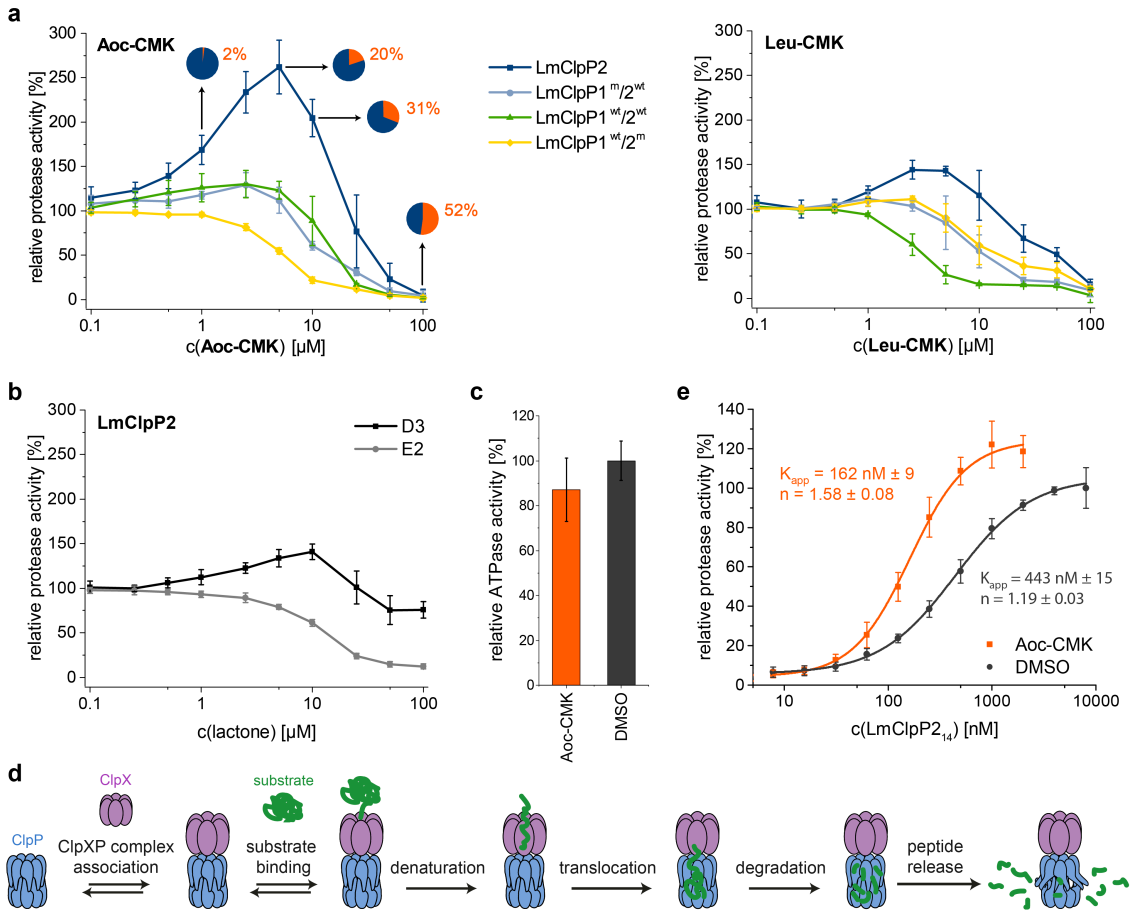

Figure 7 Activation of the ClpXP proteolysis by small molecules. **a** Protease activity of ClpP variants with **Aoc-CMK** and **Leu-CMK**. Pie diagrams illustrate the degree of modification of ClpP2 with **Aoc-CMK**, determined by intact protein mass spectrometry (means from triplicate experiments are shown). **b** Protease activity of the ClpP2 homocomplex with lactones **D3** and **E2**. **c** ATPase activity of $ClpX_6$ (0.2 µM) in the presence of $ClpP2_{14}$ (0.1 µM) and **Aoc-CMK** (4.25 µM) with 20 mM ATP. Data represent three independent experiments which were measured in quadruplicate (mean ± standard deviation). **d** Kinetic scheme for protein degradation by ClpXP. (Parts of this figure have been adapted from Kim et al.[87]) **e** Protease activity of ClpP (varying concentrations of $ClpP_{14}$) with and without **Aoc-CMK** (in 25-fold excess to $ClpP2_{14}$). Curves were fit to the Hill equation: $y = V_{min} + (V_{max} - V_{min})x^n / (K_{app}{}^n + x_n)$. Protease activity data represent at least two independent experiments which were measured in triplicate (mean ± standard deviation).

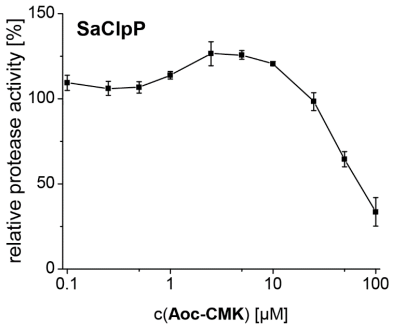

Figure 8 Protease activity of SaClpP with Aoc-CMK. 0.2 µM $SaClpP_{14}$, 0.4 µM $SaClpX_6$ and 0.4 µM eGFP-SsrA were used. Data represent two independent experiments which were measured in triplicate (mean ± standard deviation).

First, we focused on the homocomplex and addressed the nature of its activation by studying its conformational stability. Select lactones, including **E2** and phenylesters such as **AV170**, are known to destabilize tetradecameric ClpP and to induce its dissociation into inactive

heptamers.[38,79]. In fact, deoligomerization of ClpP2 could be observed upon **E2** binding, while the tetradecameric complex was retained with both the CMKs and **D3** (fig. 9). This demonstrates a principle difference in the binding mode, in which those molecules that disrupt the oligomeric state thereby inactivate ClpP, while those that only partially modify ClpP and retain the tetradecameric state stimulate ClpP.

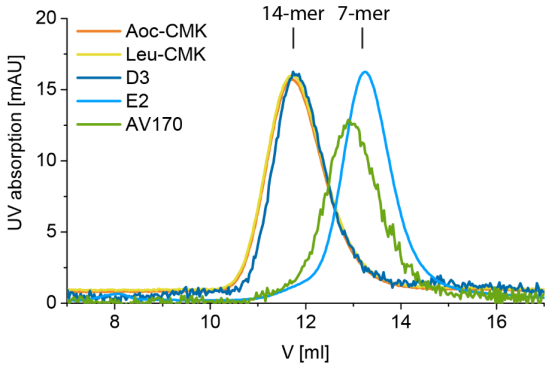

Figure 9 Size-exclusion chromatograms of ClpP2 treated with inhibitors. Treatment with **Aoc-CMK**, **Leu-CMK** and **D3** results in retention of the tetradecamer whereas **E2** and **AV170** induce deoligomerization to heptamers.

Second, as partial inhibition does not trigger peptidolysis but proteolysis, we investigated the role of the associated ClpX chaperone. ClpX recognizes tagged substrates and catalyzes their ATP-dependent unfolding, which represents the rate-determining step of proteolysis.[87] Thus, ClpX ATPase activity was determined in the presence of partially **Aoc-CMK**-inhibited ClpP2. No increase in ATP turnover could be observed, suggesting that ATP hydrolysis occurs independently of the association with **Aoc-CMK**-modified ClpP (fig. 7c).

Third, ClpXP2 assembly is in equilibrium with individual ClpP2 and ClpX complexes. This equilibrium precedes all subsequent steps required for protein turnover, including ClpX-mediated substrate binding, unfolding and translocation into the proteolytic chamber (fig. 7d). A shift in equilibrium towards the proteolytically-active ClpXP2 complex could therefore significantly enhance overall activity. We thus elucidated the direct interaction between ClpP2 and ClpX in proteolytic assays, in which the concentration of ClpP2 was systematically varied and an apparent affinity constant was calculated. Importantly, while the K_{app} of ClpXP2 with unmodified ClpP2 was 443 nM, the K_{app} for partially **Aoc-CMK**-modified ClpP2 dropped to 162 nM. This increase in affinity through partial inhibitor binding to ClpP reveals an intriguing mechanism of activation (fig. 7e). A similar enhancement in ClpX affinity was previously observed for **E. coli** ClpP fully inactivated by diisopropylfluorophosphonate (DFP) which contributed to a model of functional communication between ClpX and ClpP during substrate processing.[88] Here, we show that the mechanism of proteolytic stimulation extends beyond complete active site binding and is largely affected by the degree of modification, inhibitor structure as well as the ClpP isoform investigated.

3.2.6. Heterooligomeric ClpP1/2 is intrinsically stimulated by enhanced ClpX binding

Proteolytic studies of the three heterocomplexes did not reveal pronounced activation upon partial modification with **Aoc-CMK**. However, it should be noted that all heterocomplex constructs, including those that contain an active-site mutated ring, are about 10-fold more active compared to the ClpXP2 homocomplex for yet unknown reasons.[14] An effect on ClpX ATPase activity by heterooligomerization has already been excluded in previous studies.[14] In order to understand the basis for the enhanced activity, we dissected the mechanism and investigated key steps relevant for proteolysis.

Inspired by the results of partial **Aoc-CMK** inhibition, we focused on the interaction between ClpP1/2 and ClpX, and determined their affinity. Proteolytic assays were performed with varying ClpP1/2 concentrations, and apparent affinity constants were calculated as outlined above (fig. 10a). Importantly, the K_{app} for ClpXP1/2 was 85 nM and thus about 7-fold lower compared to the ClpXP2 homocomplex. These results suggest a strong shift in the equilibrium of complex formation to the ClpXP1/2 form, thereby enhancing substrate turnover.

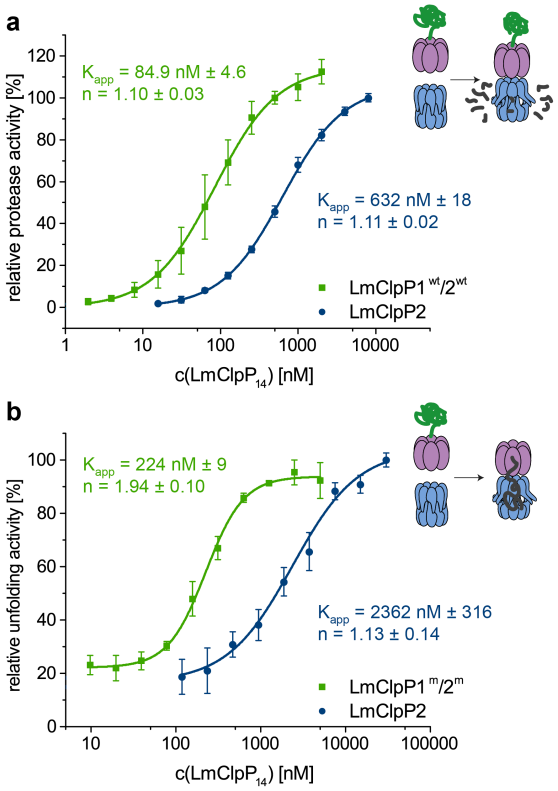

Figure 10 Stimulation of ClpXP activity by heterooligomerization. a Protease activity of hetero- and homocomplex of ClpP (varying concentrations of $ClpP_{14}$). The data set represents three independent experiments which were measured in triplicate (mean ± standard deviation). **b** Unfolding activity of hetero- and homocomplex of ClpXP(S98A) (0.4 µM $ClpX_6$, varying concentrations of $ClpP_{14}$) in presence of GFP-SsrA (0.125 µM). The data set represents two independent experiments which were measured in triplicate (mean ± standard deviation).

To further prove this theory, we determined the K_{app} for protein unfolding, which is the rate-limiting step before proteolysis.[87] To focus on ClpX activity, we utilized ClpP2 and ClpP1/2 containing Ser98 to Ala mutations. While catalytically inactive, these mutant proteins are still

able to bind ClpX and facilitate the translocation of the linear peptide chain into the barrel. Systematic variation of ClpP concentrations revealed K_{app} values of 2362 nM and 224 nM for homo- and heterocomplexes, respectively (fig. 10b). In agreement with the proteolysis data, these results indicate that ClpX and ClpP1/2 form the functional complex with higher affinity at the rate-limiting, substrate-unfolding step, thereby enhancing the overall activity.

Although these studies provide a mechanistic basis for understanding the elevated proteolytic activity, the nature of this high-affinity interaction, as well as how the heterocomplex or partially-inhibited homocomplex facilitate tighter ClpX binding, remain to be explored. No significant structural differences between the ClpP2 homocomplex and heterocomplex with respect to ClpP1 were observed.[14] However, the N-terminal regions, which are crucial for chaperone interaction, could not be characterized with high resolution so far. In order to unravel more general aspects of heterocomplex assembly, analysis of its quaternary structural organization would be required.

3.3. Conclusion

Protein degradation is tightly controlled by the cell in order to prevent unwanted proteolytic damage. Thus, major proteases such as ClpP and DegP are only activated for proteolysis in association with cognate chaperones and oligomerization, respectively.[89] The chaperones act as gatekeepers and bind to conserved hydrophobic pockets on the apical sites of ClpP[32,77,90] in order to initiate protein degradation by substrate recognition and unfolding. The mechanism of activation was more closely investigated with acyldepsipeptide (ADEP)[32], which are small-molecule chaperone mimics that bind to the same hydrophobic pockets and thereby, like ClpX, induce pore opening and conformational changes of ClpP to the activate state.[91] Thus, binding to chaperones, or mimics thereof,[92] represents the first known method of ClpP activation. Surprisingly, we identify here additional mechanisms of activation of ClpPs, based on their affinity for chaperones. Key to this analysis was the fact that ClpP and ClpX are in a dynamic equilibrium for the formation of the proteolytically competent ClpXP complex, which is the critical first step for proteolysis (fig. 7d).[87]

We initiated our studies by inspecting both ClpP isoforms and discovered that the ClpP2 peptidase, similar to its *S. aureus* homolog,[85] prefers substrates with a long aliphatic side chain at the P1 site. As ClpP exhibits hydrolytic activity of small substrates that access the proteolytic chamber by diffusion, it is possible that it may have specialized functions beyond the cleavage of proteins. Although the preference for aliphatic amino acids such as Leu and Met, similar to other ClpPs, was retained in proteolytic studies, the overall selectivity observed for peptidase activity was largely abrogated.[40,85] However, a striking feature of ClpP1 is its additional preference for Gln at the P1 site.

An additional feature of ClpP1/2 is the accelerated proteolytic rate when associated with ClpX. We show that the reason for this second principle of ClpP activation is a higher affinity between ClpP1/2 and ClpX, which shifts the equilibrium to the active ClpXP1/2 heterocomplex. As the

apical sites of ClpP1 and ClpP2 do not significantly change in the homo- and heterocomplexes, structural differences in the loop regions, which could not be resolved so far, may be responsible for a tighter interaction. Importantly, ClpP2 is prone to a third mechanism of activation based on partial active site binding by irreversible inhibitors. While modification of 20% of all catalytic serines by a CMK inhibitor increased proteolysis by 160%, alkylation of approximately 50% of the sites resulted in full inhibition. Again, the reason for this proteolytic stimulation was an increase in binding affinity of the chaperone for partially CMK-modified ClpP2, which shifted the equilibrium to the active proteolytic complex. Thus, modulating the affinity between ClpP and ClpX seems to be a unifying principle for proteolytic fine tuning. Interestingly, the activation heavily depended on the inhibitor used. While **Aoc-CMK** induced the strongest effect, a CMK-inhibitor containing Leu at the P1 site was only marginally stimulatory, suggesting that binding of long aliphatic chains into the S1 pocket could be a crucial parameter. Similarly, the long aliphatic β-lactone inhibitor **D3** also stimulated proteolysis, although to a much lesser extent, which suggests that this effect is more general and can also be observed by lactone active-site acylation in addition to CMK alkylation. On the contrary, aromatically decorated lactone **E2**, a known disruptor of the ClpP tetredecamer[79], inhibited turnover, which emphasizes the importance of the ligand introduced into the S1 pocket. While a slight activation by **Aoc-CMK** was also observed for SaClpP, the more pronounced effects in ClpP2 suggest a more functionally relevant role in this system. Based on this data, the ClpP2 active site and substrate pocket seem to control the fate of proteolytic activity. Partial binding of long aliphatic ligands or heterooligomerization with ClpP1 induce proteolysis via tighter binding to ClpX, which may be necessary under certain stress conditions. For instance, heat stress was previously shown to induce the expression of *clpP1* and *clpP2*, resulting in an increased number of heterocomplexes, which might result in elevated proteolytic rates for removal of misfolded proteins.[14] In addition, it is intriguing to speculate that metabolites containing long aliphatic chains may act as native stimulants. While the existence of such metabolites has to be investigated in future studies, it is important to note that activating peptides have previously been reported for heterooligomeric MtClpPs.[15,16] In fact, these small molecules bind to active sites and thereby enhance activity.[15,33,81]

In total, our in-depth analysis of ClpP1/2 activity revealed two principles of proteolytic stimulation that both rely on elevated affinity between ClpPs and ClpX. This phenomenon appears to be special to the Listeria system, which is already unique through its unusual expression of two ClpP isoforms. Due to the fundamental relevance of ClpP for cell homeostasis under stress conditions, both activation pathways ensure a boost in ClpP activity when needed, while remaining tightly regulated by ClpX interactions in order to prevent uncontrolled damage.

3.4. Materials and methods

3.4.1. Cloning, protein overexpression

ClpP variants

ClpP2, ClpP2(S98A), ClpP1(N172D) and SaClpP were obtained as described previously.[6,7] Expression constructs with C-terminal Strep-tag II were cloned in pET301 plasmids, overexpressed in *E. coli* BL21(DE3) and purified with affinity chromatography and gel filtration. ClpP1(N172D) was prepared by Dr. Maria Dahmen.

ClpP1/2, ClpP1/2(S98A), ClpP1(S98A)/2 and ClpP1(S98A)/2(S98A) heterocomplex variants were overexpressed and purified as detailed previously.[14] In short, C-terminally Strep-II-tagged ClpP1 and C-terminally His_6-tagged ClpP2 were introduced into pETDuet-1 vector. Proteins were overexpressed in *E. coli* BL21(DE3) at 37 °C for 6 h after induction with 1 mM isopropyl-β-D-thiogalactoside (IPTG). After harvest the cells were lysed in His-lysis-buffer (20 mM MOPS, 100 mM KCl, 1% CHAPS, 5% glycerol, pH 8.0). The proteins from the cleared cell lysate were captured by Ni^{2+} affinity chromatography in His buffers (20 mM MOPS, 100 mM KCl, 5% glycerol, pH 8.0, + 40 mM imidazole for washing, + 300 mM imidazole for elution) and a subsequent StrepTactin chromatography step in Strep buffers (100 mM Tris, 150 mM NaCl, 1 mM EDTA, pH 8.0, + 2.5 mM desthiobiotin for elution). A final gel filtration was performed in ClpP-GF buffer (20 mM MOPS, 100 mM KCl, 5% glycerol, pH 7.0).

ClpX variants

Tagfree ClpX was overexpressed in *E. coli* BL21(DE3) or in SG1146a (Δ*clpP*). In both cases, an expression construct equipped with an N-terminal His_6-tag and a TEV cleavage site in pET300 vector was used.[14] 4 L LB medium were inoculated (1:100) and grown to an optical density (OD_{600}) of 0.6 at 37 °C. After induction with 0.5 mM IPTG the cells were incubated over night at 25 °C. The cells were harvested by centrifugation, washed in PBS, resuspended in ClpX lysis buffer (25 mM HEPES, 200 mM KCl, 1 mM DTT, 5% glycerol, 0.5 mM ATP, 5 mM $MgCl_2$, pH 7.6) and lysed by ultrasonication. The cell debris was removed by centrifugation (39 000 g, 40 min, 4 °C) and the cell lysate was loaded on a 5 mL HisTrap HP column (GE Healthcare) using an ÄKTA Purifier 10 system (GE Healthcare). The column was washed with 12 column volumes (CV) ClpX wash buffer (25 mM HEPES, 200 mM KCl, 1 mM DTT, 5% glycerol, 40 mM imidazole, pH 7.6). The protein was eluted with 6 CV ClpX elution buffer (25 mM HEPES, 200 mM KCl, 1 mM DTT, 5% glycerol, 300 mM imidazol, pH 7.6). The protein fractions were pooled, 1 mM EDTA and 1.25 mg TEV protease were added and the reaction mixture was incubated at 10 °C over night. The completeness of the TEV cleavage was verified by intact protein mass spectrometry. The protein solution was loaded on a Superdex 200 pg 16/60 column (GE Healthcare) and eluted in ClpX lysis buffer.

Tagfree SaClpX was purified as described previously.[91] In short, for the overexpression of SaClpX with an N-terminal His_6-tag and TEV site pET301 vector was used in *E. coli* BL21(DE3) cells. The cell lysate was loaded on a HisTrap HP column (GE Healthcare). TEV protease and 1 mM EDTA were added to the pooled fractions. After cleavage and removal of imidazole,

the protein solution was loaded on a HisTrap HP column and the flow-through was collected which was further purified by gel filtration.

ClpXP substrate proteins

N-terminally Strep-II-tagged eGFP with a C-terminal SsrA tag (AGKEKQNLAFAA for *L. monocytogenes* and AANDENYALAA for *E. coli*) was overexpressed in *E. coli* KY2266 (Δ*clpXP*, Δ*lon*, Δ*hslVU*)[93] using pDEST007 expression vector and purified by affinity chromatography and gel filtration as described previously.[14,94]

Table 2 List of primers used in this study.

Primer	Sequence (5'→3')
LmGlyA_for	GGGGACAAGTTTGTACAAAAAAGCAGGCTTTGTCTATTTACAAAAGCAAGATAAGGAAG
LmGlyA_rev	GGGGACCACTTTGTACAAGAAAGCTGGGTGTTATTAGGCAGCGAAAGCTAGGTTTTGTTTTT CTTTGCCTGCGCTGCCTAAACTTGGATAAAGCGGATATTCATTTG
LmPncB_for	GGGGACAAGTTTGTACAAAAAAGCAGGCTTTACAAATTTATTTCAAGATGATAGTC
LmPncB_rev	GGGGACCACTTTGTACAAGAAAGCTGGGTGTTATTAGGCAGCGAAAGCTAGGTTTTGTTTTT CTTTGCCTGCGCTGCCAAACGGCATATCTAGTTCAAC

GlyA (UniProt entry Q8Y4B2) and PncB (UniProt entry Q8Y826) with an N-terminal Strep-II tag and a C-terminal LmSsrA tag were constructed from *L. monocytogenes* EGD-e genomic DNA in pDEST007 plasmid vector with Gateway® Technology using the primers listed in table 2. The plasmids were transformed into *E. coli* SG1146a cells. 2 L LB culture was induced with 0.2 μg/mL anhydroteracycline after reaching an OD_{600} of 0.6. GlyA was incubated at 37 °C for 5 hours and PncB at 25 °C over night. Cells were harvested by centrifugation, washed with PBS, resuspended in PBS and ultrasonicated on ice. The cell lysate was cleared by centrifugation (39 000 g, 40 min, 4 °C) and loaded on a pre-equlibrated 5 mL StrepTrap HP column (GE Healthcare). The column was washed with 6 CV binding buffer (100 mM Tris-HCl, 150 mM NaCl, 1 mM EDTA, pH 8.0) and eluted with 5 CV binding buffer + 2.5 mM desthiobiotin. EcRpoS and SaGudB with SsrA tags (AANDENYALAA and AGKSNNNFAVAA, respectively) were purified similarly as described elsewhere.[85]

Other enzymes

Creatine kinase (10 127 566 001), lactate dehydrogenase (10 128 155 001) and pyruvate kinase (10 127 876 001) were purchased from Roche.

3.4.2. Kinetic assays

Peptidase assay

The substrate library screening was conducted by Dr. Maria Dahmen and by Dr. Malte Gersch.

Following fluorogenic tripeptide substrate libraries were used: Ac-Ala-hArg-Xaa-ACC for P1 site, Ac-Ala-Xaa-Leu-ACC for P2 site and Ac-Xaa-hArg-Leu-ACC for P3 site.[85] 1 μL substrate (100× stock in DMSO, 100 μM final concentration) was added to a flat bottom black 96-well plate and equilibrated to 32 °C. ClpP (1 μM) in preheated peptidase buffer (100 mM HEPES, 100 mM

KCl, 15% glycerol, pH 7.0) was added to a final volume of 100 µL to start the reaction, and fluorescence (excitation: 380 nm, emission: 440 nm) was measured with an infinite M200Pro plate reader (Tecan). Data were recorded in triplicate.

For the testing of inhibitors 1 µL inhibitor (100× stock in DMSO, 1 µM, 10 µM and 100 µM final concentrations) and ClpP (1 µM) in peptidase buffer (100 µL final volume) were incubated for 30 min at 32 °C. 1 µL (100 ×stock in DMSO, 200 µM final concentration) Ac-Ala-hArg-Leu-ACC substrate was added and the fluorescece was measured (380 nm, 430 nm). Data were recorded in triplicate and two independet experiments were performed. Peptidase activity was determined by linear regression using Microsoft Excel and plots were made with Microcal OriginPro 2016.

The CMK inhibitors and the Ac-Ala-hArg-Leu-ACC substrate was provided by Marcin Poręba (Wrocław University of Technology). For the synthesis see the electronic supplementary section of Balogh et al.[95]

Protease assay

Protease assays were carried out in flat bottom white 96-well plates in a final volume of 60 µL. 0.6 µL inhibitor (100×DMSO stock, 0.1 – 100 µM final concentrations), $ClpP_{14}$ (0.2 µM), $ClpX_6$ (0.4 µM) and ATP regeneration mix (4 mM ATP, 16 mM creatine phosphate, 20 U/mL creatine kinase) were pre-incubated for 15 min at 30 °C in PZ buffer (25 mM HEPES, 200 mM KCl, 5 mM $MgCl_2$, 1 mM DTT, 10% glycerol, pH 7.6). 0.4 µM eGFP-SsrA substrate was added and fluorescence was measured (485 nm, 535 nm). Data were recorded in triplicate and at least two independent experiments were performed. Protease activity was determined by linear regression using Microsoft Excel and plots were made with Microcal OriginPro 2016.

For the determination of K_{app} values the $ClpP_{14}$ concentration was varied (2 nM – 8000 nM). If needed, **Aoc-CMK** (100× stock in DMSO, final concentration = 25 ×$ClpP_{14}$ concentration) or DMSO was added. In case of the GFP unfolding assay, ClpP2(S98A) and ClpP1(S98A)/ ClpP2(S98A) mutants were used in varying concentrations (10 nM – 30 µM) in presence of 0.4 µM $ClpX_6$ and 0.125 µM eGFP-SsrA. Data were recorded in triplicate and at least two independent experiments were performed. Slopes were determined by linear regression using Microsoft Excel. Protease activity was plotted against $ClpP_{14}$ concentration in Microcal OriginPro 2016 and was fitted to the Hill equation:

$$y = V_{min} + \frac{(V_{max} - V_{min})x^n}{K_{app}^n + x^n}$$

ATPase assay

0.85 µL **Aoc-CMK** (100× DMSO stock, 4.25 µM final concentration) or DMSO were added to a flat bottom transparent 96-well plate. $ClpX_6$ (0.2 µM) and $ClpP2_{14}$ (0.1 µ) were added in ATPase buffer (100 mM HEPES, 200 mM KCl, 20 mM $MgCl_2$, 1 mM DTT, 1 mM NADH, 2 mM phosphoenolpyruvate, 50 U/mL lactate dehydrogenase, 50 U/mL pyruvate kinase, 5% glycerol, pH 7.5) and incubated for 12 min at 37 °C. The reaction was started by the addition of 20 mM

ATP. Absorption at 340 nm was measured. Three independent experiments with four replicates each were carried out. ATPase activity was determined by linear regression using Microsoft Excel after substraction of the background signal (measurement without ClpX), the plot was made with Microcal OriginPro 2016.

3.4.3. Analysis of ClpXP protein substrate digests

$ClpP_{14}$ (0.2 µM), $ClpP_6$ (0.4 µM), SsrA-tagged substrate protein (1 µM) and ATP regeneration mix (4 mM ATP, 16 mM creatine phosphate, 20 U/mL creatine kinase) were incubated over night at 37 °C in PZ buffer (25 mM HEPES, 200 mM KCl, 5 mM $MgCl_2$, 1 mM DTT, 10% glycerol, pH 7.6).

The samples were desalted using reverse phase extraction cartridges (tC18 SepPak, 50 mg, Waters) on a vacuum manifold. Cartridges were washed three times with 1 mL acetonitrile (ACN), 1 mL 50% ACN with 0.5% formic acid (FA) and twice with 1 mL 0.1% FA. After addition of FA to a final concentration of 0.5% FA, the samples were loaded on the cartridges, washed with 1 mL 0.1% FA and twice with 1 mL 0.5% FA. Peptides were eluted into low binding reaction tubes (Eppendorf) with 3× 200 µL 80% ACN with 0.5% FA. The eluates were vacuum dried. The dried samples were dissolved in 100 µL 1% FA, ultrasonicated for 15 min and filtered on a 0.45 µm pore size filter.

LC-MS/MS analysis was carried out on a Dionex UltiMate 3000 nano HPLC coupled to a Thermo Finnigan Orbitrap XL. Samples were loaded onto a C18 NanoTrap Column (Acclaim C18 PepMap100, 2 cm × 10 µm inner diameter (I.D.), 5 µm particle size, 300 Å pore size) and separated on a Dionex C18 PepMap RSLC (Acclaim C18 PepMap RSLC, 50 cm × 75 µm I.D., 2 µm particle size, 100 Å pore size) column. Solvent A consisted of water + 0.1% FA + 5% DMSO and solvent B consisted of ACN + 0.1% FA + 5% DMSO. Separation was achieved at a constant flow rate of 0.2 µL/min using a gradient from 4% B to 30% B over 90 min and a subsequent wash-out to 80% B over 33 min. Full scans were carried out with an m/z range of 350 – 1400 at a resolution of 60 000 followed by a TOP5 CID fragmentation step (35 eV collision energy, activation time: 30 ms) using dynamic exclusion (30 s).

Fragmentation spectra were searched using the SEQUEST HT algorithm against a custom compiled proteome including contaminants using Proteome Discoverer 1.4. Cleavages were allowed after every amino acid, but the search was limited to monoisotopic precursor ions and a peptide mass tolerance of < 10 ppm. Oxidation (+15 995 Da) was set as dynamic modification at methionine residues in all runs. Peptides were validated by the Percolator algorithm with FDR = 0.01 and $\Delta Cn = 0.05$. All peptide-to-spectrum matches passing the validation were then exported and further analyzed in a custom-built and openly available web-script called Protein|Clpper (www.oc2.ch.tum.de). For a detailed depiction of the workflow see Gersch et al.[85]

3.4.4. Intact protein mass spectrometry

0.2 µM $ClpP2_{14}$, 0.4 µM $ClpX_6$, and **Aoc-CMK** (100× DMSO stock, 1 µM, 5 µM, 10 µM and 100 µM final concentrations) were incubated with ATP regeneration mix (4 mM ATP, 16 mM creatine phosphate, 20 U/mL creatine kinase) in PZ buffer (25 mM HEPES, 200 mM KCl, 5 mM $MgCl_2$, 1 mM DTT, 10% glycerol, pH 7.6) at 30 °C for 15 min. Measurements were carried out on a Dionex Ultimate 3000 HPLC system coupled to a Thermo LTQ-FT Ultra mass-spectrometer with electrospray ionisation source (spray voltage 4.0 kV, tube lens 110 V, capillary voltage 48 V, sheath gas 60 a.u., aux gas 10 a.u., sweep gas 0.2 a.u.). 5 µL of reaction mixtures were desalted with a MassPREP desalting cartridge (Waters). The mass spectrometer was operated in positive mode collecting full scans at high resolution (R = 200 000) from m/z = 600 to m/z = 2000. Collected data was deconvoluted using the Thermo Xcalibur Xtract algorithm. Data was recorded in triplicate.

3.4.5. Analytical gel filtration

20 µM ClpP2 was incubated for 10 min at room temperature with 100 µM inhibitor in ClpP-GF buffer (20 mM MOPS, 100 mM KCl, 5% glycerol, pH 7.0). 150 µL of the samples were loaded on a pre-equilibrated Superdex 200 10/300 gel filtration column (GE Healthcare) connected to an ÄKTA Purifier 10 system (GE Healthcare) and eluted with 1 CV ClpP-GF buffer. UV absorption was recorded at 280 nm. The oligomerization state was determined by comparison of the elution volumes to the calibration curve of the column (Gel Filtration Calibration Kit, GE Healthcare).

4. Cryo-EM structure of the ClpXP protein degradation machinery

Published in *Nature Structural & Molecular Biology*, **2019**, 26, pp 946-954
by Christos Gatsogiannis*, Dóra Balogh*, Felipe Merino, Stephan A. Sieber and Stefan Raunser.

*equal contribution

DOI: 10.1038/s41594-019-0304-0

Author contributions

Stephan A. Sieber and Stefan Raunser designed the study. Dóra Balogh cloned, overexpressed and purified proteins, optimized sample preparation, conducted activity assays and gel filtration measurements and analyzed HDX-MS data. Christos Gatsogiannis screened and optimized samples, prepared cryo-EM grids and processed and analyzed cryo-EM data. Christos Gatsogiannis and Felipe Merino built atomic models. Christos Gatsogiannis and Dóra Balogh prepared figures, Christos Gatsogiannis, Dóra Balogh, Stephan A. Sieber and Stefan Raunser wrote the manuscript. All authors discussed the results.

4.1. Introduction

Caseinolytic protease P (ClpP) represents a major proteolytic protein in prokaryotes and in organelles of eukaryotes which is involved in protein homeostasis, bacterial pathogenesis as well as cancer progression.[8,36,43] ClpP is highly conserved, essential for virulence and regulation of stress responses in several pathogenic bacteria and therefore considered as a promising therapeutic target for novel antibiotics.[32] ClpP associates with diverse ATP-dependent AAA+ chaperones such as ClpX, ClpC and ClpA to form a complex for the recognition, unfolding and digestion of substrate proteins.[96] To date, a large fraction of research has been dedicated to functionally exploit ClpP and its cognate chaperones, foremost ClpX, in terms of their enzymatic activity, individual structures and conformational control.

Previous low resolution electron microscopy (EM) studies of ClpXP and ClpAP from *E. coli* revealed that up to two hexameric ClpX chaperones bind to a ClpP tetradecameric barrel.[96,97] The barrel consists of two stacked heptameric rings, forming a degradation chamber with 14 proteolytic sites.[75]

Each ClpX subunit consists of an N-terminal zinc binding domain (ZBD) and a C-terminal AAA+ domain. The ZBDs at the periphery of ClpX are responsible for recognition and engagement of several substrates.[98] ClpX hydrolyzes ATP to unfold the target substrates and translocate the

unfolded polypeptides through a central pore into the proteolytic chamber of the ClpP barrel (for review see Baker et al.[23]).

Early on, the hexamer-heptamer ClpX-ClpP interface fascinated researchers and several studies characterizing the role of putative interaction motifs have led to the proposition of models explaining the symmetry mismatch and functional interaction between the two proteins.[22,88,97,99] Sequence alignments and mutational studies of AAA+ chaperones identified loops in ClpX, that interact with the hydrophobic clefts on the periphery of ClpP. They contain the highly conserved (I/L/V)-G-(F/L) motif and are essential for complex formation.[17]

More recently, cyclic acyldespipeptides (ADEPs), a novel class of anti-bacterial compounds, have been identified to bind to the same peripheral hydrophobic clefts on ClpP and to induce the opening of the axial pores of ClpP.[32,81,91,100] They stabilize ClpP in an "open" activated state in the absence of the chaperone, leading to unregulated proteolysis of substrates and finally to cell death.[101] This suggests that the protruding loops in ClpX that contain the (I/L/V)-G-(F/L) motif, also called IGF loops, are sufficient to activate ClpP. It has also been speculated that this activation involves the opening of the axial pore to allow translocation of the substrate into the proteolytic chamber of ClpP. However, due to the lack of high-resolution structures, a detailed understanding of the interaction between ClpX and ClpP is missing.

Contacts between the pore-2 loops of ClpX and the N-termini of ClpP represent a second set of well-characterized interactions between ClpX and ClpP, which are, however, more dynamic and dependent on the nucleotide state of ClpX.[22] A crucial function of the ClpP N-termini is to gate the entrance of the proteolytic chamber.[99] Despite these detailed biochemical insights, a high-resolution structure of the whole proteolytic complex is lacking, thereby limiting our understanding of this important protein degradation machinery. Here we present the first high-resolution cryo-EM structure of ClpXP from *L. monocytogenes*.

4.2. Results

4.2.1. Cryo-EM structure of ClpXP1/2

In order to obtain a ClpXP complex that is suitable for structural studies, we used the heterotetradecameric ClpP1/2 complex from *L. monocytogenes*. Recent studies have revealed that this complex has a higher affinity to ClpX in comparison to the more conserved ClpP2 homocomplex,[9,95] suggesting a superior stability of the heterooligomer. As ClpP1/2 might cleave ClpX to a small extent during sample preparation, we mutated one residue of the catalytic triad (S98A) in both ClpP isoforms. Furthermore, we mutated the nucleotide binding site of ClpX (E183Q) to allow ATP binding, but to prevent hydrolysis, which results in a tighter binding to ClpP.[102,103]

We formed a complex of ClpX and ClpP1/2 and obtained a large fraction of ClpXP1/2 dimers (ClpP1/2–ClpX–ClpX–ClpP1/2) that were in equilibrium with ClpXP1/2 monomers (fig. 11a–c). It has been demonstrated before that two ClpX or ClpA hexamers can bind to one ClpP barrel

from both sites, resulting in a ClpX–ClpP–ClpX or ClpA–ClpP–ClpA complex.[20,96,97] However, ClpXP1/2 dimers (fig. 11a–d) have, to our knowledge, not been described so far. We therefore concentrated our structural analysis first on these intriguing dimers and determined their structure by cryo-EM and single particle analysis using crYOLO[104] and SPHIRE[105] (fig. 11e–g, fig. 12a–b,). Although the intrinsic flexibility of the complexes did not allow the determination of a high-resolution structure (fig. 11e–g), the fitting of the crystal structure of ClpX into the cryo-EM density suggests that the flexible N-terminal zinc binding domains (ZBDs) of ClpX mediate the interaction between two ClpX hexamers (fig. 12c). While ZBD-deleted ClpX still associated with ClpP to a small extent, ClpX dimerization was completely abolished supporting our structural data (fig. 11a).

The ZBDs are involved in substrate binding and cofactor recognition and were shown to dimerize when expressed as single domain.[24,106] Based on these results it has been previously proposed that the ZBDs of neighboring subunits within a single ClpX hexamer dimerize resulting in a trimer-of-dimer model.[106] In this model the ZBD dimers interact with the adjacent dimers, creating a ring structure that is aligned with the central channel of ClpX. The structure of the ClpXP1/2 dimer, however, reveals that the ZBDs do not form rings, but arrange in a flexible half-cone spiral with the first and last ZBD dimer positioned directly above or at the rim of the axial pore entry of the upper and lower ClpX hexamer, respectively (fig. 11e, fig. 12c). The ZBDs are apparently interacting with the ZBDs from oppositely positioned subunits leading to the cross-linking of the two opposing ClpX hexamers (fig. 12c–d). In total, four ZBD dimers fit into the cryo-EM density (fig. 12c). Because of the limited resolution in this region, however, we cannot determine if the cross-bridges are mediated by single ZBDs that dimerize with ZBDs of the other ClpX or by ZBD dimers that interact with dimers of the other ClpX. Based on these results, we propose that ZBD dimers form stable structures only at the interface between two oppositely positioned ClpX hexamers (fig. 12d).

To obtain a cryo-EM structure at higher resolution, we focused the structural analysis on one ClpXP1/2 subunit in the dimer and solved its structure using the same dataset (fig. 12e-l, fig. 13). The final cryo-EM reconstruction has an average resolution of 3.6–4 Å for ClpP1/2 and 6–7 Å for ClpX (fig. 13e–g). The overall lower resolution of ClpX indicates that the chaperone is intrinsically more flexible and heterogeneous than the ClpP barrel in the ClpXP1/2 complex. To build a complete atomic model of ClpXP1/2, we fitted a homology model of ClpX and the available crystal structure of ClpP1/2 (PDB-ID 4RYF) into the cryo-EM density and refined the model using Molecular Dynamics Flexible Fitting (MDFF).[107]

The structure of ClpXP1/2 reveals that ClpP1 forms the upper homoheptamer of the ClpP barrel, whereas ClpP2 sits below and interacts with ClpX (fig. 12g–l). Our cryo-EM structure is consistent with previous binding studies on *L. monocytogenes* and *M. tuberculosis* ClpP proteases, showing ClpX-ClpP1/2 interactions exclusively via the ClpP2 ring surface.[14,83,108]

Interestingly, the ClpX hexamer is not centrally aligned, but slightly tilted by ~11°towards ClpP2. The structure of ClpP1/2 is almost identical to the available crystal structure of apo-ClpP1/2 (PDB-ID 4RYF), indicating that the binding of ClpX does not induce large conformational changes in ClpP1/2. In contrast, interaction with ClpP1/2 has an effect on the overall

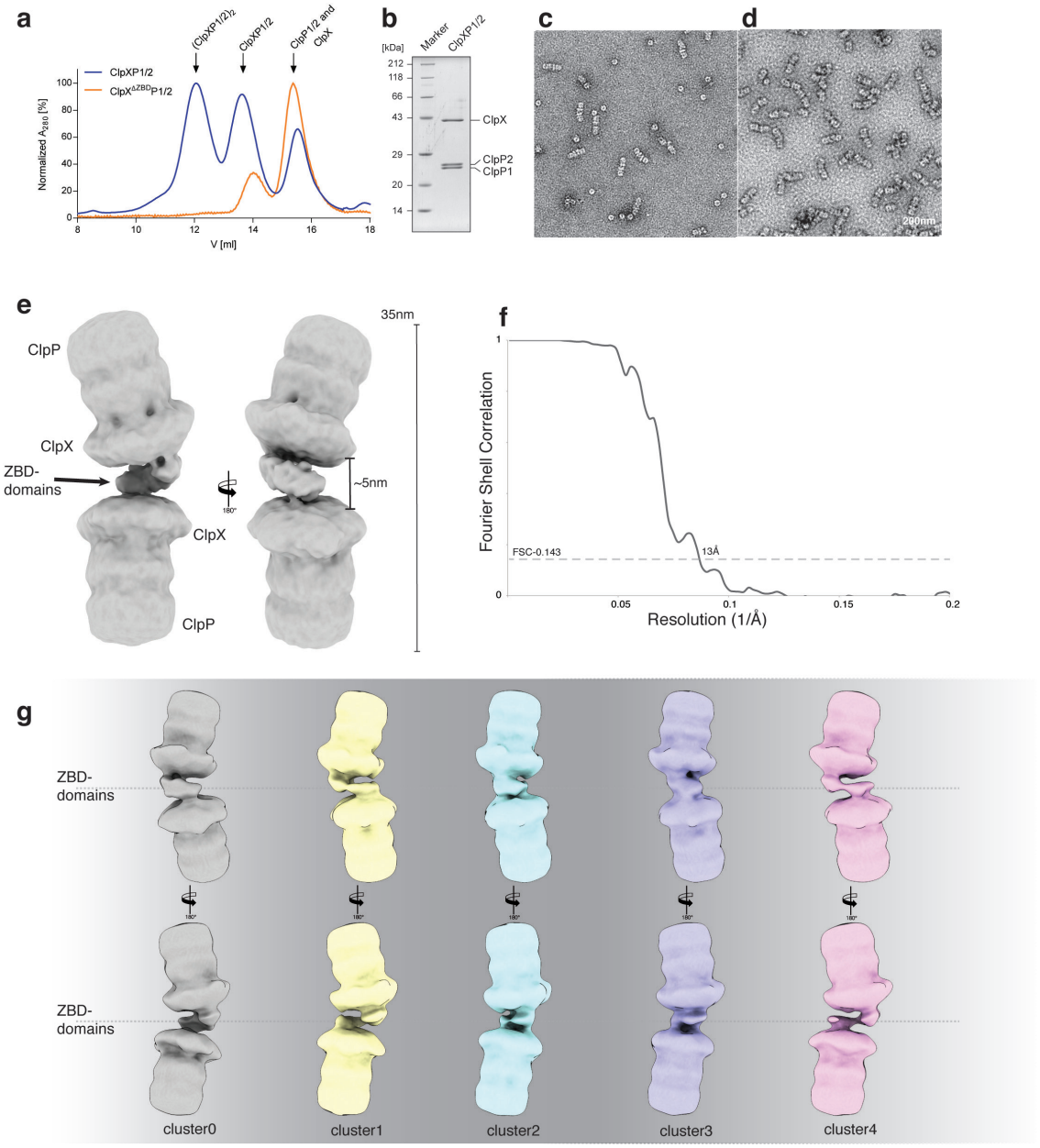

Figure 11 EM analysis of the ClpXP1/2 dimer. a Size exclusion chromatography of ClpX and ClpP1/2 mixtures on a Superose 6 increase 10/300 column. For the EM studies, a sample at 12 mL was taken. Note that the $(ClpXP1/2)_2$ peak is absent with $ClpX^{\Delta ZBD}$. **b** SDS-PAGE of the isolated $(ClpXP1/2)_2$ complex. **c–d** Subarea of a negative stain EM micrograph of the isolated $(ClpXP1/2)_2$ prior (**c**) and after (**d**) crosslinking. Scale bar: 200 nm. **e** Low resolution cryo-EM density of the ClpXP1/2-dimer. **f** Fourier Shell Correlation (FSC) between two independently refined half maps. **g** 3D clustering of the ClpXP1/2-dimer dataset.

conformation of ClpX. Whereas the crystal structure of *E. coli* ClpX shows the ATPase domains in a "dimer-of-trimers" arrangement,[109] our structure shows that upon ClpP1/2 binding, these domains become more regularly arranged and are related by pseudo-six-fold symmetry. Unlike recent substrate bound AAA+ structures that show a "spiral-staircase" arrangement with one "seam" subunit moderately displaced from the pore,[110–112] all neighboring AAA+ domains of ClpX pack closely with each other. The resolution at the nucleotide pocket is not high enough to visualize nucleotides, but the structure reveals that all six ClpX protomers are in the "loadable" conformation (fig. 14). This is in contrast to ClpX with the E183Q mutation in its apo-state.[109,113] There, two subunits are in the "loadable" (L) and four are in the "unloadable"

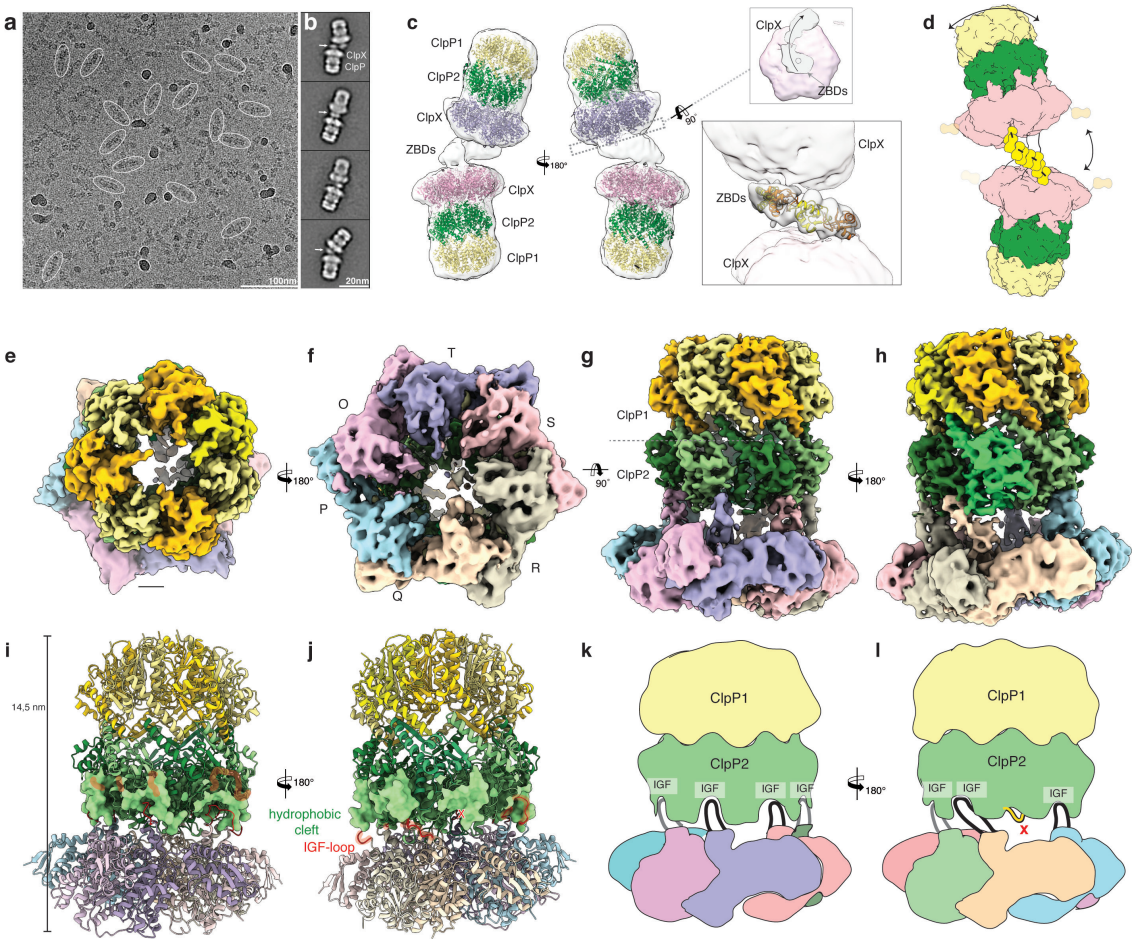

Figure 12 Cryo-EM structure of the ClpXP1/2 protein degradation machinery. a Typical low-dose cryo-EM micrograph of the ClpXP1/2 dimer from *L. monocytogenes*. Some particles are highlighted with ovals. Scale bar: 100 nm. **b** Typical reference-free 2D class averages. Arrows indicate additional densities corresponding to ZBDs at the interface between two ClpX hexamers. Scale bar: 20 nm. **c** Ribbon Model of ClpP1 (yellow), ClpP2 (green) and ClpX (orange) superimposed with the cryo-EM density map of the ClpXP1/2 dimer (white and transparent). The upper inset shows the complex shown as slice at the position of the axial pore entry of the upper ClpXP1/2 complex. ClpX and ClpX-ZBD densities are colored magenta and gray transparent, respectively. The arrow indicates the spiral arrangement of the ZBD domains. The lower inset shows four copies of ZBD-dimers (PDB: 1OVX) placed into the cryo-EM density at the interface between the ClpX hexamers. The low resolution density did not allow automated rigid-body fitting, therefore the dimers were placed manually and interconnected as proposed in Donaldson et al.[106] **d** Cartoon depicting ClpXP1/2 dimerization via the ZBD domains of two opposing ClpX hexamers. Arrows indicate the flexibility of the complex. **e–h** Cryo-EM density of ClpXP1/2 shown from the top (**e**), bottom (**f**) and side (**g**, **h**). ClpP1 and ClpP2 subunits are colored in khaki, orange and dark, light green, respectively. ClpP2 subunit J is highlighted in mint green. Note that this is the only ClpP2 subunit not interacting with ClpX via an IGF loop. Each subunit of ClpX is assigned a different color. This color code is maintained throughout this chapter. **i–j** Molecular model of ClpXP. The hydrophobic pockets of ClpP2, each spanning two ClpP2 subunits, are shown as surface. The IGF interaction loops are highlighted in red. **k–l** Cartoon depicting how the ClpX hexamer interacts with the ClpP2 heptamer via the six IGF loops. Note the extended conformation of IGF loop of ClpX subunit Q.

(U) conformation (fig. 14). In the L state, the arrangement of the small and large AAA+ domains results in an open binding cleft, to which the nucleotide can bind. In the U state, this site is blocked. A dynamic interconversion between L and U conformations is required to couple ATP hydrolysis by ClpX to mechanical work.

However, the arrangement is not a direct consequence of the bound nucleotide or the presence of specific mutation.[113] To further examine the interaction between ClpP1/2 and ClpX we used hydrogen-deuterium exchange mass spectrometry (HDX-MS) to monitor the accessibility of residues at the interface. In line with our structural observations, complex formation between

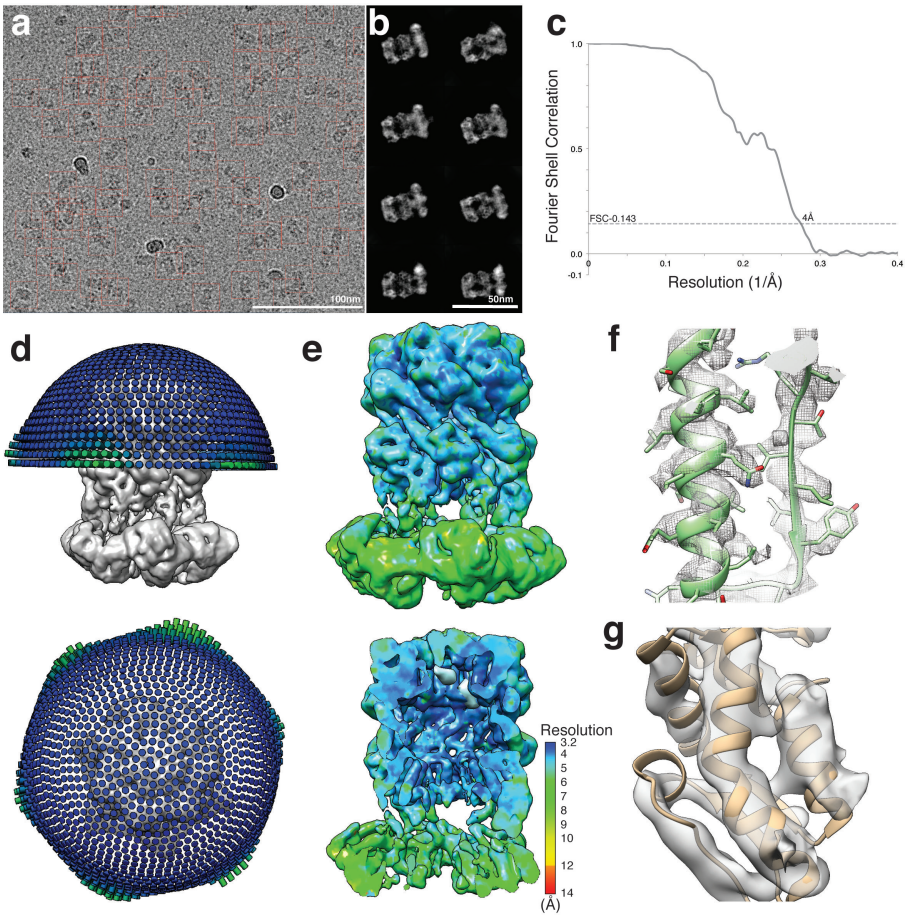

Figure 13 Cryo-EM analysis of ClpXP1/2. **a, b** Subarea of a typical low-dose cryo-EM micrograph of ClpXP1/2. ClpXP1/2 particles were selected and extracted from ClpXP1/2-ClpXP1/2 dimers using crYOLO and highlighted in red boxes. Scale bar, 100 nm. **c** Fourier Shell Correlation (FSC) between two independently refined half maps. **d** Orientation distribution of the particles used in the final refinement round. **e** Side and cut-off view of the density map colored according to the local resolution. **f–g** Superposition of segments of the molecular model of ClpP (**f**) and ClpX (**g**) with the cryo-EM density (transparent surface).

ClpP1/2 and ClpX only changes the accessibility of residues of ClpX and ClpP2, but not of ClpP1 (fig. 15). This not only corroborates that ClpX solely interacts with the ClpP2 isoform, but also indicates that ClpX binding does not induce major allosteric conformational changes in the ClpP1 heptamer.

4.2.2. Symmetry mismatch of the IGF loop interaction

The most interesting part of the structure is the interface between ClpP2 and ClpX, which involves a C6/C7 symmetry mismatch. As predicted by biochemical studies,[17,75,88] it is mediated mainly by the flexible IGF loops of ClpX interacting with hydrophobic grooves in ClpP2 (fig. 12g–h, fig. 16). The tilted arrangement of ClpX results in part of the loops interacting stronger with ClpP2 than others (fig. 17a).

The large domains of the respective ClpX subunit from which the loops protrude are positioned directly below the deep hydrophobic grooves of ClpP2 which are formed at the interface of two subunits. This arrangement allows a direct interaction of the IGF loops with the opposing grooves. The hydrophobic grooves of ClpP are arranged in a circular manner with seven-

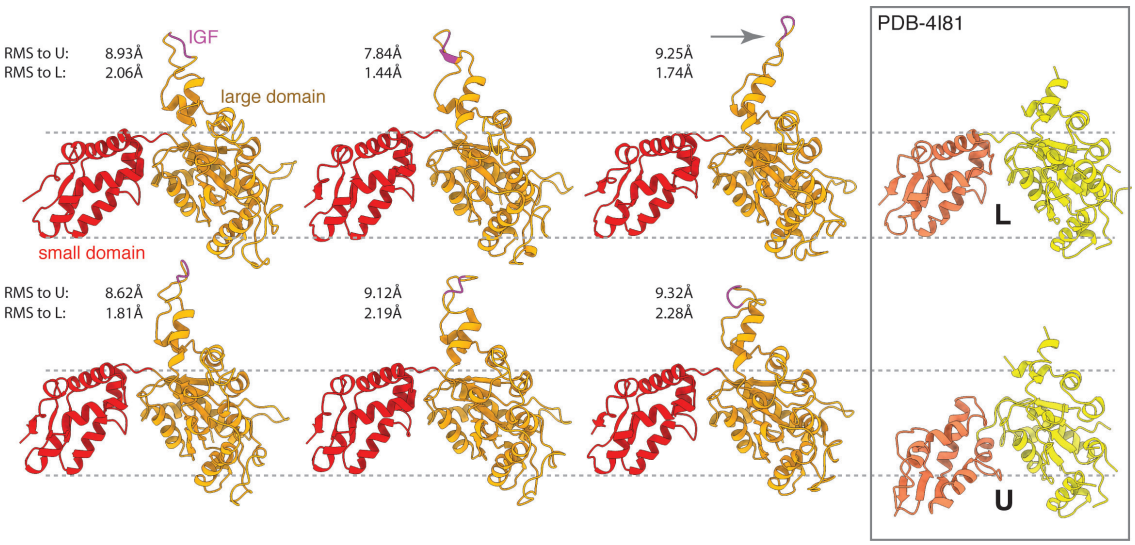

Figure 14 ClpP-bound ClpX subunits adopt a nucleotide-loadable conformation. Molecular models of the six ClpX subunits are shown as ribbon diagrams, with the large domain highlighted in orange and the small domain in red. Note the high similarity between the ClpX subunits, except the arrangement of their IGF loops. The gray arrow indicates the IGF loop of subunit Q that adopts an "extended" conformation. The inset shows nucleotide-loadable (L, upper image) and unloadable (U, lower image) subunits of ATPγS-bound *E. coli* ClpX (EcClpX, PDB-ID 4I81). Structural comparison of the six ClpX subunits with the L and U subunit of EcClpX (note the respective RMSD values of the Cα atoms) indicate that all subunits of ClpP-bound ClpX adopt a loadable conformation.

fold symmetry and the positions of the ClpX IGF loops in the complex, perfectly match this arrangement. Interestingly, both rings display similar diameters (fig. 17b–c), except that the IGF-ring remains open at the position of the seventh, free hydrophobic cleft.

Five of the six IGF loops (subunits O, P, R, S, T) display an overall similar arrangement. Due to the symmetry mismatch the large domain of the sixth subunit (subunit Q), is positioned in-between two hydrophobic grooves. The respective IGF loop, however, still interacts with one of the opposing grooves by adopting an "extended" conformation (fig. 12g–i). The other groove stays empty. Although the distance between the IGF loop and the "left" or "right" ClpP hydrophobic groove are similar, we only obtained a high-resolution structure with the IGF loop binding exclusively to the left binding pocket.

To support our structural findings, we performed HDX-MS measurements and mutational studies. Upon complex formation deuterium uptake of the IGF loop is strongly reduced (fig. 15) and mutations in the IGF loops of ClpX and the hydrophobic grooves of ClpP2 result in impaired complex formation (fig. 18). This is in line with our ClpXP1/2 structure that demonstrates that the interaction between the IGF loops with the hydrophobic grooves is crucial for complex formation and function.

Taken together, tilting of the ClpX ring and stretching of one of the IGF loops is sufficient for the hexameric ClpX to adapt to the seven-fold symmetry of the heptameric ClpP, leaving out one of the binding pockets (fig. 12k–l). Due to multivalence, this results in strong, but at the same time flexible binding, which is likely necessary to accommodate the different conformations of ClpX protomers during ATP hydrolysis and substrate processing.[88,102,109]

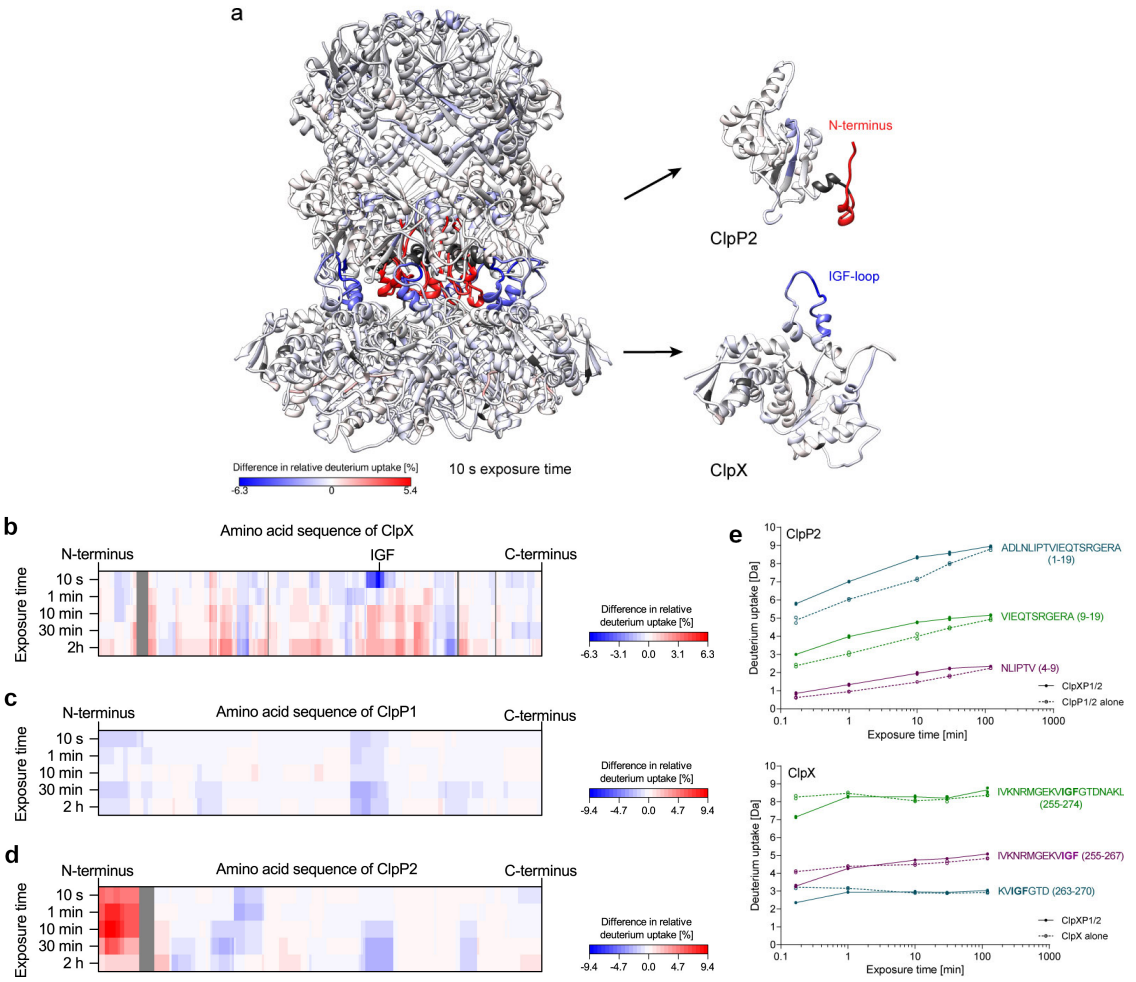

Figure 15 HDX-MS analysis of ClpXP1/2 complex formation. a Difference in relative deuterium uptake after 10 s exposure is mapped on the structure of ClpXP1/2 (left), ClpP2 monomer (right top) and ClpX monomer (right bottom). Increased deuterium uptake upon complex formation is shown in red, decreased deuterium uptake is depicted in blue. Dark gray represents no coverage. **b–d** Changes in deuterium uptake after complex formation are mapped on the amino acid sequence of ClpX (**c**), ClpP1(**d**) and ClpP2 (**e**) for the respective exposure times. Increased deuterium uptake upon complex formation is shown in red, decreased deuterium uptake is depicted in blue. Dark gray represents no coverage. Averages of two independent measurements are shown. **e** HDX kinetics of exemplary peptides in the N-terminus of ClpP2 (top) and in the IGF loop of ClpX (bottom). Solid lines and filled circles represent the ClpXP1/2 complex, dashed lines and empty circles represent ClpP1/2 or ClpX. Two independent replicates are shown, lines denote the mean.

4.2.3. N-termini of ClpP2 and pore-2 loops of ClpX regulate the entry portal

ClpX is not only tilted, but also laterally shifted respective to ClpP2 (fig. 17a, d, e). Such an arrangement has also been described for other complexes that display a symmetry mismatch.[114–116] In the case of ClpXP1/2, this results in a misalignment of the central channels of ClpP and ClpX, creating in a twisted translocation channel with a constriction site at the interface between ClpP2 and ClpX (fig. 17d). At this position, the N-terminal loops of ClpP2 and pore-2 loops of ClpX interact with each other. These interactions are expected to be even more dynamic than the flexible contacts mediated by the IGF loops, and coupled to ATP-hydrolysis.[17,25,88] Indeed, the densities corresponding to the N-terminal loops of ClpP2 and pore-2 loops of ClpX are very weak indicating a higher degree of flexibility in this region of the complex (fig. 19, fig. 20).

Different conformations of the ClpP N-terminal loops have been previously identified in crystal

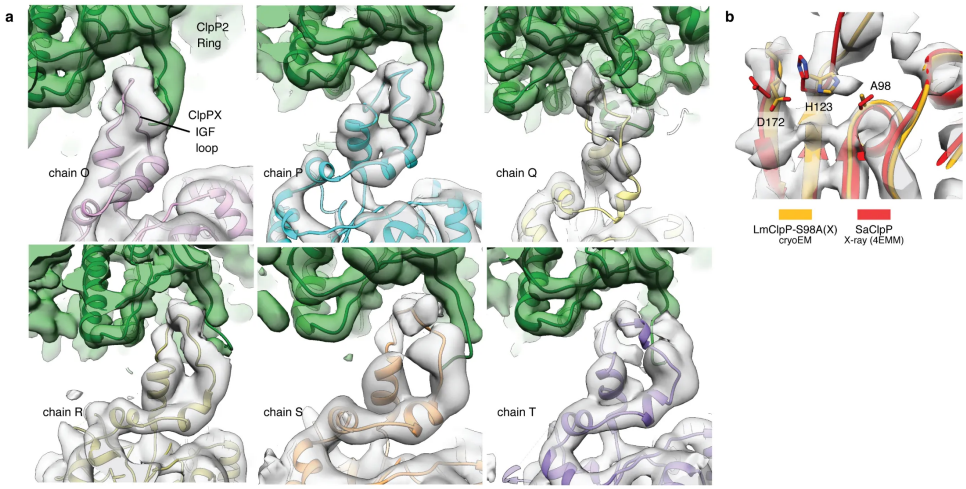

Figure 16 Cryo-EM density of the IGF loops interfaces and the ClpP2 catalytic active site. **a** Densities for the six IGF loops interactions are shown with the corresponding atomic models. ClpX and ClpP2 densities are shown as gray and green transparent isosurface, respectively. **b** Superposition of the catalytic residues S98 (S98A), H123 and D172 in ClpX-bound ClpP1(S98A)/2(S98A) (cryo-EM) (extended active state) and *S. aureus* ClpP (inactive compact state) (PDB-ID 4EMM), shown with the cryo-EM density. The catalytic residues of ClpX-bound ClpP1/2 adopt the active conformation.

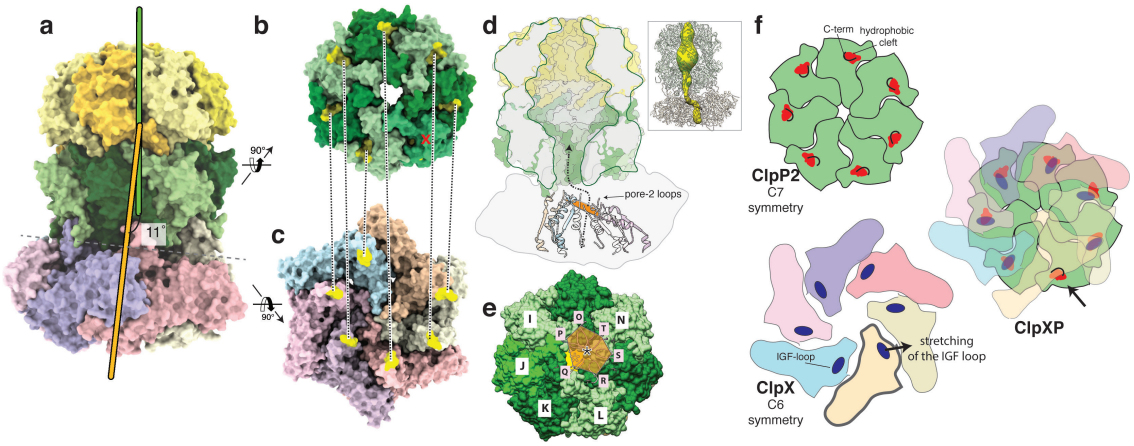

Figure 17 Symmetry mismatch between ClpP1/2 and ClpX. **a** Molecular model of ClpXP1/2 shown as surface. The symmetry axes of the ClpP tetradecamer and the ClpX hexamer are shown in green and orange, respectively. **b–c** The ClpP2 heptamer (**b**) and the ClpX hexamer (**c**) are shown from the bottom and the top, respectively, perpendicular to the plane of the ClpP2-ClpX interface. The positions of the IGF loops and the hydrophobic grooves are highlighted in yellow and connected by dashed lines. **d** Cut-away view of the ClpP density to visualize its axial pores and central lumen. Secondary structure elements directly prior (residues 170–189) and after the pore-2 loops (residues 202–220) of ClpX are shown in ribbon representation. The pore-2 loops are not resolved in the cryo-EM density and not shown here. In order to indicate the arrangement and positioning of the pore-2 loops, as well as the position of the upper opening of the ClpX channel relative to the ClpP2 pore, a plane was calculated using the Cαatoms of Gly202 as anchor points and depicted here in orange. Note that the plane is tilted and shifted relative to the ClpP channel axis, suggesting a spiral staircase-like arrangement of the pore-2 loops. The dashed line with the arrowhead indicates the pathway of substrate translocation from ClpX towards the ClpP proteolytic chamber. The inset shows the skin surface of the ClpXP pore. For calculation and visualization of the pore, the pore-2- and RKH-loops were modeled using Rosetta. **e** Molecular surface of ClpP2 shown from the bottom. Rosetta models of the pore-2 loops of ClpX are shown as ribbons. The black star at the center of the pore-2 plane indicates the positioning of the ClpX channel opening relative to the ClpP channel opening (yellow star). **f** Schematic model of the ClpX-ClpP2 binding mechanism. Left images depict axial views of the ClpP2 heptamer (green) and the ClpX hexamer (colouring similar to fig. 12) prior assembly of the ClpXP protease. The main interaction elements, the ClpX IGF loops and ClpP2 hydrophobic grooves are highlighted. The C-terminus of each ClpP2 subunit (black) blocks the respective ClpP2 hydrophobic groove. During binding (right image), ClpX is tilted so that five IGF loops come in close proximity to five hydrophobic grooves without major conformational changes. The sixth IGF loop stretches anti-clockwise to reach the next "free" hydrophobic groove, enabling the symmetry mismatch. Thereby, the six IGF loops push the C-termini of ClpP2 away and bind tightly to the hydrophobic groove. The remaining "free" ClpP2 hydrophobic groove stays shielded by the respective C-terminus (arrow).

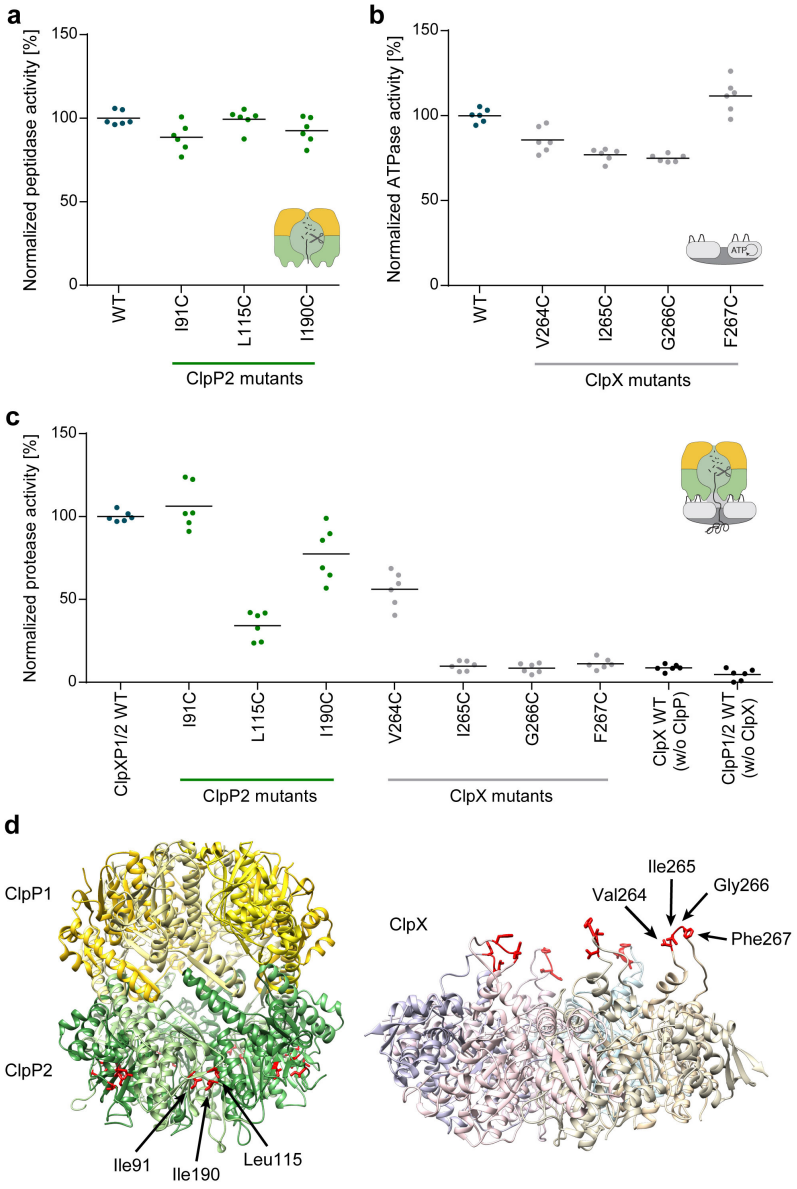

Figure 18 Activity assays of ClpX and ClpP2 mutants of the IGF loop/hydrophobic groove interface. a Peptidase activity of ClpP1/2 with respective ClpP2 mutants (0.71 μM $(ClpP1/2)_{14}$, 100 μAc-Ala-hArg-2-Aoc-ACC). **b** ATPase activity of ClpX mutants (0.33 μM ClpX6, 20 mM ATP). **c** Protease activity of ClpXP1/2 with ClpP2 and ClpX mutants (0.2 μM $(ClpP1/2)_{14}$, 0.4 μM $ClpX_6$, 0.8 μM GFP-SsrA). Data are normalized to the wild type as 100% (n = 6, black lines denote means). **d** Mapping of the ClpP2 and ClpX mutations on the protein structure. Mutation sites are shown with red sticks.

structures of apo and ADEP-bound ClpPs.[77,90,99] In the *E. coli* apo ClpP structure, the N-termini on the apical side of the ClpP barrel are in the "down" conformation, opening one axial pore of the barrel. On the basal side six of the N-termini are in the "up" conformation, with the loops moving out of the axial pore, thereby covering and closing it. It was speculated that the six ClpP N-termini in the "down" conformation would open to match the six-fold symmetry of ClpX and the seventh non-interacting N-terminus would stay in the "down" conformation upon binding to the chaperone. However, in the ADEP-bound structure of *E. coli* ClpP all loops point upwards while they are not resolved in a *Bacillus subtilis* ADEP-bound ClpP structure having made general conclusions difficult so far.[77,90]

In our cryo-EM structure, residues 6 to 17 are not resolved, but the rest of the density reveals

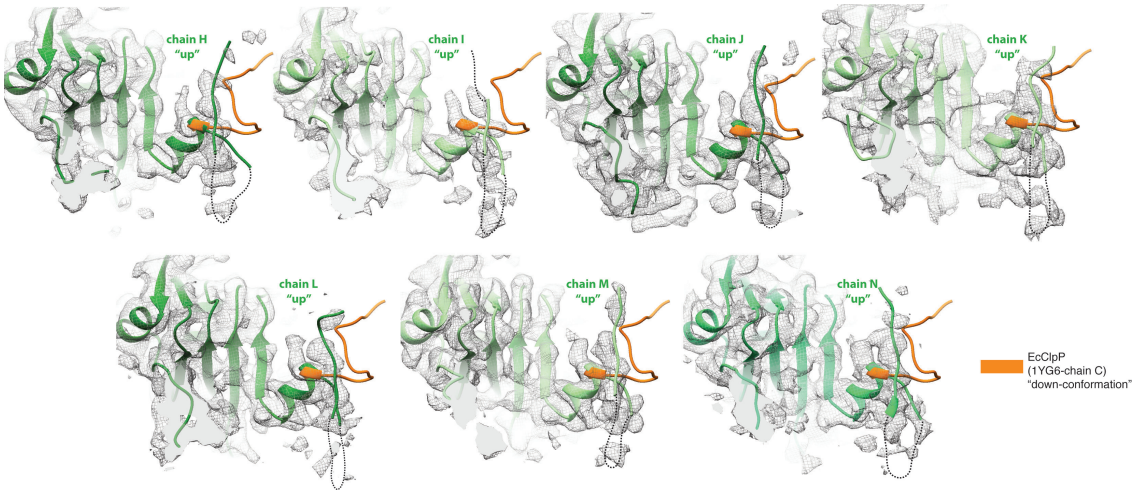

Figure 19 The N-terminal loops of ClpX-bound ClpP2 subunits adopt the "up" conformation. Cryo-EM density map (mesh) with the molecular model highlighting the N-terminal domain of the seven ClpP subunits. Residues 8–17 are not resolved, but the fragmented cryo-EM density indicates that all flexible N-terminal loops adopt the "up" conformation (indicated by dashed lines). For better comparison, the molecular model of a subunit of *E. coli* ClpP (PDB-ID 1YG6) with the N-terminus in the "down" conformation (orange) is also shown.

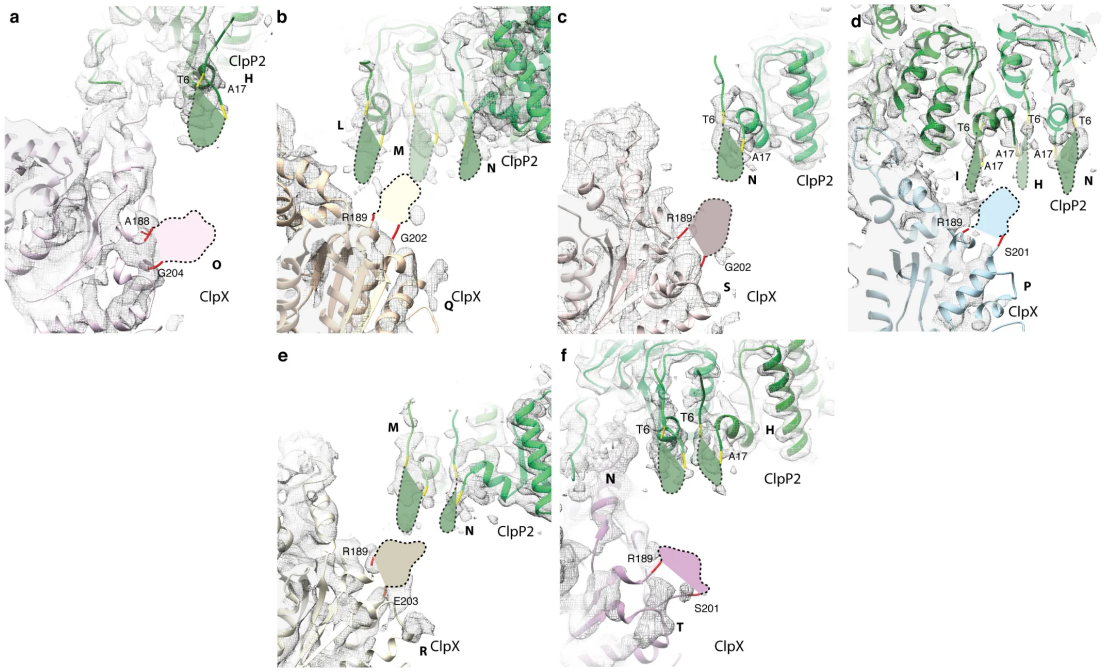

Figure 20 Possible interactions between pore-2 loops of ClpX with the N-termini of ClpP. Cryo-EM density map with the molecular model, highlighting the interaction area between the pore-2 loops of ClpX and the N-termini of ClpP. The six pore-2 loops of ClpX and residues 7–16 of the N-termini of seven subunits of ClpP2 are not resolved. Possible arrangements of these regions are indicated by dashed lines, based on their anchor points and number of residues. Note that the pore-2 loops of chains Q and P point into a cleft formed by three ClpP N-termini (**b, c**). This topological analysis also suggests that the pore-2 loops of chains O and T (**a, f**) do not show any interactions with the N-termini of ClpP. However, an unusual stretched conformation of these pore-2 loops towards ClpP cannot be excluded. Pore-2 loop of chain S is positioned in direct proximity to the N-terminus of chain N (**c**) whereas the pore-2 loop of chain R is positioned between two ClpP N-termini (M and N) (**e**).

that all seven N-termini of ClpP2 (the apical side of the barrel facing the chaperone) adopt the "up" conformation resolving the controversy about their positioning and the accessibility of the pore (fig. 20). The cryo-EM structure demonstrates that the interaction site between the ClpP2 N-termini and the ClpX pore-2 loops is not shielded and freely solvent accessible.

In addition, the N-termini undergo a conformational change upon complex formation and adopt the “up” conformation, by which the protein backbone likely gets more solvent exposed and/or flexible. In line with this, deuteration of the ClpP2 N-terminus increased after complex formation (fig. 15). This observation is also supported by reported synchrotron hydroxyl radical footprinting data showing that ClpA binding enhanced the modification rate of an N-terminal peptide of ClpP, pointing towards a higher solvent accessibility.[117]

4.2.4. The C-terminus of ClpP2 shields the hydrophobic groove prior to ClpX binding

The C-termini of the ClpP2 show two conformations in our structure: a compact conformation that blocks the hydrophobic groove when it does not accommodate an IGF loop, and an extended conformation enlarging the groove when occupied by an IGF loop (fig. 21a). Since the residues of the C-terminus are not conserved (fig. 22) and the conformational change is not transmitted to the rest of the protein, an allosteric regulation is rather unlikely. The C-termini probably shield the hydrophobic grooves, when ClpX is not bound and thereby prevent the interaction with other hydrophobic molecules and increase the stability of the protein in a hydrophilic environment.

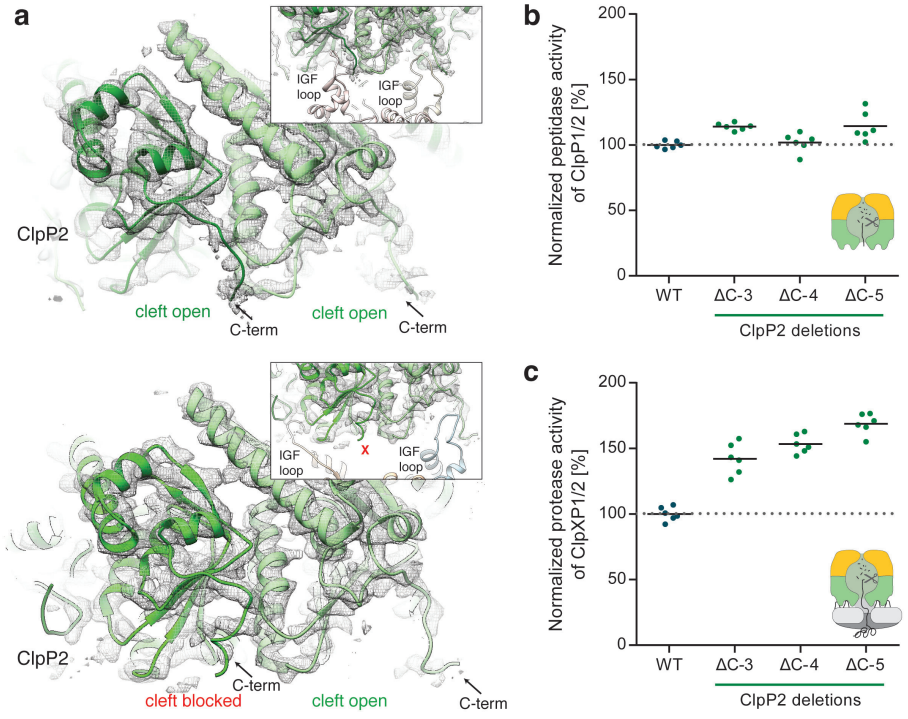

Figure 21 Role of the ClpP2 C-terminus in ClpXP1/2 binding. **a** Molecular model and cryo-EM density of IGF loop bound (upper image) and not bound to hydrophobic pockets of ClpP2 (lower image). The insets show the respective IGF loops in ribbon representation. Arrows indicate the C-terminus of ClpP2. **b** Peptidase activity of ClpP1/2 with C-terminally truncated ClpP2 (0.71 µM $(ClpP1/2)_{14}$, 100 µM Ac-Ala-hArg-2-Aoc-ACC). **c** Protease activity of ClpXP1/2 with C-terminally truncated ClpP2 (0.2 µM $(ClpP1/2)_{14}$, 0.4 µM $ClpX_6$, 0.8 µM GFP-SsrA). Data are normalized to the wild type as 100% (n = 6, black lines denote means).

To probe this, we deleted the last three to six amino acids of ClpP2. $ClpP1/2^{\Delta C\text{-}6}$ precipitated during purification, suggesting that a certain length of the C-terminus is important to protect the hydrophobic groove and facilitate protein stability. ClpP2 mutants bearing three to five

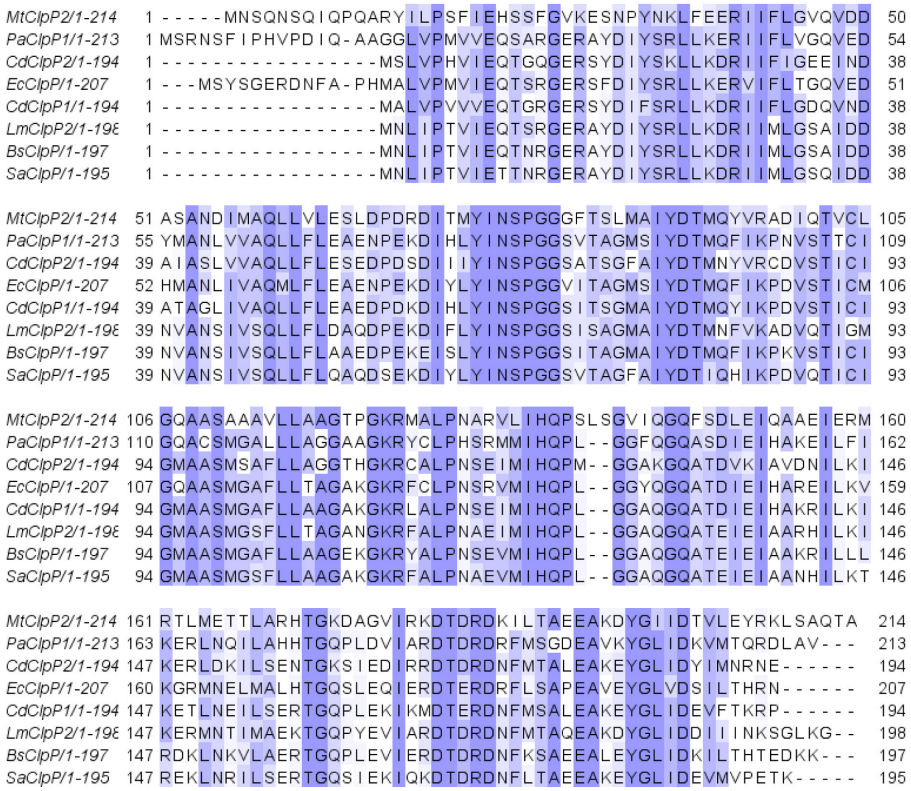

Figure 22 Alignment of ClpP sequences. Mt: *Mycobacterium tuberculosis* (ClpP2), Pa: *Pseudomonas aeruginosa* (ClpP1), Cd: *Clostridium difficile* (ClpP1 and ClpP2), Ec: *Escherichia coli*, Lm: *Listeria monocytogenes* (ClpP2), Bs: *Bacillus subtilis*, Sa: *Staphylococcus aureus*.

amino acid deletions were however soluble and exhibited a similar peptidolytic activity as the wild type complex (fig. 21b). Interestingly, in protease assays requiring the binding of ClpX, the activity increased with a growing number of amino acid deletions in comparison to the wild type complex (fig. 21c). We interpret this result such that when the C-termini are shorter more complexes are formed because ClpX can easier access the hydrophobic grooves via the IGF loops. Indeed, in line with this finding the C-termini of most ClpPs which were shown to interact with ClpX are shorter in length (fig. 22).

4.2.5. ClpP activation mechanism by ClpX

Previous crystal structures of ClpP in its apo-form, i.e. without ClpX or compound bound, revealed three different conformational states of the protein: “compressed”, “compact” and “extended”[6,118–121] (fig. 23). The catalytic triad of the peptidase is only intact in the extended state, suggesting that this is the only active state. ADEPs, that bind to the same site on ClpP as the IGF loops, can induce the transition from the compressed to the extended conformation.[91] In addition, a ∼90°rotation of Tyr63 in the hydrophobic pocket results in the widening of the axial pore by 10–15 Å. A mutation of this residue to alanine has the same effect.[122] This “open” extended conformation of ClpP deregulates the protein. Instead of only processing short peptides of five to six residues, it is now capable to degrade large unfolded polypeptides that otherwise could not be processed in the absence of the chaperone (fig. 24d-e).[77,117,123] It has been speculated that the mechanism of ClpP activation by ClpX would imply similar

conformational changes.[101,122]

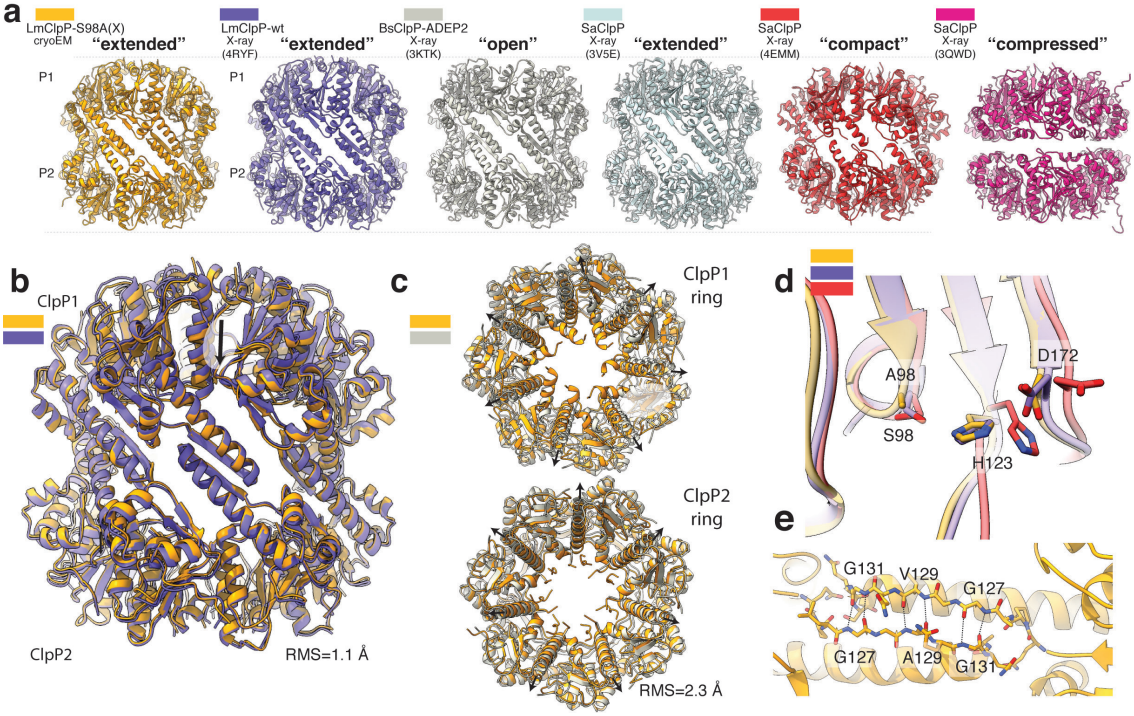

Figure 23 Comparison of ClpX-bound ClpP1/2 with available structures of active and inactive ClpP. a Side view of the structure of ClpX-bound LmClpP1/2 (gold) and the crystal structures of LmClpP1/2 in the extended active state (PDB-ID 4RYF) (purple), *B. subtilis* ClpP (BsClpP) in complex with ADEP2 in the extended open active state (PDB-ID 3KTK) (gray), *S. aureus* ClpP (SaClpP) in the extended active state (PDB-ID 3V5E) (cyan), SaClpP in the compact inactive state (PDB-ID 4EMM) (red) and SaClpP in the compressed inactive (PDB-ID 3QWD) (purple) conformation are shown in ribbon representation. **b** Structural superposition of ClpX-bound and unbound (PDB-ID 4RYF) LmClpP1/2. The low R.M.S.D. suggests that binding of ClpX to ClpP1/2 does not induce large conformational changes to ClpP1/2. **c** Structural superposition of ClpX bound ClpP1/2 heterocomplex and ADEP2-bound ClpP homocomplex (PDB-ID 3KTK) shown in top- and bottom view. Black arrows indicate the characteristic opening of the ClpP pore upon ADEP binding. **d** Superposition of the catalytic residues S98 (S98A), H123 and D172 (N172) in ClpX-bound LmClpP1(S98A)/2(S98A), LmClpP1/2 (extended active state) (PDB-ID 4RYF), SaClpP (compact inactive state) (PDB-ID 4EMM). Note that despite the S98A mutation, the catalytic residues of ClpX-bound LmClpP1/2 adopt the active conformation. **e** Opposing subunits of ClpX-bound ClpP1 and ClpP2 rings interact via an antiparallel β-sheet.

Our ClpXP1/2 structure demonstrates that this is not the case. ClpP is in the active extended conformation which is very similar to its conformation in the apo-state (fig. 23a, b). Despite the S98A mutation, the catalytic triad is aligned and in its active conformation (fig. 23d, fig. 16b). The ClpP1 and ClpP2 heptamers are interconnected via typical interactions of antiparallel β9 strands, characteristic for the "extended" active conformation (fig. 23e).[6] Importantly, the axial pore of ClpP is not widened, when compared to the crystal structure of *B. subtilis* ADEP-bound ClpP (fig. 23c). A comparison of the interface between the IGF loop and ADEP with the hydrophobic ClpP pocket reveals that both interact with the same non-polar residues including Ile28, Leu49, Tyr63, Phe83, Ile90, Leu115 (fig. 24a–c). However, binding of ClpX does not induce the rotation of Tyr63 (fig. 24c), which is key to opening the pore. Thus, despite the fact that ADEPs and ClpX share the same binding sites, ClpX does not induce the conformational changes resulting in the opening of ClpP. Instead, binding does not induce any major conformational changes and the diameter of the ClpP channel is sufficient to accommodate the unfolded peptides that are threaded into the ClpP pore by the chaperone to be processed sequentially within the chamber of the peptidase (fig. 24f).

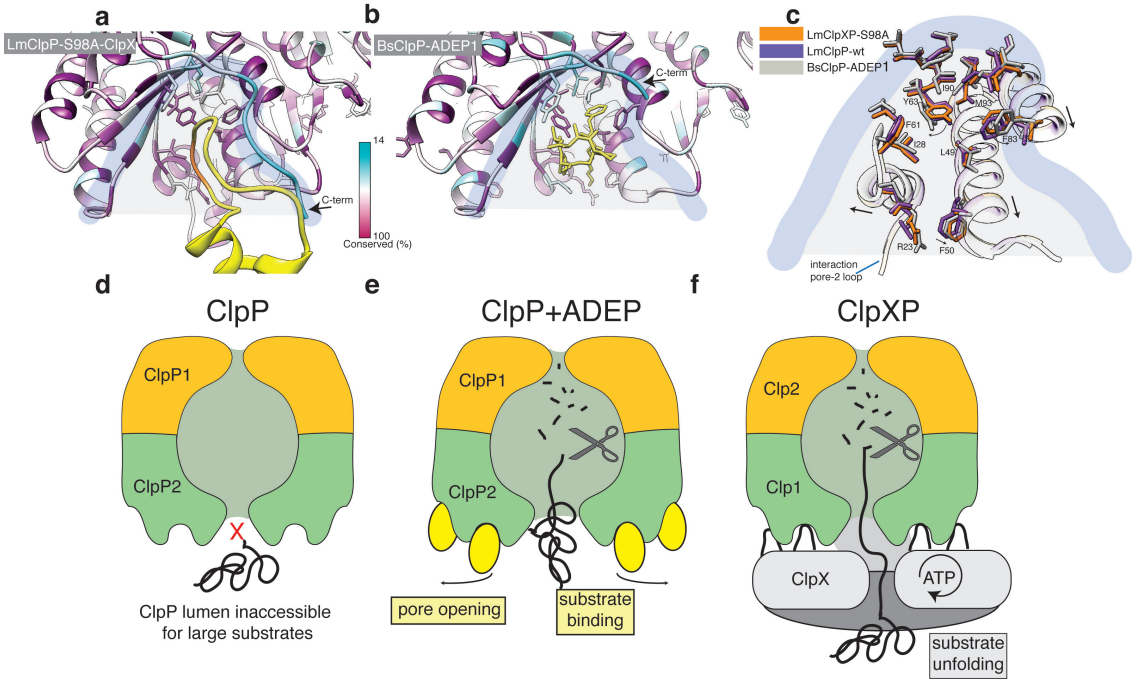

Figure 24 ClpX binds to ClpP in a similar manner like ADEP, but does not induce ClpP pore widening. **a** Local molecular interactions at one of the seven binding pockets between ClpP and the IGF loop of ClpX. Residues of ClpP are coloured by sequence conservation. The IGF loop is shown in yellow with the IGF residues highlighted in orange. **b** Interface of ADEP2 (yellow) with BsClpP (PDB-ID 3KTI) (coloured by conservation). **c** Structural superposition of the binding pockets of ClpX-bound LmClpP2(S98A), ADEP1-bound BsClpP (PDB-ID 3KTI) and "free" LmClpP2 (PDB-ID 4RYF). Arrows indicate changes upon ADEP binding. **d–f** Regulation of ClpP by ClpX and ADEP. The central pore of the ClpP protease is closed and entry of folded proteins into the proteolytic chamber is not allowed (**d**). ADEP binding to the binding pockets of ClpP induces pore opening. The proteolytic chamber is now accessible for unfolded proteins, leading to unregulated protein degradation and cell death (**e**). ClpX binds in the same hydrophobic pockets on ClpP but does not induce pore opening. ClpP and ClpX form a continuous pore instead, with ClpX unfolding target proteins and forwarding them to the proteolytic chamber of ClpP for degradation in a regulated manner (**f**).

4.3. Discussion

ClpXP plays a significant role in the production and regulation of bacterial virulence factors during host infection and is therefore considered as a promising target for antimicrobial therapy.[18,34] On the other hand, targeting of the mitochondrial homologues is considered as a novel approach to halt tumor cell proliferation and metastatic competence.[44] Despite the important role of ClpXP in protein degradation, biology and medicine in general, structural knowledge of the dynamic two-component proteolytic machinery has lagged behind. The flexible and dynamic interaction between ClpX and ClpP via long flexible IGF and pore-2 loops, involving a symmetry mismatch, together with the asymmetry of the ClpX ATPase make this complex a difficult specimen for structural analysis and probably explain why a high-resolution structure of the complex has been missing so far.

In contrast to previous works, here we utilized the ClpP1/2 heterocomplex from *L. monocytogenes*, showing a higher affinity to ClpX than the homocomplex. We mutated the proteolytic site and nucleotide binding site of ClpP1/2 and ClpX, respectively, and cross-linked the sample, in order to obtain a ClpXP1/2 complex with superior stability for cryo-EM studies. We believe that this was key to determine the ClpXP1/2 structure at an average resolution of 4 Å. The resolution for ClpX, however, is lower and therefore does not allow modeling of side chains.

The probably most interesting finding of the current study is the structural visualization of the interface between the hexameric ClpX ATPase and the heptameric ClpP protease, which involves a symmetry mismatch. The structural plasticity, which is necessary for the interaction of the symmetrically different proteins is provided by the flexibility of the IGF loops. The binding of ClpP to ClpX does not induce major conformational changes of ClpX and delocalization of distinct AAA+ subunits. The flexibility of ClpP-ClpX interface might be crucial to accommodate different conformations of the ATPase during hydrolysis and proteolysis, and might even allow rotational movement of the ATPase during the repeating cycles of substrate unfolding and translocation. However, further studies are necessary in order to support this scenario. ClpX is tilted and slightly shifted relative to ClpP2 and the symmetry axes of the protease and the ATPase are therefore not aligned. Thus, upon complex formation, the translocation pathway for unfolded peptides is not straight but twisted. A similar arrangement involving a symmetry mismatch and formation of a twisted peptide translocation channel has been recently described for the PAN-proteasome[116] and the bacterial ABC toxin comple[114]. The binding of proteasomal ATPases to the 20S core particle also involves a six-seven symmetry mismatch. However, in this case, the interface is more rigid, since the ATPases bind with their hydrophobic C-termini tightly into pockets at the surface of the 20S core particle ("key-in-lock" mechanism).[124,125] Noteworthily, whereas most ATPases induce pore opening to allow substrate entry into the proteasomal core, several eukaryotic ATPases (Rpt2, Rpt3 and Rpt5) stably bind to the same pockets of the core particle, but similar to ClpX, do not trigger gate-opening.[124,126]

Surprisingly, although ClpX interacts via the IGF loops with the same site on ClpP as the potential antibiotic ADEP,[81], it does not induce the opening of the ClpP1/2 pore, as previously suggested. Thus, the underlying mechanisms of ClpP activation by ClpX and ADEP are distinct.

Our structure further reveals, that the extended C-terminus of *L. monocytogenes* ClpP1/2 shields the IGF-binding sites prior to ClpX binding. The length of the C-terminus is apparently crucial to fine-tune the binding affinity to ClpX, among the different species, which might be important for the future design of ClpP-based antibiotics.

The pore-2 loops, that control the peptidase gate and thread the substrate into the ClpP1/2 chamber, are disordered in our structure, underlining the dynamic nature of these interactions. However, the overall arrangement of adjacent structural elements suggest that the pore-2 loops are arranged in a spiral-staircase-like manner, similarly to other AAA+ complexes.[115,127] The pore-2 loops interact in this case with the opposing N-termini of ClpP2. In contrast to an earlier crystal structure of ClpP2, all seven N-termini adopt the "up" conformation. Thus, the local symmetry match is not facilitated by the different conformations of the ClpP2 N-terminus, as previously suggested.[99]

Interestingly, the ClpXP1/2 complex from *L. monocytogenes* dimerizes. Only ClpP2 binds to ClpX and two opposing ClpX hexamers dimerize head-to-head through the ZBDs. In contrast, the *E. coli* ClpP homocomplex is doubly-capped by ClpX.[20] It is unclear whether the dimerization of the ClpXP1/2 complexes is biologically relevant. The termini of this arrangement of up to four ZBD dimers linking the ClpX hexamers, point directly to their distal pore entries. It is therefore tempting to speculate that this interaction might play a role in substrate binding

and even help guiding it into the ClpX pores. Another explanation might be that, at the high concentrations used for EM, two copies of ClpX might recognize each other as substrate. This scenario is however unlikely, because most of ClpX stays intact after incubation of wild-type ClpX with wild-type ClpP1/2.

In summary, the cryo-EM structure of ClpXP1/2 provides the necessary basic insights into ClpXP architecture, essential to understand the molecular mode of action of this dynamic and highly flexible protein degradation machinery. Our results set the stage for future investigations into conformational changes underlying ClpXP ATP hydrolysis and substrate translocation during protein degradation.

4.4. Materials and methods

4.4.1. Cloning

The cloning of pETDuet-1_ClpP1/2 and pET300_ClpX were described previously.[14] ClpX and ClpP1/2 point mutants, ClpP1/2$^{\Delta C\text{-}3}$, ClpP1/2$^{\Delta C\text{-}4}$ and ClpP1/2$^{\Delta C\text{-}5}$ were generated using the QuikChange™ technology. For ClpP1/2$^{\Delta C\text{-}4}$ and ClpP1/2$^{\Delta C\text{-}4}$, the pETDuet-1_ClpP1/2$^{\Delta C\text{-}3}$ plasmid was used as a template. ClpP1/2$^{\Delta C\text{-}6}$ and ClpX$^{\Delta ZBD}$(E183Q) were obtained with primers containing non-overlapping sequences.[128] All primers are listed in table 3.

4.4.2. Protein overexpression and purification

ClpP1/2 and its mutants were overexpressed and purified as follows. The proteins were overexpressed in *E. coli* BL21(DE3) bearing a pETDuet-1 vector with C-terminally Strep-II-tagged ClpP1 and C-terminally His_6-tagged ClpP2.[14] The bacteria were grown in LB medium until OD_{600} 0.6 at 37 °C. Following induction with 1 mM IPTG, the bacteria were incubated at 37 °C for 6 h. After harvest, the cells were sonicated on ice in lysis buffer (20 mM MOPS, 300 mM KCl, 1% CHAPS, 10% glycerol, pH 7.5) and then kept at room temperature during the rest of the purification. The proteins from the cleared cell lysate were captured in a HisTrap HP 5 ml column (GE Healthcare) in His buffers (20 mM MOPS, 300 mM KCl, 10% glycerol, pH 7.5; + 40 mM imidazole for washing) using an ÄKTA Purifier 10 system (GE Healthcare). The proteins were eluted by a 15 mL gradient from 40 mM to 300 mM imidazole, and the second elution peak was collected. A subsequent chromatography step was carried out on a StrepTrap HP 5 ml column (GE Healthcare) in Strep buffers (20 mM MOPS, 300 mM KCl, 10% glycerol, pH 7.5; + 2.5 mM desthiobiotin for elution). A final gel filtration was performed on a Superdex200 pg 16/60 column (GE Healthcare) in ClpP SEC buffer (20 mM MOPS, 300 mM KCl, 15% glycerol, pH 7.0). In the case of the cystein-containing mutants, 1 mM tris(2-carboxyethyl)phosphine (TCEP) was added to all buffers.

ClpX(E183Q) and ClpX$^{\Delta ZBD}$(E183Q) were overexpressed in *E. coli* BL21(DE3). An expression construct equipped with an N-terminal His_6-tag and a TEV cleavage site in pET300 vector was used.[14] The bacteria were grown in LB medium to OD_{600} 0.6 at 37 °C. After induction with 0.5 mM IPTG, the cells were incubated overnight at 25 °C. After harvest, the cells were

resuspended in ClpX lysis buffer (25 mM HEPES, 200 mM KCl, 1 mM DTT, 0.5 mM ATP, 5 mM $MgCl_2$, 10 mM imidazole, 5% glycerol, pH 7.6) and lysed by ultrasonication. The cleared cell lysate was loaded on a 5 mL HisTrap HP column (GE Healthcare). The column was washed with ClpX wash buffer (25 mM HEPES, 200 mM KCl, 1 mM DTT, 5% glycerol, 40 mM imidazole, pH 7.6). The protein was eluted with ClpX elution buffer (25 mM HEPES, 200 mM KCl, 1 mM DTT, 5% glycerol, 300 mM imidazole, pH 7.6). The protein fractions were pooled, 1 mM EDTA and TEV protease [1.25 mg for ClpX(E183Q) and 3.75 mg for $ClpX^{\Delta ZBD}$(E183Q)] were added and the reaction mixture was incubated at 10 °C overnight. Complete TEV cleavage was verified by intact-protein mass-spectrometry. The protein solution was loaded on a Superdex200 pg 16/60 column (GE Healthcare) and eluted in ClpX SEC buffer (25 mM HEPES, 200 mM KCl, 1 mM DTT, 0.5 mM ATP, 5 mM $MgCl_2$, 5% glycerol, pH 7.6). ClpX(WT), ClpX(V264C), ClpX-(I265C), ClpX(G266C) and ClpX(F267C) were overexpressed and purified similarly with the following modifications: the buffers contained 1 mM TCEP instead of DTT, and the ClpX wash

Table 3 Cloning primers.

Primer	Sequence (5'→3')
ClpP2 ΔC-3 fwd	TGATATTATCATTAATAAATCTGGCCATCATCATCATCATCACTAACTCG
ClpP2 ΔC-3 rev	CGAGTTAGTGATGATGATGATGATGGCCAGATTTATTAATGATAATATCA
ClpP2 ΔC-4 fwd	GGCTTAATTGATGATATTATCATTAATAAATCTCATCATCATCATCATCACTAACT
ClpP2 ΔC-4 rev	AGTTAGTGATGATGATGATGATGAGATTTATTAATGATAATATCATCAATTAAGCC
ClpP2 ΔC-5 fwd	AGATTACGGCTTAATTGATGATATTATCATTAATAAACATCATCATCATCATCACTA
ClpP2 ΔC-5 rev	TAGTGATGATGATGATGATGTTTATTAATGATAATATCATCAATTAAGCCGTAATCT
ClpP2 ΔC-6 fwd	TATCATTAATCATCATCATCATCATCACTAACTCGAGTC
ClpP2 ΔC-6 rev	GATGATGATGATTAATGATAATATCATCAATTAAGCCGTAATC
ClpX ΔZBD fwd	TTGGCACTTCACCAAAGCCCTGAAAATAAAGATTCTCAAAG
ClpX ΔZBD rev	TCTTTATTTTCAGGGCTTTGGTGAAGTGCCAAAACC
ClpX V264C fwd	CGTTAAAAATCGAATGGGTGAAAAATGCATTGGATTTGGTACAGATAATGC
ClpX V264C rev	GCATTATCTGTACCAAATCCAATGCATTTTTCACCCATTCGATTTTTAACG
ClpX I265C fwd	TAAAAATCGAATGGGTGAAAAAGTCTGTGGATTTGGTACAGATAATGCGAAA
ClpX I265C rev	TTTCGCATTATCTGTACCAAATCCACAGACTTTTTCACCCATTCGATTTTTA
ClpX G266C fwd	CGTTAAAAATCGAATGGGTGAAAAAGTCATTTGCTTTGGTACAGATAATGC
ClpX G266C rev	GCATTATCTGTACCAAAGCAAATGACTTTTTCACCCATTCGATTTTTAACG
ClpX F267C fwd	TCGAATGGGTGAAAAAGTCATTGGATGTGGTACAGATAATGC
ClpX F267C rev	GCATTATCTGTACCACATCCAATGACTTTTTCACCCATTCGA
ClpP2 I91C fwd	GGACGTACAAACATGCGGCATGGGTATGGCAGC
ClpP2 I91C rev	GCTGCCATACCCATGCCGCATGTTTGTACGTCC
ClpP2 L115C fwd	GCAAATGGCAAACGTTTTGCCTGCCCAAACGCTGAAATTATG
ClpP2 L115C rev	CATAATTTCAGCGTTTGGGCAGGCAAAACGTTTGCCATTTGC
ClpP2 I190C fwd	CAAAAGATTACGGCTTAATTGATGATATTTGCATTAATAAATCTGGCTTAAAAGGCC ATC
ClpP2 I190C rev	GATGGCCTTTTAAGCCAGATTTATTAATGCAAATATCATCAATTAAGCCGTAATCTT TTG

buffer and ClpX elution buffer contained additionally 0.5 mM ATP and 5 mM $MgCl_2$. The TEV digestion step was omitted.

N-terminally Strep-II-tagged eGFP with a C-terminal SsrA tag (AGKEKQNLAFAA) was overexpressed in *E. coli* SG1146a (Δ*clpP*) using pET55-Dest expression vector and purified by affinity chromatography and gel filtration as described previously.[14,91]

4.4.3. Isolation of the ClpXP complex

4.4 nmol $(ClpP1/2)_{14}$ and 3.3 nmol $ClpX_6$ were incubated for 10 min at 37 °C in PZA buffer (25 mM HEPES, 200 mM KCl, 5 mM $MgCl_2$, 1 mM DTT, 0.5 mM ATP, 15% glycerol, pH 7.6). The samples were loaded onto a Superose 6 increase 10/300 column (GE Healthcare) connected to an ÄKTA Purifier 10 system (GE Healthcare) and eluted at 0.2 mL/min flow rate. Samples were taken at 12 mL retention volume for EM and HDX-MS measurements. For cryo-EM, the sample was diluted 1:3 with glycerol-free PZA buffer and 0.1% glutaraldehyde was added. The reaction was quenched after 30 s with 2 equivalents of Tris-HCl. For SDS-PAGE, 4.4 µg protein was loaded on a gel and stained with Coomassie blue after separation.

4.4.4. Hydrogen/deuterium exchange mass spectrometry (HDX-MS)

HDX-MS experiments were performed using an ACQUITY UPLC M-class system equipped with automated HDX technology (Waters). HDX kinetics were determined by taking data points at 0, 10, 60, 600, 1800 and 7200 s at 20 °C. At each data point of the kinetic, 3 µL of a solution of 30 µM „free" ClpP1/2 and „free" ClpX were analyzed and compared to the $(ClpXP1/2)_2$ complex (1.4 µM). The respective protein solutions were diluted automatically 1:20 into 99.9% D_2O-containing buffer (25 mM HEPES, 200 mM KCl, 5 mM $MgCl_2$, 0.5 mM ATP, 1 mM TCEP, 5% glycerol, pH 7.6). As reference, all samples were analyzed in H_2O–containing buffers. The reaction mixture was quenched by the addition of 1:1 200 mM KH_2PO_4, 200 mM Na_2HPO_4, pH 2.3 (titrated with HCl) at 1 °C and 50 µL of the resulting sample were subjected to on-column peptic digest on a Waters Enzymate BEH pepsin column 2.1 × 30 mm at 20 °C. Peptides were separated by reverse phase chromatography at 0 °C in trapping mode using a Waters Acquity UPLC C18 1.7 µm Vangard 2.1 × 5 mm pre-column and a Waters Aquity UPLC BEH C18 1.7 µm 1 × 100 mm separation column. For separation, a gradient increasing the acetonitrile concentration stepwise from 5 to 35% in 6 min, from 35 to 40% in 1 min and from 40 to 95% in 1 min was applied and the eluted peptides were analyzed using an in-line Synapt G2-S QTOF HDMS mass spectrometer (Waters). UPLC was performed in protonated solvents (0.1% formic acid), allowing deuterium to be replaced with hydrogen from side chains and amino/carboxyl termini that exchange much faster than backbone amide linkages.[129] All experiments were performed in duplicate. Deuterium levels were not corrected for back exchange and are therefore reported as relative deuterium levels.[130] The use of an automated system, i.e. handling all samples at identical conditions, negotiates the need for back exchange correction. MS data were collected over an m/z range of 100–2000. Mass accuracy was ensured by calibration with Glu-fibrino peptide B (Waters) and peptides were identified by triplicates MSE ramping the collision energy from 20–50 V. MS data were analyzed with the

PLGS 3.0.3 and DynamX 3.0 software packages and all spectra were checked manually. For each peptide, relative uptake values were determined as follows:

$$\text{relative uptake}[\%] = \frac{\text{deuterium uptake} \times 100}{\text{maximal uptake}}.$$

For each amino acid, the average of the relative uptake of all peptides covering the amino acid was calculated. The difference of the relative deuterium uptake between the "free" and "complex" states was calculated for each amino acid. Data were analyzed and visualized using custom MATLAB and python scripts, UCSF Chimera 1.12[131] and OriginPro 2016.

4.4.5. Biochemical assays

Peptidase assay

In this assay, the degradation of a fluorogenic tripeptide was measured, for which ClpX was not required. 99 µL 1 µM ClpP1/2 was incubated in PZ buffer (25 mM HEPES, 200 mM KCl, 5 mM $MgCl_2$, 1 mM DTT, 10% glycerol, pH 7.6) in flat bottom black 96-well plates for 15 min at 30 µC. 1 µL Ac-Ala-hArg-2-Aoc-ACC substrate (10 mM stock in DMSO) was added and the fluorescence was measured (380 nm, 430 nm) with an infinite M200Pro plate reader (Tecan) at 30 °C. Data were recorded in triplicate and two independent experiments were performed. Peptidase activity was determined by linear regression using Microsoft Excel and plots were made with GraphPad Prism 6.

Protease assay

Protease assays were carried out in flat bottom white 96-well plates in a final volume of 60 µL. $(ClpP1/2)_{14}$ (0.2 µM), $ClpX_6$ (0.4 µM) and ATP regeneration mix (4 mM ATP, 16 mM creatine phosphate, 20 U/mL creatine kinase) were pre-incubated for 15 min at 30 °C in PZ buffer. 0.8 µM eGFP-SsrA substrate was added and fluorescence was measured (485 nm, 535 nm) at 30 °C. Data were recorded in triplicate and at least two independent experiments were performed. Protease activity was determined by linear regression using Microsoft Excel and plots were made with GraphPad Prism 6.

ATPase assay

90 µL 2 µM ClpX in ATPase buffer (100 mM HEPES, 200 mM KCl, 20 mM $MgCl_2$, 1 mM DTT, 1 mM NADH, 2 mM phosphoenolpyruvate, 50 U/mL lactate dehydrogenase, 50 U/mL pyruvate kinase, 5% glycerol, pH 7.5) was added to a flat bottom transparent 96-well plate and incubated for 15 min at 37 °C. The reaction was started by the addition of 10 µL 200 mM ATP in 100 mM HEPES, pH 7.5. Absorption at 340 nm was measured at 37 °C. Two independent experiments with three replicates each were carried out. ATPase activity was determined by linear regression using Microsoft Excel after subtraction of the background signal (measurement without ClpX), and the plot was made with GraphPad Prism 6.

4.4.6. Electron microscopy

Electron microscopy was performed by Dr. Christos Gatsogiannis at the Max Planck Institute of Molecular Physiology (Dortmund, Germany).

Sample quality was examined by negative stain EM. Sample from the respective fraction was further diluted to a concentration of 0.01–0.03 mg/mL and negative stain EM was performed as described previously.[132] Images were recorded with a JEOL JEM-1400 equipped with a 4K CMOS detector F416 (TVIPS) at a pixel size of 1.84 Å. For cryo-EM, 4 µL of cross-linked ClpXP1/2 dimers at a concentration of 0.045 mg/mLwere applied to a glow-discharged quantifoil 2/1 Cu grid with an additional 2 nm thin carbon layer and after an incubation time of 45 sec, rapidly plunge-frozen using a CryoPlunge3 (Cp3, Gatan) at 90% humidity. To improve ice quality and thickness distribution, 0.01% Tween-20 was added shortly prior plunging. The quality of the grids was screened with a JEOL JEM 1400 and a FEI Tecnai Spirit, both equipped with a LaB6 cathode and a 4K CMOS detector F416 (TVIPS). A cryo-EM dataset was acquired on a FEI Titan KRIOS at 300 kV equipped with spherical aberration corrector and a Falcon III direct detector (linear mode) at a ×112 807 magnification (×59 000 nominal magnification), corresponding to a pixel size of 1.1 Å(table 4). Each exposure was recorded with a total dose of ∼114 electrons/Å^2 and a total exposure time of 2 sec (frame rate of 50 msec). A total of 3200 micrographs were collected using the EPU software (FEI).

4.4.7. Image processing and reconstruction

Image processing and reconstruction was performed by Dr. Christos Gatsogiannis at the Max Planck Institute of Molecular Physiology (Dortmund, Germany).

The frames were aligned, averaged and dose-weighted using unblur and sum_movie.[133] Unweighted full-dose images were further used to estimate the CTF parameters using CTER[134] (SPHIRE[105]). Dose weighted full-dose images were used for all other steps of image processing. ClpXP1/2 dimers were picked automatically using EMAN2's[135] neuralnet e2boxer. Further data processing was performed using the software package SPHIRE.[105] After inspection of micrographs using the CTF-assessment-GUI, 273 300 single particles were selected for further processing. The particle stack was subjected to 2D-clustering using ISAC2 (SPHIRE), resulting in a "clean" stack of 143 901 single particles producing stable and reproducible 2D-class averages (table 4). The 2D class-averages were used to calculate a 3D volume, using VIPER. After masking, this volume was used as the reference for a 3D refinement using Meridien (SPHIRE), which resulted in a 13 Ådensity map, as estimated by the "gold-standard" FSC. In agreement to the 2D clustering results, further 3D clustering using Sort3D (SPHIRE) confirmed that the ClpXP1/2 dimer is a continuously flexible structure (fig. 11g). Independent refinement of the resulting subsets did not, however, further improve the resolution of the volume.

We then manually picked the ClpXP1/2 monomers within each ClpXP1/2-dimer for 10 representative micrographs of the dataset and used these data to train crYOLO,[104] which then automatically selected 613 322 single particles. After 2D and 3D clustering, a final "clean" stack of 383 927 particles was used for further refinement. During the first rounds of the

refinement, we applied local symmetrization of the reference after each refinement round, as previously described[114] i.e. after each refinement round the density of ClpP was symmetrized using D7 symmetry, whereas the density of ClpX was scaled in order to put an additional weight on this region during the asymmetric refinement. Finally, both densities (ClpX and ClpP) were combined and the resulting volume was used as a reference for the subsequent refinement iteration. This procedure was performed during the initial rounds in order to obtain global projection parameters. The user function was not applied during the local refinements. This resulted in a density map with an average resolution of 4 Å, where the resolution of the density decreases towards ClpX (fig. 13). The average resolution was calculated between two independently refined "half maps" at the 0.143 FSC criterion. The estimated accuracy of rotation and translation search during the last refinement round was estimated to 1.78°and 1.02 pixels, respectively. Local resolution was computed using the "Local Resolution" tool in SPHIRE. 3D clustering into four groups was performed using the RSORT3D tool of SPHIRE. However, according to the ANOVA analysis, the resulting volumes were not reproducible and were therefore not considered for further analysis. 3D refinement and clustering focusing on the density of ClpX, after removing the ClpP signal from the dataset, did also not result into further improvement of the ClpX density. The density of ClpP was auto-sharpened locally using phenix.auto_sharpen[136] and filtered to its average resolution of 3.9 Å. The ClpX desnity was filtered to an average resolution of 6.5 Åand sharpened with an ad-hoc b-factor of -240 Å^2. Angular distribution plots were computed using SPHIRE. Beautified 2D class averages were computed with 3500 members per group.

4.4.8. Atomic modelling

Atomic modelling was done by Dr. Christos Gatsogiannis and by Dr. Felipe Merino at the Max Planck Institute of Molecular Physiology (Dortmund, Germany).

We built a homology model of ClpX with SWISS-MODEL[137] using ADP-bound *E. coli* ClpX (PDB-ID 3HWS, Chain A) and ATPγS-bound *E. coli* ClpX (PDB-ID 4I81, Chain B). We then used UCSF Chimera[131] to fit the structures of ClpX's homology model and ClpP1/2 (PDB-ID 4RYF)[14] into the cryo-EM density. We used the RosettaES protocol[138] to build the missing residues 9–16 for each ClpP2 subunit. Residues 1–2 were manually built in Coot.[139]

With the complete model, we performed several iterative runs of molecular dynamics flexible fitting (MDFF)[140] and manual adjustment with Coot, paying particular attention to the fitting of the IGF loops. In the initial run, we applied 6-fold symmetry to ClpX, allowing regions poorly supported by the density to settle into reasonable conformations. This restraint was later removed. For the final iterations, we also included a step of real-space refinement in Phenix (ref), to decrease the number of Ramachandran outliers and to fit the atomic B-factors. The necessary files for the MDFF runs were set up with VMD[141] and all simulations were performed in NAMD,[142] using the CHARMM 36 m force field[143] with the implicit solvation model implemented in NAMD.

For the proper modeling of the structure with MDFF, we included all missing regions of the structures, even if their density does not allow full atomic modeling. After refinement, we

removed all those from the final model. The quality of this model was assessed in Phenix, using the Molprobity[144] and EMRinger scores[145] as well as the overall geometry of the structure.

Sequence conservation was analyzed using the ConSurfserver.[146] Analysis of the channel pathway was performed with ChExVis.[147] Electron density maps and models were visualized using Chimera[131] and Chimera X[148].

Table 4 Cryo-EM data collection, refinement and validation statistics

	ClpXP1/2 dimer	ClpXP1/2 EMD-10162 (PDB-IDs 6SFX, 6SFW)	
Data collection and processing			
Magnification	112 807	112 807	
Voltage (kV)	300	300	
Electron exposure (e^{-}/Å^2)	114	114	
Defocus range (μm)	0.5 to −3.0	−5 to −3.0	
Pixel size (Å)	1.1	1.1	
Symmetry imposed	C1	C1	
Initial particle images (no.)	273 300	613 322	
Final particle images (no.)	143 901	383 927	
Map resolution (Å)	13	4	
FSC threshold	0.143	0.143	
Map resolution range (Å)	–	3.2 – 10	
Refinement		**6SFX**	**6SFW**
Initial model used (PDB code)	–	4RYF	–
Model resolution (Å)	–	2.8	–
Model resolution range (Å)	–	–	–
Map sharpening B factor (Å^2)	–	−214	−240
Model composition			
Nonhydrogen atoms	–	20 196	15 225
Protein residues	–	2 602	1 955
B factors (Å^2)	-	100.8	187.87
R.M.S. deviations			
Bond lengths (Å)	-	0.012	0.018
Bond angles (°)	-	1.233	1.978
Validation			
MolProbity score	–	2.34	2.30
Clashscore	–	22.88	22.43
Poor rotamers (%)	–	0.18	0.20
Ramachandran plot			
Favored (%)	–	92.0	92.9
Allowed (%)	–	7.65	6.40
Disallowed (%)	–	0.31	0.70

5. ClpP1/2 as an intracellular thermometer for proteome regulation in *L. monocytogenes*

The submission of this chapter to a peer-reviewed journal is planned after publication of the thesis.

5.1. Introduction

Listeria monocytogenes is a highly stress resistant pathogenic bacterium that can survive under rapidly changing conditions: in the soil under varying temperatures, in food during processing and storage, in the gastrointestinal tract, in lysosomes and in the cytosol of mammalian cells.[48,49] In order to cope with these different conditions, the cells must detect environmental changes and promptly adjust their protein expression as well as turnover in a strictly regulated manner.

It has been shown that different stressors often induce the same stress response pathways.[66] For example, there is an overlap between oxidative stress and heat stress response genes.[60,64] As a consequence, cross-protective stress response has been observed. For example, sublethal acid stress enhances the heat and osmotic resistance of *L. monocytogenes* cells.[149] This can be a useful strategy in the infection process, where the cells have to withstand different stressors at the same time, e.g. bile acids, elevated temperatures, rapid pH changes (while entering and leaving the lysosome) and oxidative stress.

L. monocytogenes can grow at temperatures varying from −0.4 to 45 °C.[49] In order to achieve this, it must be able to sense temperature changes to control gene expression. There are several temperature detection systems in *L. monocytogenes* including the CtsR protein, which acts as a negative regulator of class III heat shock proteins.[58] CtsR itself can sense heat as it is destabilized at high temperatures resulting in its dissociation from DNA and subsequent transcription of the above mentioned heat shock proteins.[150]

GmaR is another a thermo-sensing protein, which undergoes conformational changes at elevated temperatures and controls the expression of flagellar motility genes. *L. monocytogenes* uses flagella for extracellular motility but stops their expression after infection of mammalian cells. At temperatures below 37 °C, GamR forms a complex with the repressor MogR, inducing the expression of flagellar proteins. Vice versa, the complex gets destabilized at physiological temperatures, leading to repression of flagellar motility genes by MogR.[151]

Further important temperature sensing macromolecules are non-coding RNAs that change their secondary structures at different temperatures and thereby affect the translation of genes. The 5' untranslated region on the transcript of the virulence factor activator gene *prfA* forms a hairpin, which relaxes above 37 °C, allowing the ribosome to bind to the mRNA and PrfA to be translated.[152]

It has been demonstrated that heat shock also induces the SOS genes in *L. monocytogenes*.[60] The SOS response is a conserved DNA damage response mechanism in bacteria, which is induced after accumulation of ssDNA in cells. It is induced by a variety of stressors such as UV light and DNA damaging agents,[59] certain antibiotics,[153–155] and hydrogen peroxide[156]. In *L. monocytogenes* heat stress has also been shown to induce the SOS pathway.[60] The RecA activator protein forms filaments after binding to ssDNA and induces the autocleavage of LexA, the repressor of the SOS genes[59]. The N- and C-terminal LexA domains (NTD and CTD respectively) retain a weak DNA binding capacity after cleavage. They are further digested by ClpXP in *S. aureus* and additionally by the Lon protease in *E. coli*.[157–159] LexA binds to the conserved SOS box sequence upstream of the regulated genes.[59] In different species, different genes are regulated by the SOS box. In *L. monocytogenes*, 28 genes have been identified.[64] Most of them are DNA polymerases required for DNA repair. Furthermore, the induction of the SOS pathway inhibits bacterial growth, probably in order to prevent cell division after incomplete DNA replication.[64,160]

L. monocytogenes is one of the bacteria that possesses two ClpP isoforms that can build a hetero-oligomeric complex.[9,14] It is hitherto unknown why some bacteria have homotetradecameric and others heterotetradecameric ClpPs. In this study, we revealed the thermosensing ability of ClpP1/2 heterooligomerization and we investigated the unique cellular functions of ClpP1 and ClpP2. To achieve this, the phenotypes of Δ*clpP1*, Δ*clpP2* and double knockout (Δ*clpP1/2*) strains were examined in an integrative proteomic approach using mass spectrometry-based whole proteome analysis and co-immunoprecipitation. Our data suggest that ClpP plays an important role in the oxidative processes of the cells.

5.2. Results and discussion

5.2.1. ClpP1 and ClpP2 form a heteroxomplex at elevated temperatures

Heterologous expression and production of the *L. monocytogenes* ClpP1/2 in *E. coli* revealed that the heterocomplex is unstable at 4 °C or on ice. Pure tetradecameric ClpP1/2 could be only obtained when the whole purification process after cell lysis was performed at room temperature (~26 °C, fig. 25). It is known from transcription analyses that both *clpP* genes show up to 7-fold higher expression levels under heat stress,[14,60] indicating that heterocomplex formation is preferred at high temperatures and might have a specific biological role. ClpP1 is not active by itself, however, the heterocomplex exhibits ten times higher protease activity compared to the ClpP2 homocomplex due to its enhanced affinity to the chaperone ClpX.[14,95] Taking these data together, a ~140-times increase of ClpXP1/2 proteolytic activity per subunit can be expected during heat stress due to higher expression levels and heterooligomerization. *M. tuberculosis* ClpP1 and ClpP2 also heterooligomerize at elevated temperatures,[83] which suggests that temperature sensing could be a conserved biological function of ClpP.

To assess whether the temperature-dependent stabilization is a general feature of ClpP1/2 and not a result of the co-expression and purification conditions, we measured hetero-

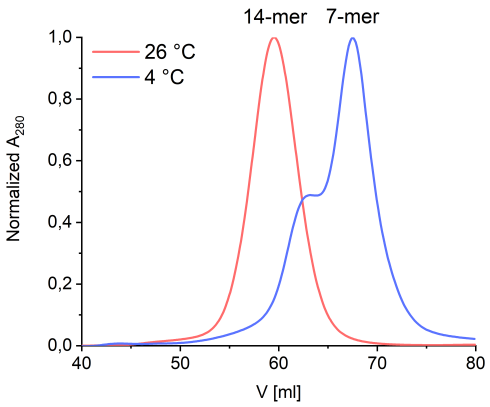

Figure 25 Purification of ClpP1/2 at 4 °C and at room temperature. Size exclusion chromatography on a Superdex200pg 16/60 coloumn.

oligomerization at temperatures ranging from 0 °C to 48 °C. Equal amounts of separately overexpressed and purified $ClpP1_7$ and $ClpP2_{14}$ were mixed and incubated at different temperatures. The samples were subjected to analytical size-exclusion chomatography (SEC), and the protein composition of the tetradecamer peak was analyzed by intact protein mass spectrometry (ip-MS) (fig. 26a). The ratio of the tetradecamer (ClpP2 and ClpP1/2) and heptamer peaks (ClpP1) differed temperature-dependently, with the highest 14-mer amount observed at 42 °C (fig. 26b); however at 48 °C, the 7-mer:14-mer ratio remained 1:1. Ip-MS analysis revealed an increasing ClpP1 fraction within the tetradecameric complex up to 37 °C with a maximum content of 44% (fig. 26c). However, at 48 °C, the 7-mer:14-mer ratio declined to 1:1. Accordingly, the ClpP1 partition decreased. As a control, the ClpP1/2 complex assembled at 42 °C was cooled down to 0 °C which resulted in disassembly of the newly built heterooligomers suggesting that heterocomplex formation is reversible (fig. 26d). In order to rule out the existence of $ClpP1_{14}$ homocomplexes, we incubated ClpP1 at 42 °C. No shift in the chromatogram compared to 0 °C occurred, which implies that ClpP1 is not able build homotetradecamers even under elevated temperatures (fig. 26e).

In order to assess whether the heterocomplex formation translates to increased protease activity at high temperatures, we monitored the degradation of GFP-SsrA by ClpXP in the presence of an ATP regeneration system.[87] Using this assay, we compared the protease activity of mixed $ClpP1_7$ and $ClpP2_{14}$ to solely $ClpP2_{14}$ at different temperatures. While ClpP1 alone is known to be inactive because of its impaired catalytic triad (Ser98, His123, *Asn172*) and its inability to bind AAA+ chaperones,[7,14,95] co-inbubation with ClpP2 at 37 °C and 42 °C resulted in an elevated proteolytic activity (fig. 27). The slower kinetics of the GFP degradation at 42 °C are attributed to the low thermal stability of ClpX and the ATP regenerating enzyme creatine kinase.

5.2.2. Intracellular heterooligomerization of ClpP1 and ClpP2 under heat stress

Next, we set out to investigate whether temperature-dependent heterooligomerization also occurs in living *L. monocyotgenes* as a response to heat stress. For this purpose, we performed selective co-immunoprecipitation (co-IP) with ClpP1 and ClpP2 at low and high temperatures.

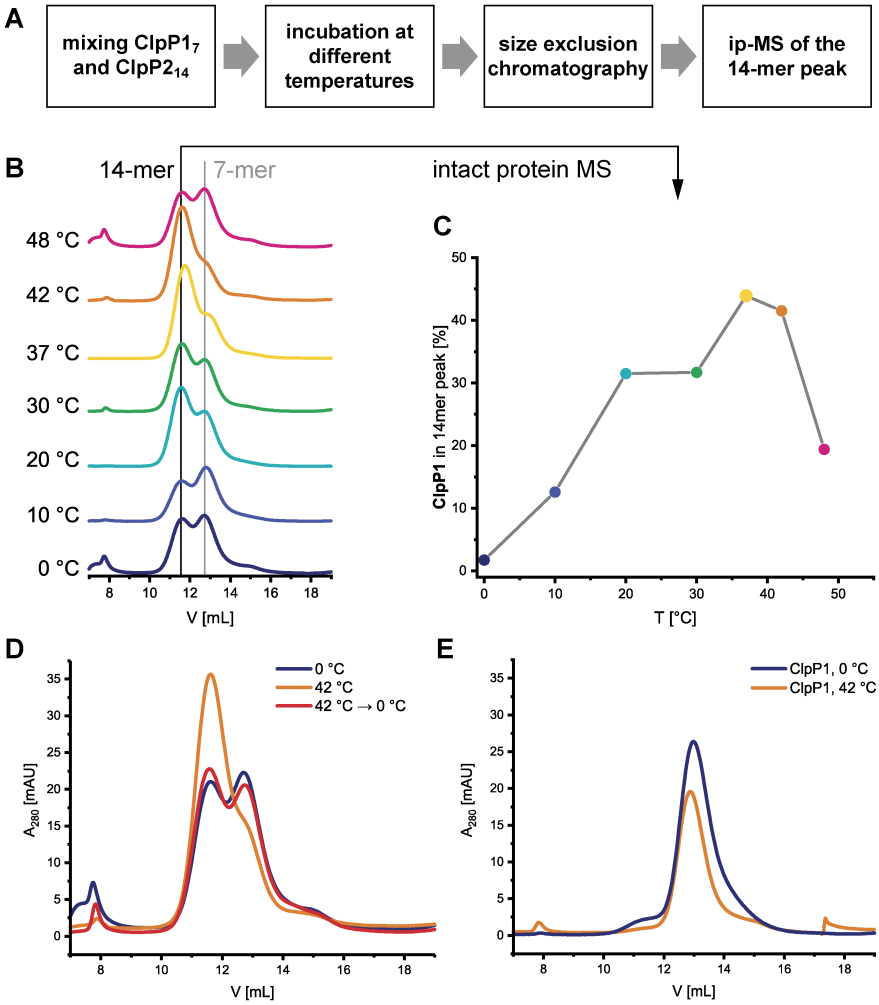

Figure 26 Temperature-dependent formation of the ClpP1/2 heterocomplex. a Scheme of the SEC/ip-MS workflow. **b** Size-exclusion chromatography of ClpP1$_7$ and ClpP2$_{14}$ after incubation at the indicated temperatures for 30 min. Black line: tetradecamer, gray line: heptamer. **c** Percentage of ClpP1 in the 14-mer peaks of panel b, measured by intact protein mass spectrometry. **d** Size-exclusion chromatography of ClpP1/2 after incubation at 0 °C for 30 min (blue), 42 °C for 30 min (orange) and 42 °C for 30 min followed by 0 °C for 30 min (red). **e** Size-exclusion chromatography of ClpP1$_7$ after incubation at 0 °C for 30 min (blue) and at 42 °C for 30 min (orange).

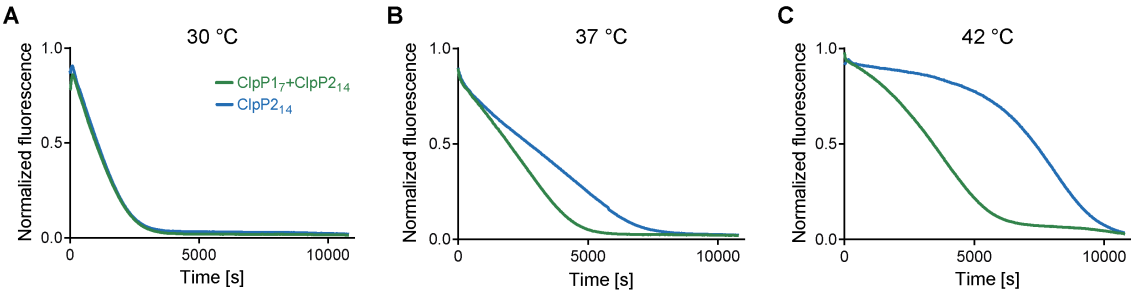

Figure 27 Protease activity of ClpP1$_7$ and ClpP2$_{14}$ at different temperatures. ClpP (green line: 0.1 µM ClpP2$_{14}$ and 0.2 µM ClpP1$_7$, blue line: 0.1 µM ClpP2$_{14}$) and 0.4 µM ClpX were pre-incubated for 30 min at 30 °C (**a**), 37 °C (**b**) and 42 °C (**c**), subsequently the degradation of 0.4 µM GFP-SsrA was measured. Means of triplicates are shown. The experiments were independently repeated with qualitatively identical results (data not shown).

Because of their similar structure, both ClpP1 and ClpP2 bind to the anti-ClpP antibody. In order to pull-down ClpP isomers selectively, we inserted a 2×myc tag at the end of the *clpP2* gene. The *L. monocytogenes clpP1(191)*::2×myc and *L. monocytogenes clpP2(199)*::

2×myc strains constitutively expressed C-terminally myc-tagged ClpP1 (ClpP1-2×myc) and ClpP2 (ClpP2-2×myc) respectively, which can be selectively precipitated with an anti-c-Myc antibody.

The strains were grown to stationary phase at 20 °C and 42 °C, harvested the bacteria and incubated with an MS-cleavable amine-reactive disuccinimidyl sulfoxide (DSSO) crosslinker in order to stabilize transient protein-protein interactions.[108] After cell lysis, proteins were precipitated with immobilized polyclonal anti-c-Myc antibody. An isotype control was used to account for background binding. The captured proteins were subjected to tryptic digest, and the isolated peptides were measured by LC-MS/MS.

When ClpP2-2×myc was used as a bait, analysis of the ClpP1 intensities revealed a 6-times higher enrichment at 42 °C compared to 20 °C (fig. 28a, c), which suggests that temperature plays a role in the heterocomplex formation of ClpP1 and ClpP2. However, in case of ClpP1-2×myc, ClpP2 was similarly enriched at both temperatures (fig. 28b, d). Further experiments must clarify why the reverse co-IP yielded differing results. As previously observed by SEC, at 20 °C heterooligomerization takes place only to a small degree (fig. 26b). It is therefore possible that the co-IP workflow is not sensitive enough to robustly detect this difference in the heterocomplex amount. Another possibility is that if the cellular amount of ClpP1 is lower than that of ClpP2, ClpP1 can easily get saturated with ClpP2 but a larger amount of ClpP2 must stay in the homocomplex, which is detectable at 20 °C.

5.2.3. Phenotypic characterization of *L. monocytogenes* Δ*clpP* mutants

To further investigate the cellular role of ClpP1 and ClpP2, we constructed Δ*clpP1* and Δ*clpP2* single mutants, as well as a Δ*clpP1/2* double knockout strain (fig. 29a, top) in *L. monocytogenes* EGD-e. The Δ*clpP1* mutant was provided by Dr. Christian Fetzer. We assessed the activity of ClpPs by labelling the whole cells with vibralactone probe (VLP) (fig. 29b). Vibralactone is the only known small molecule, which is able to label both ClpP1 and ClpP2 by binding to the active site serine.[9] VLP is equipped with a terminal alkyne tag which enables the coupling of an azide-tagged fluorescent dye to the probe by Click reaction. This way, proteins that covalently bind VLP can be visualized on a polyacrylamide gel by fluorescence. As expected a strong ClpP2 signal is detected in Δ*clpP1*. Interestingly, a weak band was seen in Δ*clpP2*. In contrary to the in vitro activity assays,[7,14] this indicates that ClpP1 has some residual activity in vivo in the absence of ClpP2 since the catalytic serine is activated to some extent and it can react with the lactone ring. It is possible that other cognate interaction partners partially push ClpP1 into an active conformation where the catalytic triad is correctly aligned as in ClpP1/2.[7,14] Still, it is unlikely that ClpP1 alone would be able to act as a protease, because it does not have hydrophobic pockets where AAA+ ATPases could attach.[14,161]

The growth curves of the mutants show that the single mutants grow at a similar rate to the wild type strain but reach stationary phase at a lower cell density (fig. 29c). The growth of the ΔclpP1/2 mutant is substantially slower, but shows the highest optical density in the stationary phase.

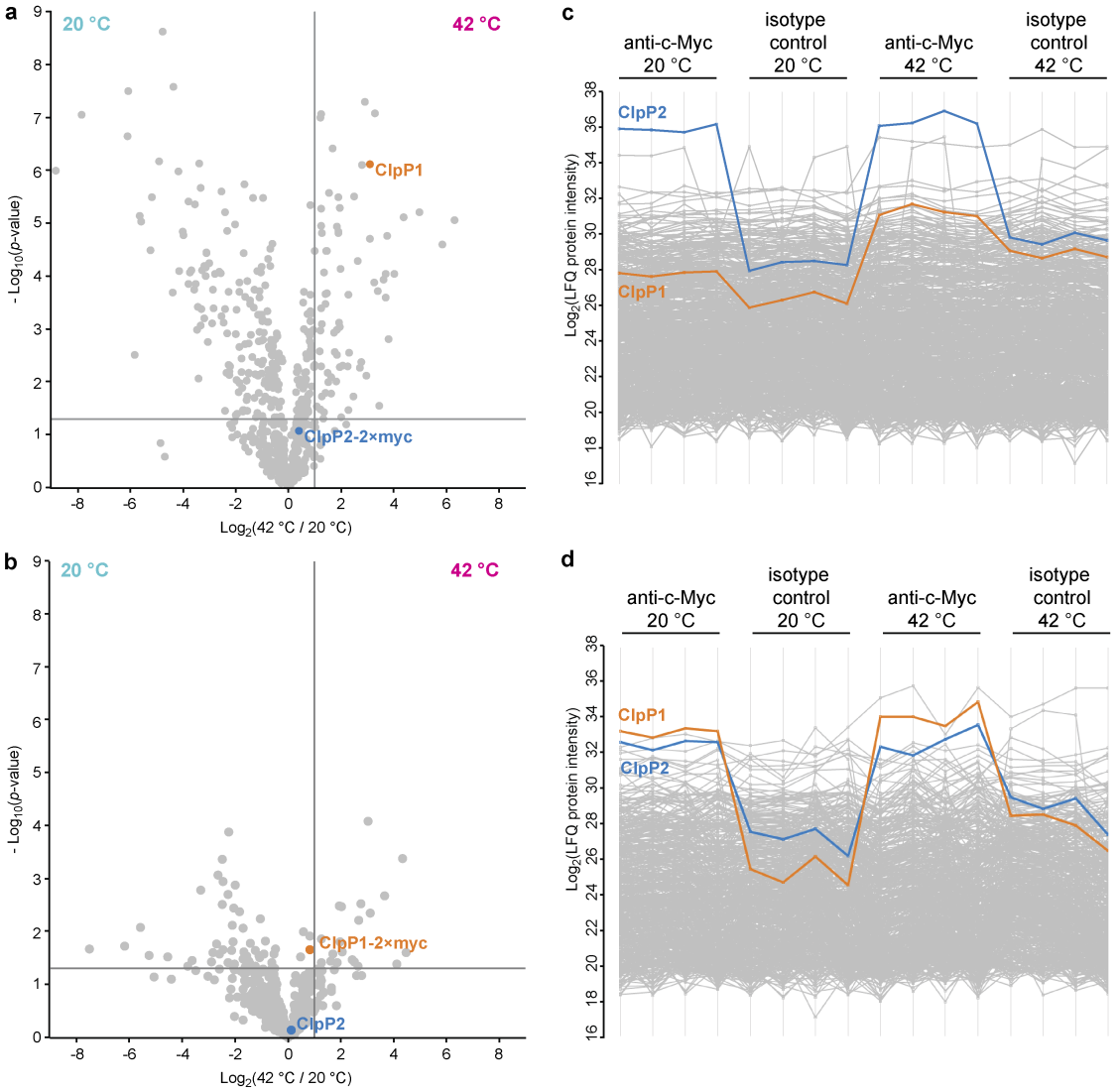

Figure 28 Intracellular hetero-oligomerization of ClpP1 and ClpP2 in *L. monocytogenes* demonstrated by co-immunoprecipitation. a, b Volcano plots of co-IPs using ClpP2-2×myc (**a**) and ClpP1-2×myc (**b**) as baits after growing the *L. monocytogenes* cultures at 20 °C and 42 °C to stationary phase. $-\text{Log}_{10}$ *p*-values from two-samples Student's *t*-test are plotted against $\log_2$ ratios of label-free quantification (LFQ) protein intensities. The vertical grey lines show 2-fold enrichment at 42 °C compared to 20 °C, the horizontal grey lines show *p*-value = 0.05 (n = 4). **c, d** Profile plots showing the $\log_2$ LFQ intensities of all measured proteins across all replicates after missing value imputation. ClpP1 and ClpP2 are highlighted with orange and blue respectively.

ClpP2 has been shown to be important for intracellular growth in macrophages.[36] We decided to investigate the role of ClpP1 as well. For this, we infected mouse-derived macrophages with *L. monocytogenes* EGD-e (WT), Δ*clpP1*, Δ*clpP2* and Δ*clpP1/2* and measured the colony forming units (CFUs) after 7 hours (fig. 29d). All mutants were able to enter and replicate inside the cells, but the replication of the double knockout was strongly reduced. Contrary to previous findings,[36] the intracellular growth of Δ*clpP2* was only weakly inhibited. It is possible that ClpP2 is more important for infection in the *L. monocytogenes* LO28 strain, which was used by Galliot et al., than in *L. monocytogenes* EGD-e. Deletion of both *clpP* genes seems to strongly impair the intracellular growth but this can also be a result of the generally slower growth kinetics (fig. 29c) of this strain.

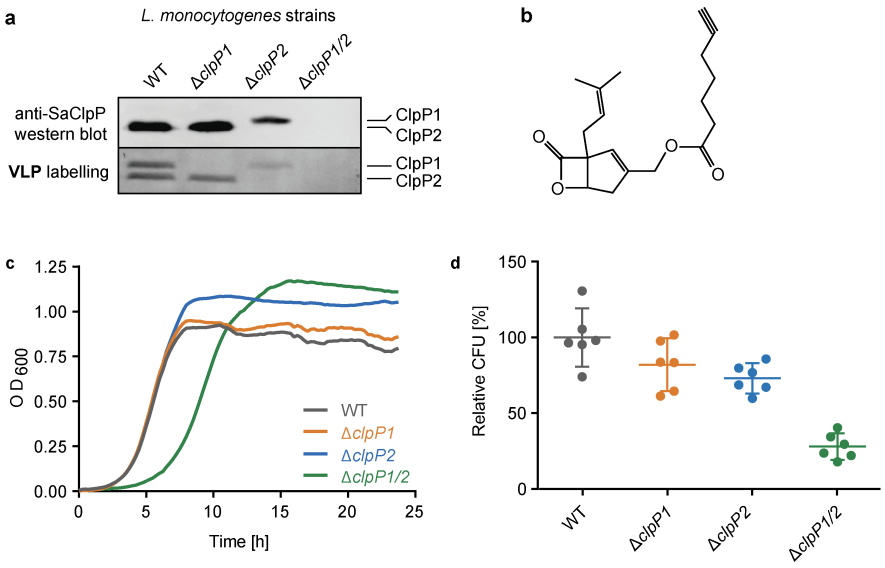

Figure 29 ***L. monocytogenes ΔclpP*** **mutants. a** Validation of the Δ*clpP* mutants by western blot (top) and by fluorescent labelling with vibralactone probe (bottom). **b** Structure of the vibralactone probe. **c** Growth curves of the Δ*clpP* mutants in BHI medium at 37 °C. Means of triplicates are shown. The experiment was independently repeated with qualitatively identical results (data not shown). **d** Intracellular growth of the Δ*clpP* mutants in murine macrophages. CFUs were determined after 7 h, and normalized to WT as 100% (n = 6, two independent experiments in triplicates were performed, mean ± 95% confidence interval).

5.2.4. Whole-proteome analysis of ClpP1 and ClpP2 deletion mutants

ClpP is required for the maintenance and regulation of the proteome by clearing damaged proteins and degrading transcription factors. So far, the specific roles ClpP1 and ClpP2 in *L. monocytogenes* are elusive. We analyzed the proteomes of *L. monocytogenes* EGD-e (WT), Δ*clpP1*, Δ*clpP2* and Δ*clpP1/2* at early stationary phase at 37 °C. The proteome of Δ*clpP1* does not differ markedly from the wild type (fig. 30a) but in Δ*clpP2* and in Δ*clpP1/2* many proteins are dysregulated (fig. 30b–c). The dysregulated proteins in Δ*clpP2* and Δ*clpP1/2* are highly overlapping: 89% of the proteins that are upregulated in Δ*clpP1/2* compared to the wild type are also upregulated in Δ*clpP2*, and the same is true for 82% of the downregulated proteins in the double mutant. However, these mutants have greatly different phenotypes, which is not reflected by the respective in the proteome changes.

UniProt Keyword and Gene Ontology Biological Process (GOBP) term analyses of the proteomic data were performed with the aGOtool (agotool.sund.ku.dk).[162] This tool corrects for the cellular abundances and for differences in detection by LC-MS/MS of the proteins. The whole proteome of the wild-type strain *L. monocytogenes* EGD-e was used as background.

Among the upregulated proteins, the GOBP term "response to stimulus" was significantly enriched in both Δ*clpP2* and in Δ*clpP1/2*, and the SOS response was preferentially enriched in Δ*clpP1/2*. In case of double *clpP1/2* deletion, the bacteria's ability to cope with stress was attenuated and the SOS response was induced. Activation of the SOS response inhibits cell division in *L. monocyotgenes*[60] and in *E. coli*[153], and accordingly the growth of Δ*clpP1/2* was slower compared to the wild type.

Additionally, the class III heat shock proteins (CtsR, McsB, ClpB, ClpC, ClpE and the Lmo0230

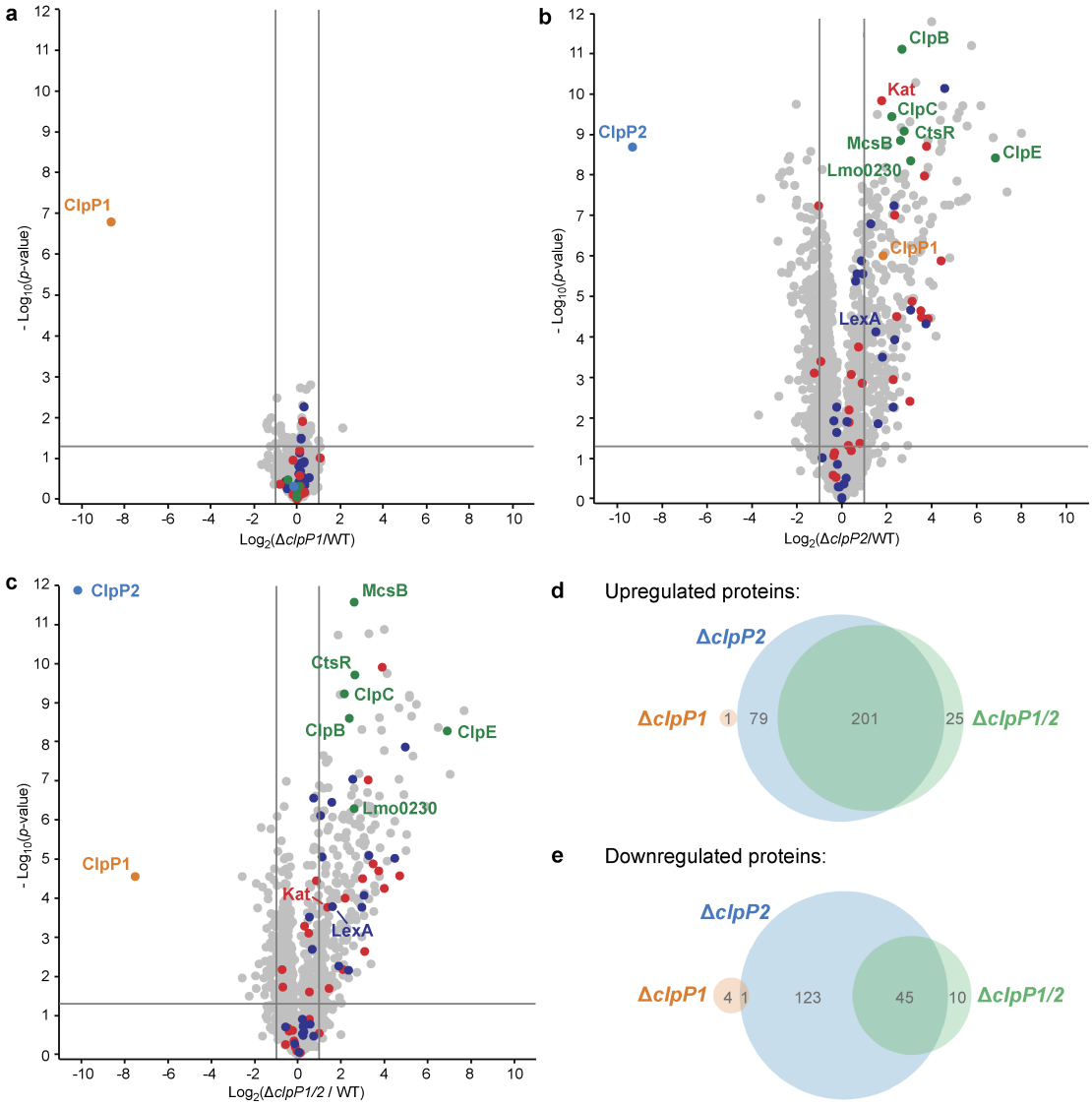

Figure 30 Whole-proteome analysis of the *L. monocytogenes* Δ*clpP* mutants. a–c Proteomes of *L. monocytogenes* Δ*clpP1* (**a**), Δ*clpP2* (**b**) and Δ*clpP1/2* (**c**)(right) compared to the WT (left). Bacterial cultures were grown to stationary phase at 37 °C. − Log_{10} *p*-values from two-sample Student's *t*-test are plotted against $\log_2$ ratios of LFQ protein intensities. The vertical grey lines show 2-fold enrichment, the horizontal grey lines show *p*-value = 0.05. Samples were prepared in triplicates in two independent experiments (n = 6). Class III heat shock proteins (green), SOS response proteins (dark blue) and iron-containing proteins (red) are highlighted. ClpP1 and ClpP2 are shown in orange and blue respectively. **d–e** Venn-diagrams showing the up-(**d**) and downregulated (**d**) proteins in the proteomes of the Δ*clpP* mutants compared to the WT (fold enrichment ≥ 4, *p*-value ≥ 0.05).

protein) were upregulated in both Δ*clpP2* and Δ*clpP1/2*. The class I heat shock proteins were not overexpressed, except for their repressor, HrcA. Most of the class II HSPs (except for GlpK and BilEA, which is also an SOS response protein) and their positive regulator σ^B were also not dysregulated. Of the 28 proteins, which have been found in a genome-wide screen for temperature sensitivity,[163] only two (ClpB and AddA) were significantly upregulated in the *clpP2* deletion mutants. This, and the fact that the class I and II heat shock proteins were not induced, highlights the differences between the stress caused by *clpP2* deletion and heat stress, even though class III heat shock proteins and the SOS response are induced in the mutants lacking *clpP2*.

Iron containing and iron-sulfur proteins were also significantly upregulated in Δ*clpP2* and

in *ΔclpP1/2*. In *S. aureus*, it has been shown that ClpP degrades damaged iron-sulfur proteins,[27,164] which could also be the case in *L. monocytogenes*. ClpP has been connected to iron homeostasis and maintaining the oxidative balance inside the cell.[37,165,166]

5.2.5. Co-immunoprecipitation of ClpP1 and ClpP2

In order to identify specific interaction partners of ClpP1 and ClpP2, we conducted a second set of co-IP experiments. The *ΔclpP1* and *ΔclpP2* mutants were grown to stationary phase at 37 °C and interacting proteins were covalently crosslinked with DSSO. The ClpPs were precipitated with the polyclonal anti-ClpP antibody and binding partners of each ClpP isoform were selectively pulled down. The precipitated proteins were digested with trypsin and analyzed by LC-MS/MS.

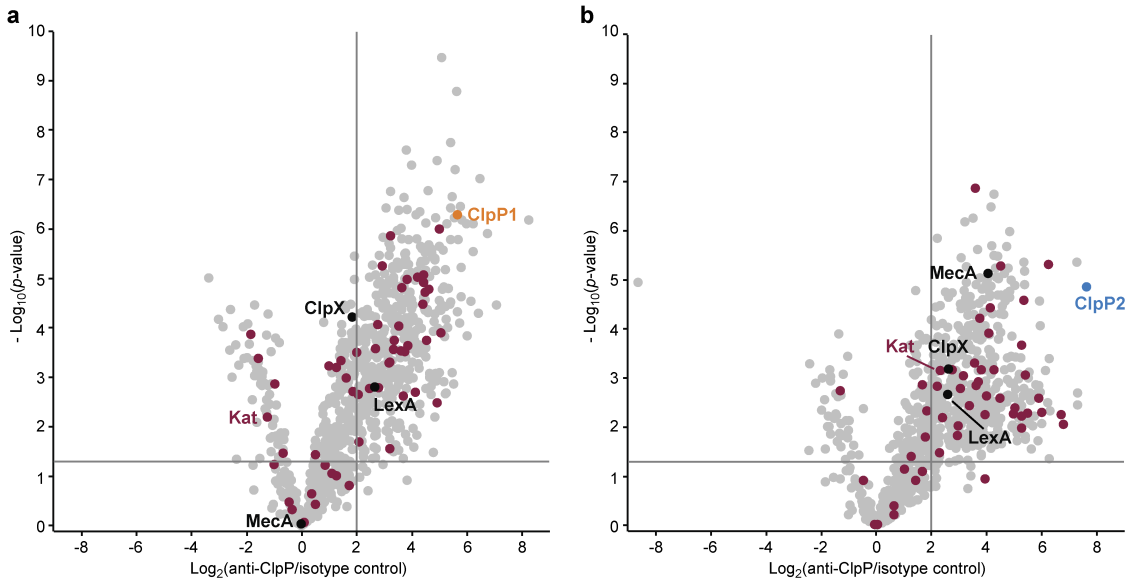

Figure 31 Co-immunoprecipitation of ClpP1 and ClpP2 in *L. monocytogenes ΔclpP* mutants. a, b Volcano plots of co-IPs with anti-ClpP antibody in *L. monocytogenes ΔclpP1* (**a**) and *ΔclpP2* (**b**) at stationary phase (37 °C). $-\text{Log}_{10}$ *p*-values from two-sample Student's *t*-test are plotted against $\log_2$ ratios of LFQ protein intensities. The vertical grey lines show 4-fold enrichment, the horizontal grey lines show *p*-value = 0.05 (n = 4). Oxidoreductases are highlighted with purple. ClpP1 and ClpP2 are shown in orange and blue respectively.

451 significantly enriched proteins were found for ClpP1 and 469 for ClpP2 (fig. 31), which is much more than in case of the anti-Myc antibody. One reason for this is that the anti-ClpP antibody is more promiscuous than the anti-Myc antibody therefore a higher background was detected. On the other hand, the heterologous C-terminal 2×myc tag are in close proximity to the hydrophobic pockets of ClpP (see section 4.2.4) and thus might interfere with chaperone binding. This can lead to the loss of interaction partners such as the chaperones themselves, adaptor proteins and substrates.

Overall, the co-IP results revealed two groups of proteins: a) chaperones and adaptor proteins that engage in a classical protein-protein interaction with ClpP and b) protein substrates that are bound to the chaperones and adaptors which are digested by ClpP. From the co-IP results alone, it is not possible to assign the hits to one of these groups, therefore more in-depth data analysis was required.

5.2.6. Integrated proteomic analysis of ClpP1 and ClpP2 cellular functions

In the *clpP* deletion mutants, ClpP substrates are expected to accumulate, because they cannot get degraded. In order to decipher these putative substrates, we looked at common hits in the whole proteome analyses of the Δ*clpP* strains and in the co-IPs with anti-ClpP antibody (fig. 32a). The proteins that were only enriched in the co-IP and not in the Δ*clpP* strains were regarded as putative interaction partners.

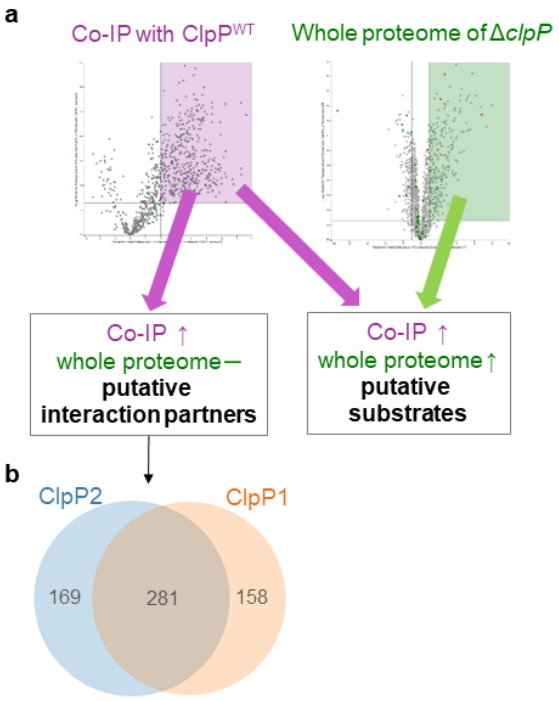

Figure 32 Proteomic analysis of the cellular functions of the ClpP isoforms. **a** Proteins were classified as putative ClpP substrates (see table 5) if they were significantly enriched both in the whole-proteome analysis and in the anti-SaClpP co-IP of the respective Δ*clpP* mutants. Proteins that were significantly enriched only in the co-IP were classified as putative interaction partners of ClpP. **b** Venn-diagram showing the putative interaction partners of ClpP1 and ClpP2.

Most of the putative interaction partners are common for both proteases (fig. 32b). In this protein group, the biological processes of amino acid metabolism and ribonucleoside metabolism are significantly upregulated suggesting an important role of ClpP in the general cellular metabolism. ClpX was identified as a specific interaction partner of solely ClpP2 which is corroborated by structural and activity data demonstrating that ClpP1 is not able the bind ClpX because it lacks the hydrophobic binding pockets needed for association with chaperones.[14,161] The large number of putative interactors (450 for ClpP1 and 440 for ClpP2) emphasizes that unspecific binders are among these proteins.

Only two proteins were significantly upregulated in the Δ*clpP1* mutant which were not enriched in the co-IP. This lack of ClpP1 substrates was expected as ClpP1 is only active in complex with ClpP2. In this complex, ClpP2 determines the substrate specificity because of its interactions with the AAA+ chaperones.

In the case of ClpP2, 26 putative substrates were identified with this method (table 5). The analogs of three proteins are known ClpP substrates in other bacteria, namely MecA, LexA and

catalase.[27,167]

Table 5 List of putative ClpP2 substrates. *The functions of not annotated proteins were derived from BLAST searches.

Gene	Uniprot ID	Description
lmo1350 (*gcvPB*)	Q8Y7D3	Probable glycine dehydrogenase (decarboxylating) subunit 2
lmo1605 (*murC*)	Q8Y6S8	UDP-*N*-acetylmuramate-L-alanine ligase
lmo2190 (*mecA*)	Q9RGW9	ClpC adapter protein MecA
lmo2526 (*murA*)	Q8Y4C4	UDP-*N*-acetylglucosamine 1-carboxyvinyltransferase 1
lmo0485	Q8Y9P0	Putative oxidoreductase, iron response*
lmo0487	Q8Y9N8	Putative hydrolase*
lmo0582 (*iap*)	P21171	Invasion-associated protein p60
lmo0640	Q8Y993	Putative oxidoreductase*
lmo0823	Q8Y8S1	Putative oxidoreductase*
lmo0930	Q8Y8H4	Putative lactamase*
lmo1302 (*lexA*)	Q8Y7H7	LexA SOS response repressor
lmo1320 (*polC*)	Q8Y7G1	PolC-type DNA polymerase III
lmo1381 (*acyP*)	Q8Y7A7	Acylphosphatase (pyruvate metabolism)
lmo1406 (*pflB*)	Q8Y786	Pyruvate formate-lyase (pyruvate metabolism)
lmo1515	Q8Y711	Similar to CymR cystein metabolism repressor*
lmo1538 (*glpK*)	Q8Y6Z2	Glycerol kinase (glycerol metabolism)
lmo1921	Q8Y5Y2	Unknown function
lmo1932	Q8Y5X2	Putative heptaprenyl diphosphate synthase (menaquinone biosynthesis)*
lmo2168	Q8Y5A1	Putative lactoylglutathione lyase*
lmo2182	Q8Y587	Putative ferrichrome ABC transporter ATP-binding protein*
lmo2205 (*gpmA*)	Q8Y571	2,3-Bisphosphoglycerate-dependent phosphoglycerate mutase (glycolysis)
lmo2743 (*tal1*)	Q8Y3T8	Probable transaldolase 1 (pentose phosphate pathway)
lmo2755	Q8Y3S6	Putative dipeptidyl-peptidase activity*
lmo2759	Q8Y3S3	Macro domain-containing protein (putative ADP-ribose binding)
lmo2785 (*kat*)	Q8Y3P9	Catalase (H_2O_2 detoxification)
lmo2829	Q8Y3K6	Putative nitroreductase*

LexA, the repressor of the SOS regulon, is a known ClpP target in *E. coli* and in *S. aureus*.[27,157] During the activation of the SOS response, LexA undergoes autocleavage and the N- and C-

terminal domains get separated.[59] Consequently, the ClpX recognition sequence gets exposed and the NTD (in some organisms also the CTD) is degraded by ClpXP.[157] While we were unable to detect any peptides that stretch across the autocleavage site, the fact that many SOS response genes were upregulated in both Δ*clpP2* and Δ*clpP1/2* suggests that the cleaved form of LexA accumulated, which can only weakly bind to the SOS box. It has been shown that various genes are repressed to different levels by the NTD of LexA.[157] It is possible, that only the upregulated SOS genes are independent of the NTD and the rest are repressed by it.

Another known substrate, MecA is an adaptor protein of ClpC, which is necessary to shift ClpC into the active hexameric state. After it delivers the target to ClpCP it also gets digested by ClpP.[157,168]

Six of the 26 substrates are oxidoreductases and four other proteins are associated with oxidative stress (LexA, Lmo1515 CymR analog, Lmo2168 putative lactoylglutathione lyase and Lmo2182 ferrichrome ABC transporter). One of the oxidoreductases, catalase is also a ClpP substrate in *E. coli*.[27] The abundance of these protein hits among the identified substrates suggests that ClpP plays a crucial role in the redox homeostasis of the cells.

In order to see how the Δ*clpP* mutants react to oxidative stress, we cultivated the respective strains in medium supplemented with H_2O_2 (fig. 33). Surprisingly, only Δ*clpP1/2* could grow in the presence of 100 ppm H_2O_2. This is in line with the observation that the SOS response was significantly upregulated in Δ*clpP1/2* and not in Δ*clpP1* and in Δ*clpP2*. In *L. monocytogenes*[64] and in *E. coli*[156] the SOS response is induced by H_2O_2. Thus a constitutively upregulated SOS response system readily protects cells from H_2O_2 effectively in the Δ*clpP1/2* strain. Although in Δ*clpP2* the oxidoreductases are upregulated, this is not sufficient for H_2O_2 protection. Additional deletion of *clpP1* is therefore necessary for suffitient SOS response induction, even though the single deletion of *clpP1* has only a minor effect on the phenotype and on the proteome of *L. monocytogenes*.

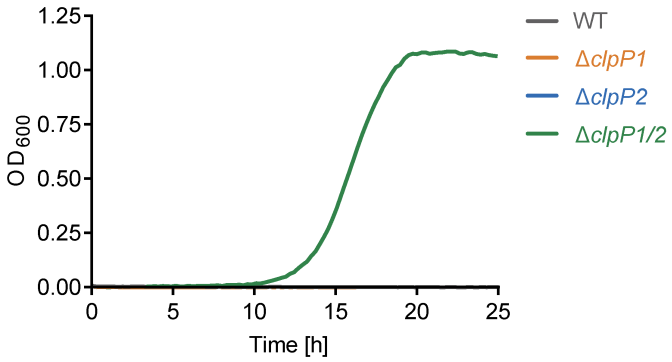

Figure 33 *L. monocytogenes* Δ*clpP1/2* is resistant against oxidative stress. Growth curves of the Δ*clpP* mutants in the presence of 100 ppm H_2O_2 (BHI medium, 37 °C). Note that the WT strain and the single *clpP* knockouts show no growth under these conditions. Means of triplicates are shown. The experiment was independently repeated with qualitatively identical results (data not shown).

5.3. Conclusion

ClpP is a conserved heat shock protein in bacteria and in eukaryotic organelles. Some organisms have more than one *clpP* gene, but the role of multiple ClpPs in these organisms is not well understood. In bacteria, it is known that two different ClpPs are able to form heterocomplexes that are either the only active form or are more active than the homocomplexes.[13,14,16] Here we examined the biological role of ClpP1/2 heterocomplex formation in *L. monocytogenes* and the specific physiological functions of both ClpPs.

We showed that ClpP1 and ClpP2 do not bind to each other at 10 °C, and under these conditions ClpP2is a homotetradecamer with low activity and ClpP1 an inactive heptamer. At high temperatures, especially above 37 °C, the ClpP1/2 heterocomplex is formed displaying enhanced activity. We suspect that this trait is important for modulation of ClpP proteolytic activity and is therefore crucial for stress response and virulence regulation. In order to study this effect in intact *L. monocytogenes* cells, we performed MS-based co-IP experiments at various temperatures. We observed enhanced ClpP1 binding to the bait ClpP2 at 42 °C as compared to 20 °C, which indeed indicates that temperature affects intracellular heterooligomer formation. However, there was no difference when we used ClpP1 as bait. Further research is needed to investigate the exact conditions under which heterooligomerization takes place and elucidate whether other factors such as other binding partners or post-translational modifications can modulate ClpP1/2 complex formation.

With the aim of dissecting the physiological functions of each ClpP isoforms, we constructed single and double *clpP* deletion mutants in *L. monocytogenes* EGD-e. Phenotypic assays showed decreased growth of Δ*clpP1/2* in culture medium and in macrophages. MS-based whole proteome analysis demonstrated that the deletion of *clpP1* only caused minimal changes in the proteome while the Δ*clpP2* and the Δ*clpP1/2* mutants differed greatly from the wild type. In these mutants, class III heat shock proteins and a subset of the SOS response proteins as well as iron-containing proteins were upregulated. These results suggest that ClpP plays an important role in the regulation of oxidative stress response, which is in line with the results of transcriptomic analysis of the *S. aureus* Δ*clpP2* mutant.[166]

We conducted co-IPs in the single mutants with anti-ClpP antibody in order to identify specific ClpP1 and ClpP2 substrates and interaction partners. Combined analysis of the co-IP and whole proteome data led us to the identification of 26 putative ClpP2 substrates and ∼600 putative ClpP1 and ClpP2 interaction partners. Almost half of the putative interaction partners are shared between ClpP1 and ClpP2 and many of them are involved in amino acid and ribonucleoside metabolism. ClpP might have an indirect effect on proteostasis via the interactions with these proteins. A large fraction of the identified ClpP2 substrates are related to oxidative stress. The Δ*clpP1/2* mutant exhibited stronger resistance to H_2O_2 than the wild type and the single mutants, thus we could show that ClpP modulates the cellular redox homeostasis. ClpP2 determines the substrate specificity via the interactions with the AAA+ chaperones, and ClpP1 fine-tunes its activity.

In summary, we found that the ClpP1/2 heterocomplex in *L. monocytogenes* acts as an intracellular thermometer and revealed ClpP's role in coping with oxidative stress. Further research is needed to determine the exact conditions for heterocomplex formation and to validate newly identified ClpP substrates. Studying ClpP heterocomplex formation in other organisms under varying conditions might reveal that thermosensitivity is a general feature of ClpPs in bacteria carrying more than one *clpP* genes. This study and initial data from *M. tuberculosis*, also showing heterooligomerization at elevated temperatures,[83] point in this direction.

5.4. Methods

5.4.1. Protein overexpression and purification

The overexpression and purification of ClpP1/2 is described in section 4.4.2. The overexpression and purification of ClpP2 is described in section 3.4.1. ClpP1 was kindly provided by Dr. Maria Dahmen.[14] Creatine kinase (10 127 566 001) was purchased from Roche.

5.4.2. Analytical size-exclusion chromatography followed by intact protein mass spectrometry

544 nmol $ClpP1_7$ (1:1 ClpP1:ClpP2 monomeric ratio) and/or 272 nmol $ClpP2_{14}$ were incubated for 30 min at the indicated temperatures (0 – 42 °C) in ClpP-GF buffer (20 mM MOPS, 100 mM KCl, 5% glycerol, pH 7.0) in a final volume of 100 µL. The samples were loaded on a pre-equilibrated Superdex 200 10/300 gel filtration column (GE Healthcare) connected to an ÄKTA Purifier 10 system (GE Healthcare) and eluted with 1 CV ClpP-GF buffer. 200 µL fractions were collected. UV absorption was recorded at 280 nm. The oligomerization state was determined by comparison of the elution volumes to the calibration curve of the column (Gel Filtration Calibration Kit, GE Healthcare). The fraction corresponding to the tetradecamer peak was analyzed by intact protein mass spectrometry as described in section 3.4.4. The experiments with a mixture of $ClpP1_7$ and $ClpP2_{14}$ at 20 °C and at 42 °C were repeated with qualitatively identical results. Plots were made with Microcal OriginPro 2018.

5.4.3. Protease assay

Protease assays were carried out in flat bottom black 96-well plates in a final volume of 60 µL. 0.1 µM $ClpP2_{14}$ or a mixture of 0.2 µM $ClpP1_7$ and 0.1 µM $ClpP2_{14}$ (1:1 ClpP1:ClpP2 monomeric ratio), $ClpX_6$ (0.4 µM) and ATP regeneration mix (4 mM ATP, 16 mM creatine phosphate, 20 U/mL creatine kinase) were pre-incubated for 30 min at the indicated temperatures (30 °C, 37 °C and 42 °C) in PZ buffer (25 mM HEPES, 200 mM KCl, 5 mM $MgCl_2$, 1 mM DTT, 10% glycerol, pH 7.6). 0.4 µM eGFP-LmSsrA substrate was added and fluorescence (485 nm, 535 nm) was measured at the respective temperatures with an infinite M200Pro plate reader (Tecan). Data were recorded in triplicate. The measurements were independently repeated with qualitatively identical results. Protease activity was determined by linear regression using Microsoft Excel and plots were made with GraphPad Prism 6.

5.4.4. Cloning of *L. monocytogenes* mutants

Generation of *L. monocytogenes clpP1(191)*::2×myc and *L. monocytogenes clpP2(199)*:: 2×myc

Construction of pLSV101_clpP-2×myc shuttle vectors Ca. 1000 base pairs upstream and downstream from the C-terminus of *clpP1* were amplified by PCR using the A–B and C–D primer pairs from table 6 (Phusion polymerase, GC buffer, NEB). For *clpP2*, ca. 700 bp upstream and downstream were amplified using the A–B and C–CD primer pairs from table 6 (Phusion polymerase, GC buffer, NEB). The 2×myc tag was added to the B primers as overhangs. The PCR products were purified with E.Z.N.A. Cycle Pure Kit (Omega Bio-tek). The AB fragments were digested with SalI-HF (NEB) and BglII (Promega), the CD fragments were digested with BglII (Promega) and BamHI (NEB) and the empty pLSV101 vector was digested with SalI-HF and BamHI-HF (NEB). The digested DNAs were purified with E.Z.N.A. Gel Extraction Kit (Omega Bio-tek) after agarose gel electrophoresis. The AB and CD fragments were ligated with T4 DNA ligase (NEB) (1:1 molar ratio, 15 °C, overnight). The ligated fragments were amplified by PCR (Phusion polymerase, HF buffer) using the clpP1_A–clpP1D and clpP2_A–clpP2_CD primer pairs (table 6). The PCR products were purified with E.Z.N.A. Gel Extraction Kit (Omega Bio-tek) after agarose gel electrophoresis. The ABCD fragments were digested with SalI-HF and BamHI-HF (NEB) and dephosphorylated with Antarctic phosphatase (NEB). The fragments were purified with E.Z.N.A. Gel Extraction Kit (Omega Bio-tek) after agarose gel electrophoresis. The fragments were ligated into the pLSV101 vector (1:1 and 3:1 molar ratios) with T4 DNA ligase (NEB) (10 °C for 30 s and 30 °C for 30 s alternating overnight). The ligated vectors were transformed into chemically competent *E. coli* TOP10. *E. coli* containing pLSV101 was grown with 200 µg/mL erythromycin. Colonies were tested with colony PCR using pLSV101_seq fwd and rev primers (table 6). The vectors were purified from positive colonies with NucleoSpin Plasmid EasyPure, Mini kit (MACHEREY-NAGEL) (elution with ddH_2O) and sequenced by Sanger sequencing with A and D primers.

Preparation of electrocompetent L. monocytogenes 200 mL BHI medium (7.5 g/L brain infusion, 1 g/L peptone, 10 g/L heart infusion, 5 g/L NaCl, 2.5 g/L Na_2HPO_4, 2 g/L glucose, pH 7.4) was inoculated to an initial OD_{600} of 0.05 with an overnight culture of *L. monocytogenes* EGD-e. The culture was grown to $OD_{600} = 0.5$ at 37 °C, 200 rpm. 5 µg/mL penicillin G was added, and the bacteria were incubated at 37 °C, 200 rpm for 15 min and on ice without shaking for 10 min. The cells were harvested (4000 g, 10 min, 4 °C) and washed with 30 mL ice-cold SMHEM medium (952 mM saccharose, 3.5 mM $MgCl_2$, 7 mM HEPES, pH 7.2). The pellet was resuspended in 2 mL cold SMHEM medium. 100 µL aliqots were prepared and shock-frozen in liquid N_2 and stored at −80 °C.

Transformation into L. monocytogenes Electrocompetent *L. monocytogenes* EGD-e aliquots were thawed on ice and 1 µg plasmid was added. The cells were transferred into ice-cold 2 mm electroporation cuvettes (Bio-Rad) and electroporated (2500 V, 200 Ω, 25 µF, exponential decay, time constant < 4 ms) using Gene Pulser Xcell (Bio-Rad). 1 mL BHI medium + 0.5 mM saccharose was added and the cells were incubated at 30 °C for 4 h and plated on BHI agar plates containing 10 µg/mL erythromycin. The plates were incubated at 30 °C for 3 days.

Table 6 List of primers used for the genomic insertion of 2×myc tag into *L. monocytogenes*.

Primer	Sequence (5'→3')
clpP1_A	GTTGCAGTCGACAGGAGGAAACCATGCAAGAG
clpP1-Myc_B	TTAGATCTAAATCTTCTTCACTAATTAATTTTTGTTCTAAATCTTCTTCACTAATTA ATTTTTGTTCTTTTAAGCCATCGCGATTTTCG
clpP1_C	CGGCAGATCTATAAAACCAAAAGGTTCACTTC
clpP1_D	CTTTATGGATCCTTGATCCGGTCACTCCAG
clpP2_A	GTTGCAGTCGACACAGGAGGAATCTTGATATGAAC
clpP2-Myc_B	TTAGATCTAAATCTTCTTCACTAATTAATTTTTGTTCTAAATCTTCTTCACTAATTA ATTTTTGTTCGCCTTTTAAGCCAGATTTATTAATG
clpP2_C	CGGCAGATCTCTAATAAAAAAAGAGGTTTTGCAC
clpP2_CD	CTTTATGGATCCTTCTGCAGTTCTAACAGGAGT
pLSV101_seq fwd	AGTACCATTACTTATGAG
pLSV101_seq rev	AGGGTTTTCCCAGTCACG
clpP1_tag fwd	CGTAATTTCTGGCTTTCTG
clpP1_tag rev	GAGTGATAAATGAATTAGGTCAAG
clpP2_tag fwd	GCGATACAGATCGTGATAATTTC
clpP2_tag rev	GAATACTAGTGTATACATTCTATGGAAG

Homologous recombination and colony selection 2.5 mL BHI medium with 10 μg/mL erythromycin was inoculated with single colonies after transformation. 10^{-2} and 10^{-6} dilutions were plated on BHI + 10 μg/mL erythromycin agar plates and incubated at 42 °C for 2 days. Colony PCR (OneTaq polymerase, NEB) with the respective primer pairs clp_A–pLSV101_seq rev and pLSV101_seq fwd–clp_D (table 6) was performed to check the genomic integration of the fragments. Positive colonies were subcultivated several times in 3 mL BHI medium without antibiotic at 30 °C (200 rpm). 10^{-6} dilutions were plated on BHI agar plates (37 °C, overnight). Single colonies were picked and transferred to BHI agar plates with and without 10 μg/mL erythromycin (37 °C, overnight). Erythromycin sensitive strains were tested with colony PCR (OneTaq DNA polymerase, NEB) using the clpP_tag fwd and rev primer pair (table 6) to check for integration of the 2×myc tag into the genome.

Generation of *L. monocytogenes* Δ*clpP1*

These experiments were conducted by Dr. Christian Fetzer.

Construction of pMAD_ΔclpP1 shuttle vector Approx. 1000 bp upstream (clpP1_KO_A and clpP1_KO_B, table 7) region of clpP1 was amplified by PCR (GC buffer, Phusion polymerase, NEB) using isolated *L. monocytogenes* EGD-e DNA as template. The PCR product was purified (Cycle Pure Kit, E.Z.N.A., Omega Bio-tek) and digested with MluI and NcoI (Promega, standard protocol). pMAD plasmid was also digested with MluI and NcoI and dephosphorylated by addition of TSAP (Promega, streamlined restriction digestion protocol) for 20 min. After restriction digest products were purified (MicroElute DNA Clean-Up Kit, E.Z.N.A., Omega Bio-tek). Ligation into pMAD vector was conducted using T4 DNA Ligase (Promega, standard protocol) overnight at 8 °C and a vector:insert ratio of 1:6. The ligation product (pMAD-AB) was

chemically transformed into *E. coli* TOP10 cells and plated onto LB agar containing ampicillin. Accordingly, a 1000 bp downstream (clpP1_KO_C and clpP1_KO_D, table 7) region of clpP1 was amplified by PCR (GC buffer, Phusion polymerase, NEB) using isolated *L. monocytogenes* EGD-e DNA as template. The PCR product was purified (Cycle Pure Kit, E.Z.N.A., Omega Bio-tek) and digested with MluI and BamHI (Promega, standard protocol). pMAD-AB plasmid was also digested with MluI and BamHI and dephosphorylated by addition of TSAP (Promega, streamlined restriction digestion protocol) for 20 min. After restriction digest products were purified (MicroElute DNA Clean-Up Kit, E.Z.N.A., Omega Bio-tek). Ligation into pMAD-AB vector was conducted using T4 DNA Ligase (Promega, standard protocol) overnight at 8 °C and a vector:insert ratio of 1:6. Insertion of the desired construct was tested after plasmid extraction (Plasmid Mini Kit I, E.Z.N.A., Omega Bio-tek) by analytical restriction digest and sequencing (pMAD-seq-for and pMAD-seq-rev, table 7).

Table 7 List of primers used for the construction *L. monocytogenes clpP* deletion mutants.

Primer	Sequence (5'→3')
clpP1_KO_A	GGACCATGGTTTCATCAGCAAACCTCCGCAC
clpP1_KO_B	GGAACGCGTGAAAAAATTCCTCCTTAAAAAGCCTTAGTTTATTTG
clpP1_KO_C	GGAACGCGTAAGCAAAAGATTACGGCATCG
clpP1_KO_D	GGAGGATCCTTGATCCGGTCACTCCAGTA
pMAD-seq-for	CCCAATATAATCATTTATCAACTCTTTTACACTTAAATTTCC
pMAD-seq-rev	GCAACGCGGGCATCCCGATG
clpP2_KO_A	CGAACAGTGTAAGTGTATGCG
clpP2_KO_B	AGTTTGAGATCTTACTGTTGGAATTAAGTTCAT
clpP2_KO_C	TACGGCAGATCTGATGATATTATCATTAATAAA
clpP2_KO_D	TTGCATTTGTAGTGGTTATGG
clpP2_AB	GTTGCAGTCGACTCTAACGATGATCTTGTTAGT
clpP2_CD	CTTTATGGATCCTTCTGCAGTTCTAACAGGAGT

Preparation of electrocompetent L. monocytogenes 100 mL of BM medium (10 g/L soy peptone, 5 g/L yeast extract, 5 g/L NaCl, 1 g $K_2HPO_4 \times 3\ H_2O$, 1 g/L glucose, pH 7.4–7.6) were inoculated with 1 mL (1:100) from a *L. monocytogenes* EGD-e overnight culture and incubated at 37 °C until an OD_{600} of 0.5 was reached. Cells were centrifuged (5000 g, 15 min, 4 °C) and washed three times with cold 10% glycerol (sterile): 1.) 100 mL; 2.) 50 mL; 3.) 25 mL. The pellet was resuspended in 400 µL cold 10% glycerol and 75 µL aliquots were frozen in liquid nitrogen and stored at −80 °C.

Transformation into L. monocytogenes Electrocompetent *L. monocytogenes* was thawed at room temperature (RT) and incubated for 10 min with > 1 µg plasmid. The suspension was transferred into a 0.1 cm electroporation cuvette (Bio-Rad) and electroporated (exponential, 25 µF, 1 kV, 400 Ω) using a Gene Pulser Xcell (Bio-Rad). Immediately after the pulse 1 mL pre-warmed BM medium was added and incubated at 30 °C for 90 min. The cell suspension was streaked onto BM agar containing selective antibiotic + X-gal and incubated until colonies were visible.

Selection protocol – pMAD After successful transformation into *L. monocytogenes* EGD-e, indicated by blue colonies, single colonies were picked and incubated overnight at 30 °C in the presence of 1 µg/mL erythromycin. 10 mL BM medium were inoculated 1:1000 from the overnight culture and incubated 2 h at 30 °C and 6 h at 42 °C. 100 µL diluted cultures (10^{-2} to 10^{-6}) were plated onto BM agar (containing 1 µg/mL erythromycin and 100 µg/mL X-gal) and incubated at 42 °C until colonies with blue coloration were visible (enrichment of single crossover). Ten light blue colonies were picked and incubated (together) in 10 mL BM medium at 3 °C for 8 h followed by overnight incubation at 42 °C. 10 mL BM medium were inoculated 1:1000 from this overnight culture and grown for 4 h at 30 °C and additional 4 h at 42 °C. 100 µL of diluted cultures (10^{-2} to 10^{-6}) were plated onto BM agar containing X-gal and incubated at 4 °C. White colonies were picked and streaked onto BM agar containing erythromycin and X-gal and onto BM agar containing only X-gal. Plates were incubated at 30 °C and erythromycin susceptible colonies further analyzed by colony PCR followed by analytical restriction digest and sequencing. For colony PCR small parts of colonies were resuspended in 50 µL sterile water and 1 µL thereof was used in PCR reactions with an initial denaturation step for 10 min (95 °C).

Generation of *L. monocytogenes* Δ*clpP1* and Δ*clpP1/2*

Construction of pLSV101_ΔclpP2 shuttle vector Ca. 1000 base pairs upstream and downstream from the *clpP2* gene were amplified by PCR using the A–B and C–D primer pairs from table 7 (Phusion polymerase, GC buffer, NEB). The PCR products were purified with E.Z.N.A. Gel Extraction Kit (Omega Bio-tek) after agarose gel electrophoresis. The fragments were digested with BglII (Promega) and purified with E.Z.N.A. Cycle Pure Kit (Omega Bio-tek). The AB and CD fragments were ligated with T4 DNA ligase (NEB) (1:1 molar ratio, 15 °C, overnight). The ligated fragment was amplified by PCR (Phusion polymerase, HF buffer) using the AB–CD primer pair (table 7). The PCR product was purified with E.Z.N.A. Cycle Pure Kit (Omega Bio-tek). The insert and the empty pLSV101 vector were digested with SalI-HF and BamHI-HF (NEB) and purified with E.Z.N.A. Gel Extraction Kit (Omega Bio-tek) after agarose gel electrophoresis. The fragment was ligated into the pLSV101 vector (3:1 molar ratio) with T4 DNA ligase (NEB) (16 °C overnight). The ligated vector was transformed into chemically competent *E. coli* TOP10. *E. coli* containing pLSV101_ΔclpP2 was grown with 300 µg/mL erythromycin. Colonies were tested with colony PCR using pLSV101_seq fwd and rev primers (table 6). The vectors were purified with E.Z.N.A. Plasmid Mini Kit I (Omega Bio-tek) from positive colonies (elution with ddH_2O) and sequenced by Sanger sequencing with pLSV101_seq fwd and rev primers.

Transformation into L. monocytogenes Electrocompetent *L. monocytogenes* EGD-e and Δ*clpP1* cells were prepared as described on page 67. Aliquots of electrocompetent cells were thawed on ice and 2 or 5 µg plasmid was added. The cells were transferred into ice-cold 2 mm electroporation cuvettes (Bio-Rad) and electroporated (2500 V, 200 Ω, 25 µF, exponential decay, time constant ~ 4 ms) using Gene Pulser Xcell (Bio-Rad). 1 mL warm BHI medium was added and the cells were incubated at 30 °C for 6 h under shaking at 200 rpm and plated on BHI agar plates with 10 µg/mL erythromycin. The plates were incubated at 30 °C for 5 days.

Homologous recombination and colony selection 2.5 mL BHI medium with 10 µg/mL erythromycin was inoculated with single colonies after transformation. 10^{-2} and 10^{-5} dilutions were plated on BHI + 10 µg/mL erythromycin agar plates and incubated at 42 °C for 2 days. Colony PCR (OneTaq polymerase, NEB) with the primer pairs clp2_KO_A–pLSV101_seq rev and pLSV101_seq fwd–clpP2_KO_D (see tables 6 and 7) was performed to check the genomic integration of the fragments. Positive colonies were subcultivated several times in 2.5 mL BHI medium without antibiotic at 30 °C (200 rpm). 10^{-6} dilutions were plated on BHI agar plates (RT, 3 days). Single colonies were picked and transferred to BHI agar plates with and without 10 µg/mL erythromycin (37 °C, overnight). Erythromycin sensitive strains were tested with colony PCR (OneTaq DNA polymerase, NEB) using the clpP2_KO_A and clpP2_KO_D primer pair (table 7) to check for *clpP2* deletion.

5.4.5. Western blot

5 mL BHI medium was incolulated with *L. monocytogenes* EGD-e, Δ*clpP1*, Δ*clpP2* and Δ*clpP1/2* strains. An amount of cells corresponding to 200 µL of $OD_{600} = 20$ of each mutant was harvested (4000 g, 10 min, 4 °C). The cells were lysed by ultrasonication (3×20 s, 75%, cooled on ice during breaks). 2× Laemmli buffer was added and 20 µL sample was separated by SDS-PAGE (12,5% polyacrylamide, 150 V, 2.5 h). The proteins from the polyacrylamide gel were transferred to a methanol-soaked PVDF membrane (Bio-Rad) in a Trans-Blot SD semi-dry western blot cell (Bio-Rad) using blotting buffer (48 mM Trizma, 39 mM glycine, 0.04% SDS, 20% methanol) (10 V, 1 h). The membrane was blocked with 5% milk powder in PBS-T (0.5% Tween-20 in PBS) for 1 h at RT and subsequently inbucated with rabbit polyclonal anti-ClpP antibody (raised against *S. aureus* ClpP, 2 mg/mL, 1:1000 dilution) in PBS-T + 5% milk powder (4 °C, overnight). The membrane was washed three times with PBS-T (15 min, RT) and incubated with Pierce Goat anti-Rabbit poly-HRP secondary antibody (1:10 000, Thermo Scientific) in PBS-T + 5% milk powder (1 h, RT). The membrane was washed three times with PBS-T (15 min, RT) and chemiluminescence was detected after 10 min incubation with freshly prepared Clarity Western ECL Substrate (Bio-Rad) with LAS-4000 gel scanning station (Fujitsu Life Sciences).

5.4.6. Fluorescent labelling

25 mL BHI medium was inoculated with *L. monocytogenes* EGD-e, Δ*clpP1*, Δ*clpP2* and Δ*clpP1/2* from a day culture to an initial OD_{600} of 0.05. The culture was grown to early stationary phase and an amount corresponding to 800 µL $OD_{600} = 20$ was harvested (4000 g, 4 °C, 10 min). The cells were washed with 1 mL PBS (4000 g, 4 °C, 5 min). The pellets were resuspended in 800 µL PBS and aliquots of 250 µL were prepared. 2.5 µL 5 mM vibralactone probe (or 5 mM D3 or DMSO as controls) from a DMSO stock was added to all strains (2 h, RT). The cells were centrifuged (4000 g, 5 min, 4 °C), the supernatant was discarded, and the pellets were washed with 1 mL PBS (4000 g, 5 min, 4 °C). The pellets were stored at −80 °C until further usage. The cells were resuspended in 250 µL PBS and transferred to 2 mL tubes containg 0.5 mL inlets filled with glass beads of 0.5 mm diameter. The cells were lysed using 2× program #2 in Precellys 24 tissue homogenizer (Bertin Instruments) coupled to liquid N_2-cooled Cryolys (flow

rate set to level I during shaking, level 0 during breaks). 200 µL of the lysates were pipetted into microcentrifuge tubes and the insoluble fractions were separated (10 000 g, 30 min, 4 °C). To 88 µL of the supernatant Click reagents were added [2 µL 5 mM rhodamine azide, 2 µL 15 mg/mL TCEP, 6 µL 1.67 mM tris((1-benzyl-4-triazolyl)methyl)amine ligand and 2 µL 50 mM $CuSO_4$] and the reactions were incubated in the dark for 1 h at RT. 2×Laemmli buffer was added and the samples were stored at −20 °C until further usage. 50 µL of the samples were separated by SDS-PAGE (12.5% polyacrylamide, 150 V, 3 h) and fluorescence was detected with LAS-4000 gel scanning station (Fujitsu Life Sciences).

5.4.7. Growth curves of *L. monocytogenes* mutants

In the inner wells of a transparent flat-bottom 96-well plate, 200 µL BHI medium (if required, supplemented with 100 ppm H_2O_2) were inoculated to a starting OD_{600} of 0.01 with overnight cultures of *L. monocytogenes* EDG-e and its mutants (Δ*clpP1*, Δ*clpP2* and Δ*clpP1/2*) or left sterile for blank measurements. The outer wells of the plate were filled with 200 µL BHI medium but were not measured. The plate was covered with a transparent lid and was incubated at 37 °C with 5 s shaking every 15 min in an infinite M200Pro plate reader (Tecan). OD_{600} was measured every 15 min for 24 h. Data was recorded in triplicates and at least two independent experiments were conducted with qualitatively identical results. Plots were made with GraphPad Prism 6.

5.4.8. Intracellular growth assay

Cultivation of the J774A.1 cell line J774A.1 murine macrophage-like cells were grown in tissue culture flasks with hydrophobic surface for suspension cells in DMEM/FCS (DMEM high glucose medium (Sigma) supplemented with 2 mM glutamine and 10% heat-deactivated FCS). The flasks were incubated at 37 °C under 5% CO_2. The cells were splitted into new flasks every 2–3 days to ca. 5×10^4 cells/cm^2. For detachment, cells were washed twice with TEN buffer (40 mM Tris-HCl, 150 mM NaCl, 1 mM EDTA, pH 7.4) and incubated with Accutase solution (Sigma) at 37 °C for 30 min.

Intracellular growth assay 10^5 J774A.1 cells in 100 µL DMEM/FCS were pipetted into the inner wells of a flat-bottom 96-well plate. The outer wells were filled with 150 µL sterile PBS. The plates were incubated overnight at 37 °C under 5% CO_2. On the next day, DMEM/FCS was inoculated with *L. monocytogenes* EDG-e, Δ*clpP1*, Δ*clpP2* and Δ*clpP1/2* overnight cultures to 10^3 CFU/µL. The J774A.1 cells were washed with 150 µL PBS and 100 µL bacterial suspension was added (multiplicity of infenction = 0.5). The plate was incubated on ice for 15 min and at 37 °C for 15 min. The cells were washed three times with 200 µL PBS. 150 µL DMEM/FCS supplemented with 10 µL gentamycin was added to kill extracellular bacteria. The plates were incubated at 37 °C under 5% CO_2. After 7 h, the cells were washed three times with 200 µL PBS, and lysed with 2× 100 µL 0.05% Triton X-100 in ddH_2O (1 min, RT). Dilution series were prepared from the lysates and plated on BHI agar plates. The agar plates were incubated at 37 °C for 2 days until colonies were counted. Data was recorded in triplicates and two independent experiments were performed. Plots were made with GraphPad Prism 6.

5.4.9. Whole-proteome analysis

Cultivation of L. monocytogenes 3×5 mL BHI medium (3 technical replicates) were inoculated 1:100 with overnight cultures of *L. monocytogenes* EGD-e, Δ*clpP1*, Δ*clpP2* and Δ*clpP1/2*. The first day culture was grown to an OD_{600} of ca. 0.5 at 37 °C under shaking at 200 rpm. For the second day culture, 3×5 mL BHI medium was inoculated with the first day cultures to a starting OD_{600} of 0.05 and incubated at 37 °C under shaking at 200 rpm. After reaching early stationary phase, 1.5 mL of the cultures were harvested (4000 g, 10 min, 4 °C). The pellet was washed with 1 mL PBS and stored at −80 °C until further usage. Two biological replicates were generated.

Cell lysis and protein precipitation Bacteria were resuspended in 150 µL lysis buffer (1% Triton X-100, 0.5% SDS, 1 tablet cOmplete EDTA-free protease inhibitor cocktail (Roche) in 10 mL PBS) and lysed by ultrasonication (5×20 s, 80%, on ice during breaks). Cell debris was pelletized (5000 g, 10 min, 4 °C) and the supernatant was sterile filtered through a 0.2 µm pore size PTFE filter. Protein concentration was determined with BCA assay (Roti-Quant universal, Roth) and all samples were brought to the same volume and concentration (ca. 1 mg/mL) and were transferred to protein low-bind microcentrifuge tubes (Eppendorf). To precipitate the proteins, 4× sample volume acetone (−80 °C) was added and the samples were stored at −80 °C overnight. The samples were centrifuged at 21 000 g and at 4 °C for 15 min and the supernatant was discarded. The pellet was resuspended in 500 µL methanol (−80 °C) with ultrasonication (10 s, 10%). After centrifugation at 21 000 g and at 4 °C for 15 min, the supernatant was discarded and the pellet was air-dried.

Sample preparation for LC-MS/MS 200 µL X buffer (7 M urea, 2 M thiourea, 20 mM HEPES, pH 7.5) was added and the pellet was resuspended by ultrasonication (10 s, 10%). The samples were reduced by the addition of 0.2 µL 1 M DTT (45 min, RT, 450 rpm), alkylated with 2 µL 0.55 M iodoacetamide (IAA) (30 min, RT, 450 rpm), the reaction was quenched with 0.8 µL 1 M DTT (30 min, RT, 450 rpm). The samples were pre-digested with 0.5 µg/µL LysC (2 h, RT, 450 rpm). For the tryptic digest, 600 µL 50 mM triethylammonium bicarbonate (TEAB) buffer and 0.5 µg/µL trypsin (sequencing grade, modified, Promega) was added (overnight, 37 °C, 450 rpm). The pH was set to < 3 with 10 µL formic acid (FA). The samples were desalted on a Sep-Pak C18 50 mg column (Waters) using gravity flow. The columns were equilibrated with 1 mL MeCN, 0.5 mL 80% MeCN + 0.5% FA and 3× 1 mL 0.1% trifluoroacetic acid (TFA). The samples were loaded on the column and washed with 2× 1 mL 0.1% TFA and with 250 µL 0.5% FA. The peptides were eluted with 3× 250 µL MeCN, 0.5 mL 80% MeCN + 0.5% FA using vacuum in the last step. The solvents were removed under vacuum at 30 °C and the samples were resuspended in 1% FA (volume set to 2 µg/µL protein concentration), with pipetting up and down, 15 min ultrasonication in water bath and vortexing. The samples were filtered through a 0.2 µm pore size centrifugal filter.

LC-MS/MS Samples were analyzed by LC-MS/MS using an UltiMate 3000 nano HPLC system (Dionex) equipped with an Acclaim C18 PepMap100 75 µm ID × 2 cm trap and an Acclaim Pepmap RSLC C18 separation column (75 µm ID × 50 cm) (25cm Aurora Series emitter (column 25 cm × 75µm ID, 1.6 µm C18) in case of the temperature-dependent co-IP with

anti-c-Myc antibody) in an EASY-spray setting coupled to an Orbitrap Fusion (Thermo Fisher Scientific). 4 µL (6 µL in case of the co-IP experiments) were loaded on the trap column with a flow rate of 5 µL/min with 0.1% TFA buffer and then transferred onto the separation column at a flow rate of 0.3 µL/min (0.3 µL/min in case of the temperature-dependent co-IP with anti-c-Myc antibody). Samples were separated using a 152 min gradient (buffer A: H_2O with 0.1% FA, buffer B: MeCN with 0.1% FA, gradient: 5% buffer B for 7 min, from 5% to 22% buffer B in 105 min, then to 32% buffer B in 10 min, to 90% buffer B in 10 min and hold at 90% buffer B for 10 min, then to 5% buffer B in 0.1 min and hold 5% buffer B for 9.9 min). Peptides were ionized using a nanospray source at 1.7–1.9 kV and a capillary temperature of 275 °C. The instrument was operated in a top speed data dependent mode with a cycle time between master scans of 3 s. MS full scans were performed in the orbitrap with quadrupole isolation at a resolution of R = 120 000 and an automatic gain control (AGC) ion target value of 2×10^5 in a scan range of 300–1500 m/z with a maximum injection time of 50 ms. Internal calibration was performed using the ion signal of fluoranthene cations (EASY-ETD/IC source). Dynamic exclusion time was set to 60 s with a mass tolerance of 10 ppm (low/high). Precursors with intensities higher than 5×10^3 and charge states 2–7 were selected for fragmentation with HCD (30%). MS2 scans were recorded in the ion trap operating in a rapid mode with an isolation window of 1.6 m/z. The AGC target was set to 1×10^4 with a maximum injection time of 35 ms (100 ms in case of the temperature-dependent co-IP with anti-c-Myc antibody) and the “inject ions for all available parallelizable time” was enabled.

Data analysis MS raw data were analyzed with MaxQuant 1.6.5.0 and default settings were used, exept for the following: label-free quantification and match between runs were activated. All replicates for one condition (n = 6) were set as one fraction. The UniProt database of *L. monocyotogenes* EGD-e proteins (taxon ID: 169963, downloaded on 25.01.2019.) was searched. Data was further analyzed with Perseus 1.6.2.3. The rows "only identified by site", "potential contaminants" and "reverse" were filtered and the data were $\log_2$-transformed. Replicates were grouped and filtered to at least 4 valid values per at least one group. Missing values were imputed for the total matrix from normal distribution. Two-sample Student’s *t*-tests were performed with default settings. Iron containing proteins were searched for with the UniProt Keyword "Iron". SOS response proteins were identified from van der Veen et al.[64] Abundance corrected UniProt keyword and GOBP term analyses were performed with aGOtool (agotool.sund.ku.dk),[162] cut-off values of fold enrichment ≥ 1.5 and *p*-value ≤ 0.05 were used.

5.4.10. MS-based co-immunoprecipitation

Temperature-dependent co-IP with anti-c-Myc antibody

Cultivation of L. monocytogenes single ΔclpP mutants 30 mL BHI medium were inoculated 1:100 with overnight cultures of *L. monocytogenes clpP1(191)*::2×myc and *L. monocytogenes clpP2(199)*::2×myc. The first day culture was grown to an OD_{600} of ca. 0.5 at 37 °C under shaking at 200 rpm. For the second day culture, 4×100 mL BHI medium was inoculated with the first day cultures to a starting OD_{600} of 0.05. 2 flasks per condition were incubated at 20 °C

and at 42 °C under shaking at 200 rpm. After reaching early stationary phase, an amount of bacteria corresponding to 4×1 mL $OD_{600} = 20$ per flask was harvested (4000 g, 5 min, 4 °C) and washed with 1 mL PBS. The pellets were resuspended in 1 mL PBS and 2 mM DSSO was added (20 µL from a 100 mM DMSO stock). The bacteria were incubated with the crosslinker for 30 min at 20 °C or 42 °C under shaking at 200 rpm. The reaction was quenched by washing twice with 50 mM Tris-HCl (pH 8.0) and the pellets were stored at −80 °C until further usage.

Cell lysis and co-IP Bacteria were resuspended in 800 µL co-IP lysis buffer (50 mM Tris-HCl, 150 mM NaCl, 5% glycerol, pH 7.4) and 120 µL lysosyme was added. The samples were incubated at 37 °C under shaking at 1400 rpm for 1 h. Afterwards, 8 µL 10% NP-40 solution was added and the bacteria were lysed by ultrasonication (5×30 s, 80%, on ice during breaks). The unsoluble fraction was pelletized (10 000 g, 30 min, 4 °C) and the supernatant was sterile filtered through a 0.2 µm PTFE filter. Protein concentration was determined with BCA assay (Roti-Quant universal, Roth). 30 µL Protein A/G agarose beads (Thermo Fischer Scientific) were transferred to protein low-bind microcentrifuge tubes (Eppendorf) and washed with 1 mL co-IP wash buffer (50 mM Tris-HCl, 150 mM NaCl, 5% glycerol, 0.05% NP-40, pH 7.4) and centrifuged for 1 min at 1000 g at 4 °C. 500 µg proteome (in 500 µL) and either 1 µL anti-c-Myc antibody (rabbit polyclonal, ab152146, 1 mg/mL, Abcam) or 0.4 µL isotype control (2.5 mg/mL, Cell Signalling Technology) were added. The samples were incubated at 4 °C for 3 h under constant rotation. The supernatant was removed after centrifugation (1000 g, 1 min, 4 °C), and the beads were washed twice with 1 mL co-IP wash buffer. The detergent was removed by washing the beads twice with co-IP lysis buffer.

Sample preparation for LC-MS/MS The samples were reduced and digested in 25 µL co-IP digest buffer (50 mM Tris-HCl, 5 ng/µL trypsin (sequencing grade, modified, Promega), 2 M urea, 1 mM DTT, pH 8.0) at 25 °C under shaking at 600 rpm for 30 min. For alkylation, 100 µL 50 mM Tris-HCl, 2 mM urea, 5 mM IAA (pH 8.0) was added (25 °C, 600 rpm, 30 min). The digestion was completed overnight at 37 °C under shaking at 600 rpm. The pH was set to < 3 with 0.75 µL FA. The samples were desalted on double layer C18-stage tips (Empore disk-C18, Agilent Technologies). The stage tips were equilibrated with 70 µL methanol and 3× 70 µL 0.5% FA. The samples were loaded and washed with 3× 70 µL 0.5% FA. The peptides were eluted with 3× 30 µL 80% MeCN + 0.5% FA. The solvents were removed under vacuum at 30 °C and the samples were resuspended in 27 µL 1% FA with pipetting up and down, 15 min ultrasonication in water bath and vortexing. The samples were filtered through a 0.2 µm pore size centrifugal filter. LC-MS/MS measurement was conducted as described for the whole proteome analysis (page 73).

Data analysis MS raw data were analyzed with MaxQuant 1.6.10.43. and default settings were used, exept for the following: label-free quantification and match between runs were activated, *N*-acetylation modification was deactivated. All replicates for one condition ($n = 4$) were set as one fraction. The UniProt database of *L. monocyotogenes* EGD-e proteins (taxon ID: 169963, downloaded on 21.10.2019.) was searched. Data was further analyzed with Perseus 1.6.10.43. The rows "only identified by site", "potential contaminants" and "reverse" were filtered and the data were $\log_2$-transformed. Replicates were grouped and filtered to at least 3

valid values per at least one group. Missing values were imputed for the total matrix from normal distribution. Two-sample Student's *t*-tests were performed with default settings.

Co-IP with anti-clpP antibody

2×20 mL BHI medium (two technical replicates) were inoculated 1:100 with overnight cultures of *L. monocytogenes* Δ*clpP1* and Δ*clpP2*. The first day culture was grown to an OD_{600} of ca. 0.5 at 37 °C under shaking at 200 rpm. For the second day culture, 2×50 mL BHI medium was inoculated with the first day cultures to a starting OD_{600} of 0.05 and incubated at 37 °C under shaking at 200 rpm. After reaching early stationary phase, an amount of bacteria corresponding to 2×1 mL $OD_{600} = 20$ per replicate was harvested (4000 g, 5 min, 4 °C) and washed with 1 mL PBS. The pellets were resuspended in 1 mL PBS and 2 mM DSSO was added (20 µL from a 100 mM DMSO stock). The bacteria were incubated with the crosslinker for 30 min at 37 °C and under shaking at 200 rpm. The reaction was quenched by washing twice with 50 mM Tris-HCl (pH 8.0) and the pellets were stored at −80 °C until further usage. Two independent biological replicates were generated.

Cell lysis, co-IP and sample preparation were conducted as described for the temperature-dependent co-IP with anti-c-Myc antibody (page 75), except that either 5 µL anti-ClpP antibody (polyclonal, raised against *S. aureus* ClpP in rabbit, 2 mg/mL) or 4 µL isotype control (2.5 mg/mL, Cell Signalling Technology) were used. LC-MS/MS measurements were performed as described for the whole proteome analysis (page 73).

Data analysis was done as described for the temperature-dependent co-IP with anti-c-Myc antibody (page 75). Oxidoreductases were searched for with the UniProt Keyword "Oxidoreductase".

6. Research conclusion and outlook

The aim of this thesis was the in-depth functional and structural characterization of the ClpXP1/2 protease complex from *L. monocytogenes*. It was already known that there are two ClpP proteins in *L. monocyotogenes* of which ClpP1 is inactive and ClpP2 is very similar to other bacterial ClpP proteases.[7,9] It has also been discovered that the ClpP1/2 heterocomplex is more active than the ClpP2 homocomplex.[14] But the physiological functions of ClpP1 and the heterocomplex have not been investigated yet. From the structural biology perspective, the crystal structures of $ClpP1_7$, $ClpP2_{14}$, $ClpP1/2_{14}$ from *L. monocyotgenes* and $ClpX_6$ from *E. coli* were available.[7,14,109] However, no high-resolution structures of AAA+ chaperone bound ClpPs from any organisms were published at the start of this work. Therefore the interaction between the two protein complexes, especially the 7/6 symmetry mismatch was not well understood. My goal was to answer the question why *L. monocytogenes* needs a second ClpP and why it builds a heterocomplex. Furthermore, the interactions between ClpP1/2 and ClpX had to be investigated in structural studies.

Looking at the cleavage specificities of ClpP1 and ClpP2, we could show that both enzymes can cleave between any amino acid when bound to ClpX. This characteristic enables ClpP to digest any unfolded or ribosome-stalled protein. We also conducted an inhibitor screening with already known and newly designed ClpP inhibitors. Interestingly, some of the inhibitors overactivated the ClpP2 homocomplex. Detailed kinetic experiments revealed that the reason for this is the enhanced ClpX affinity after partial inhibitor binding. Since then, new ClpP inhibitors with different structures that also activate the protease at low concentrations have been found, suggesting that this seems to be a general activating principle.[169,170] To completely understand this phenomenon, activator-bound ClpP or ClpXP structures are still needed. Enhanced ClpX binding was also observed in case of the ClpP1/2 heterocomplex, which explains its higher activity. Modulation of the affinity between ClpP and the chaperones could be an effective method to regulate proteolytic activity.

The high affinity between ClpP1/2 and ClpX enabled the preparation of stable ClpXP1/2 samples for cryo-EM. With the high-resolution cryo-EM structure, HDX-MS measurements and biochemical assays in hand, we could analyze the binding mode. ClpX binds with all of its IGF loops into six of ClpP's hydrophobic pockets, while the seventh pocket stays empty and is shielded by the C-terminus of ClpP. The interaction between the ClpX pore-2 loops and the ClpP N-termini is also important for binding. Previously, ADEP antibiotics were thought to be ClpX mimics that bind to the same hydrophobic pockets and open up the substrate entry pore of ClpP. Surprisingly, our structure showed that the pore of ClpP is not widened after ClpX binding. This means that the ADEPs have a different binding mode than the chaperone. ClpX unfolds the protein before translocating it into ClpP so ClpX does not need to open up the pore. There are still several unanswered questions about the mechanism of this protein degradation machinery. For example, structures of related complexes such as ClpAP, ClpCP or ClpEP could show how conserved the binding mode is. A structure that shows a substrate spanning from

ClpX to ClpP could bring to light the exact substrate processing mechanisms in both proteins. Another open question is, whether ClpX rotates on ClpP during substrate processing. Our work supplies the basis for designing further studies to answer these questions.

Lastly, we have discovered that ClpP1/2 heterooligomerization occurs at high temperatures. We hypothesize that *L. monocytogenes* cells use this feature to turn on ClpP activity under heat stress and during infection. It is an interesting question whether the presence of a second *clpP* gene in other bacteria is also required for temperature-dependent regulation of protease activity and therefore for transcription factor turnover. Further experiments at different temperatures could reveal the exact in vivo heterooligomerization conditions and its effect on the proteome of *L. monocytogenes*. In-depth proteomics studies revealed that ClpP is not only important for heat stress but also for oxidative stress. The relative large fraction of unannotated proteins in *L. monocytogenes* makes the interpretation of proteomics experiments challenging. Hopefully in the future an increasing number of proteins from less extensively studied organisms will be characterized in order to help researchers to uncover complex biological processes and their regulation.

I hope that my work will contribute to the understanding of the complicated regulatory network in *L. monocytogenes* and can serve as a model for other bacteria as well. The 3D structure of the ClpXP complex gives useful insights for all researchers of Clp proteases due to the high conservation of this ubiquitous complex.

Bibliography

1. Dikic, I. Proteasomal and Autophagic Degradation Systems. *Annual Review of Biochemistry* **86,** 193–224 (2017).
2. Mahmoud, S. A. & Chien, P. Regulated Proteolysis in Bacteria. *Annual Review of Biochemistry* **87,** 677–696 (2018).
3. Bittner, L.-M., Arends, J. & Narberhaus, F. Mini review: ATP-dependent proteases in bacteria. *Biopolymers* **105,** 505–517 (2016).
4. Olivares, A. O., Baker, T. A. & Sauer, R. T. Mechanistic insights into bacterial AAA+ proteases and protein-remodelling machines. *Nature Reviews Microbiology* **14,** 33 (2016).
5. Kirstein, J., Molière, N., Dougan, D. A. & Turgay, K. Adapting the machine: adaptor proteins for Hsp100/Clp and AAA+ proteases. *Nature Reviews Microbiology* **7,** 589–599 (2009).
6. Gersch, M., List, A., Groll, M. & Sieber, S. A. Insights into structural network responsible for oligomerization and activity of bacterial virulence regulator caseinolytic protease P (ClpP) protein. *J Biol Chem* **287,** 9484–94 (2012).
7. Zeiler, E., List, A., Alte, F., Gersch, M., Wachtel, R., Poreba, M., Drag, M., Groll, M. & Sieber, S. A. Structural and functional insights into caseinolytic proteases reveal an unprecedented regulation principle of their catalytic triad. *Proc Natl Acad Sci U S A* **110,** 11302–7 (2013).
8. Yu, A. Y. & Houry, W. A. ClpP: a distinctive family of cylindrical energy-dependent serine proteases. *FEBS Lett* **581,** 3749–57 (2007).
9. Zeiler, E., Braun, N., Bottcher, T., Kastenmuller, A., Weinkauf, S. & Sieber, S. A. Vibralactone as a tool to study the activity and structure of the ClpP1P2 complex from Listeria monocytogenes. *Angew Chem Int Ed Engl* **50,** 11001–4 (2011).
10. Benaroudj, N., Raynal, B., Miot, M. & Ortiz-Lombardia, M. Assembly and proteolytic processing of mycobacterial ClpP1 and ClpP2. *BMC biochemistry* **12,** 61 (2011).
11. Lavey, N. P., Shadid, T., Ballard, J. D. & Duerfeldt, A. S. Clostridium difficile ClpP homologues are capable of uncoupled activity and exhibit different levels of susceptibility to acyldepsipeptide modulation. *ACS infectious diseases* **5,** 79–89 (2018).
12. Hall, B. M., Breidenstein, E. B., de la Fuente-Núñez, C., Reffuveille, F., Mawla, G. D., Hancock, R. E. & Baker, T. A. Two isoforms of Clp peptidase in Pseudomonas aeruginosa control distinct aspects of cellular physiology. *Journal of bacteriology* **199,** e00568–16 (2017).
13. Pan, S., Malik, I. T., Thomy, D., Henrichfreise, B. & Sass, P. The functional ClpXP protease of Chlamydia trachomatis requires distinct clpP genes from separate genetic loci. *Scientific reports* **9,** 1–14 (2019).

14. Dahmen, M., Vielberg, M. T., Groll, M. & Sieber, S. A. Structure and mechanism of the caseinolytic protease ClpP1/2 heterocomplex from Listeria monocytogenes. *Angew Chem Int Ed Engl* **54,** 3598–602 (2015).

15. Akopian, T., Kandror, O., Raju, R. M., Unnikrishnan, M., Rubin, E. J. & Goldberg, A. L. The active ClpP protease from M. tuberculosis is a complex composed of a heptameric ClpP1 and a ClpP2 ring. *Embo J* **31,** 1529–41 (2012).

16. Li, M., Kandror, O., Akopian, T., Dharkar, P., Wlodawer, A., Maurizi, M. R. & Goldberg, A. L. Structure and Functional Properties of the Active Form of the Proteolytic Complex, ClpP1P2, from Mycobacterium tuberculosis. *Journal of Biological Chemistry* **291,** 7465–7476 (2016).

17. Kim, Y.-I., Levchenko, I., Fraczkowska, K., Woodruff, R. V., Sauer, R. T. & Baker, T. A. Molecular determinants of complex formation between Clp/Hsp100 ATPases and the ClpP peptidase. *Nature Structural Biology* **8,** 230 (2001).

18. Frees, D., Chastanet, A., Qazi, S., Sorensen, K., Hill, P., Msadek, T. & Ingmer, H. Clp ATPases are required for stress tolerance, intracellular replication and biofilm formation in Staphylococcus aureus. *Mol Microbiol* **54,** 1445–62 (2004).

19. Frees, D., Savijoki, K., Varmanen, P. & Ingmer, H. Clp ATPases and ClpP proteolytic complexes regulate vital biological processes in low GC, Gram-positive bacteria. *Mol Microbiol* **63,** 1285–95 (2007).

20. Ortega, J., Singh, S. K., Ishikawa, T., Maurizi, M. R. & Steven, A. C. Visualization of substrate binding and translocation by the ATP-dependent protease, ClpXP. *Mol Cell* **6,** 1515–21 (2000).

21. Kim, D. & Mobashery, S. Mechanism-based inhibition of zinc proteases. *Curr. Med. Chem.* **8,** 959–965 (2001).

22. Martin, A., Baker, T. A. & Sauer, R. T. Distinct Static and Dynamic Interactions Control ATPase-Peptidase Communication in a AAA+ Protease. *Molecular Cell* **27,** 41–52 (2007).

23. Baker, T. A. & Sauer, R. T. ClpXP, an ATP-powered unfolding and protein-degradation machine. *Biochim Biophys Acta* **1823,** 15–28 (2012).

24. Wojtyra, U. A., Thibault, G., Tuite, A. & Houry, W. A. The N-terminal Zinc Binding Domain of ClpX Is a Dimerization Domain That Modulates the Chaperone Function. *Journal of Biological Chemistry* **278,** 48981–48990 (2003).

25. Martin, A., Baker, T. A. & Sauer, R. T. Diverse Pore Loops of the AAA+ ClpX Machine Mediate Unassisted and Adaptor-Dependent Recognition of ssrA-Tagged Substrates. *Molecular Cell* **29,** 441–450 (2008).

26. Bell, T. A., Baker, T. A. & Sauer, R. T. Interactions between a subset of substrate side chains and AAA+ motor pore loops determine grip during protein unfolding. *eLife* **8,** e46808 (2019).

27. Flynn, J. M., Neher, S. B., Kim, Y. I., Sauer, R. T. & Baker, T. A. Proteomic discovery of cellular substrates of the ClpXP protease reveals five classes of ClpX-recognition signals. *Mol Cell* **11,** 671–83 (2003).

28. Hoskins, J. R., Yanagihara, K., Mizuuchi, K. & Wickner, S. ClpAP and ClpXP degrade proteins with tags located in the interior of the primary sequence. *Proceedings of the National Academy of Sciences* **99,** 11037–11042 (2002).

29. Himeno, H., Kurita, D. & Muto, A. tmRNA-mediated trans-translation as the major ribosome rescue system in a bacterial cell. *Frontiers in Genetics* **5,** 66 (2014).

30. Levchenko, I., Seidel, M., Sauer, R. T. & Baker, T. A. A specificity-enhancing factor for the ClpXP degradation machine. *Science* **289,** 2354–2356 (2000).

31. Brötz-Oesterhelt, H. & Sass, P. Bacterial caseinolytic proteases as novel targets for antibacterial treatment. *International Journal of Medical Microbiology* **304,** 23–30 (2014).

32. Brötz-Oesterhelt, H., Beyer, D., Kroll, H. P., Endermann, R., Ladel, C., Schroeder, W., Hinzen, B., Raddatz, S., Paulsen, H., Henninger, K., Bandow, J. E., Sahl, H. G. & Labischinski, H. Dysregulation of bacterial proteolytic machinery by a new class of antibiotics. *Nat Med* **11,** 1082–7 (2005).

33. Famulla, K., Sass, P., Malik, I., Akopian, T., Kandror, O., Alber, M., Hinzen, B., Ruebsamen-Schaeff, H., Kalscheuer, R., Goldberg, A. L. & Brötz-Oesterhelt, H. Acyldepsipeptide antibiotics kill mycobacteria by preventing the physiological functions of the ClpP1P2 protease. *Molecular Microbiology* **101,** 194–209 (2016).

34. Böttcher, T. & Sieber, S. A. Beta-lactones as specific inhibitors of ClpP attenuate the production of extracellular virulence factors of Staphylococcus aureus. *J Am Chem Soc* **130,** 14400–1 (2008).

35. Böttcher, T. & Sieber, S. A. Beta-lactones decrease the intracellular virulence of Listeria monocytogenes in macrophages. *ChemMedChem* **4,** 1260–3 (2009).

36. Gaillot, O., Pellegrini, E., Bregenholt, S., Nair, S. & Berche, P. The ClpP serine protease is essential for the intracellular parasitism and virulence of Listeria monocytogenes. *Mol Microbiol* **35,** 1286–94 (2000).

37. Frees, D., Qazi, S. N., Hill, P. J. & Ingmer, H. Alternative roles of ClpX and ClpP in Staphylococcus aureus stress tolerance and virulence. *Mol Microbiol* **48,** 1565–78 (2003).

38. Hackl, M. W., Lakemeyer, M., Dahmen, M., Glaser, M., Pahl, A., Lorenz-Baath, K., Menzel, T., Sievers, S., Bottcher, T., Antes, I., Waldmann, H. & Sieber, S. A. Phenyl Esters Are Potent Inhibitors of Caseinolytic Protease P and Reveal a Stereogenic Switch for Deoligomerization. *J Am Chem Soc* **137,** 8475–83 (2015).

39. Maurizi, M. R., Clark, W. P., Kim, S. H. & Gottesman, S. Clp P represents a unique family of serine proteases. *J Biol Chem* **265,** 12546–52 (1990).

40. Akopian, T., Kandror, O., Tsu, C., Lai, J. H., Wu, W., Liu, Y., Zhao, P., Park, A., Wolf, L., Dick, L. R., Rubin, E. J., Bachovchin, W. & Goldberg, A. L. Cleavage Specificity of Mycobacterium tuberculosis ClpP1P2 Protease and Identification of Novel Peptide Substrates and Boronate Inhibitors with Anti-bacterial Activity. *J Biol Chem* **290,** 11008–20 (2015).

41. Haynes, C. M., Petrova, K., Benedetti, C., Yang, Y. & Ron, D. ClpP mediates activation of a mitochondrial unfolded protein response in C. elegans. *Dev Cell* **13,** 467–80 (2007).

42. Jenkinson, E. M., Rehman, A. U., Walsh, T., Clayton-Smith, J., Lee, K., Morell, R. J., Drummond, M. C., Khan, S. N., Naeem, M. A., Rauf, B., Billington, N., Schultz, J. M., Urquhart, J. E., Lee, M. K., Berry, A., Hanley, N. A., Mehta, S., Cilliers, D., Clayton, P. E., Kingston, H., Smith, M. J., Warner, T. T., University of Washington Center for Mendelian, G., Black, G. C., Trump, D., Davis, J. R., Ahmad, W., Leal, S. M., Riazuddin, S., King, M. C., Friedman, T. B. & Newman, W. G. Perrault syndrome is caused by recessive mutations in CLPP, encoding a mitochondrial ATP-dependent chambered protease. *Am J Hum Genet* **92,** 605–13 (2013).

43. Bhandari, V., Wong, K. S., Zhou, J. L., Mabanglo, M. F., Batey, R. A. & Houry, W. A. The Role of ClpP Protease in Bacterial Pathogenesis and Human Diseases. *ACS Chemical Biology* **13,** 1413–1425 (2018).

44. Cole, A., Wang, Z., Coyaud, E., Voisin, V., Gronda, M., Jitkova, Y., Mattson, R., Hurren, R., Babovic, S., Maclean, N., Restall, I., Wang, X., Jeyaraju, D. V., Sukhai, M. A., Prabha, S., Bashir, S., Ramakrishnan, A., Leung, E., Qia, Y. H., Zhang, N., Combes, K. R., Ketela, T., Lin, F., Houry, W. A., Aman, A., Al-Awar, R., Zheng, W., Wienholds, E., Xu, C. J., Dick, J., Wang, J. C., Moffat, J., Minden, M. D., Eaves, C. J., Bader, G. D., Hao, Z., Kornblau, S. M., Raught, B. & Schimmer, A. D. Inhibition of the Mitochondrial Protease ClpP as a Therapeutic Strategy for Human Acute Myeloid Leukemia. *Cancer Cell* **27,** 864–76 (2015).

45. Hu, D., Sun, X., Liao, X., Zhang, X., Zarabi, S., Schimmer, A., Hong, Y., Ford, C., Luo, Y. & Qi, X. Alpha-synuclein suppresses mitochondrial protease ClpP to trigger mitochondrial oxidative damage and neurotoxicity. *Acta neuropathologica* **137,** 939–960 (2019).

46. De Noordhout, C. M., Devleesschauwer, B., Angulo, F. J., Verbeke, G., Haagsma, J., Kirk, M., Havelaar, A. & Speybroeck, N. The global burden of listeriosis: a systematic review and meta-analysis. *The Lancet Infectious Diseases* **14,** 1073–1082 (2014).

47. Pagliano, P., Arslan, F. & Ascione, T. Epidemiology and treatment of the commonest form of listeriosis: meningitis and bacteraemia. *Infez Med* **25,** 210–216 (2017).

48. Radoshevich, L. & Cossart, P. Listeria monocytogenes: towards a complete picture of its physiology and pathogenesis. *Nature Reviews Microbiology* **16,** 32 (2018).

49. Bucur, F. I., Grigore-Gurgu, L., Crauwels, P., Riedel, C. U. & Nicolau, A. I. Resistance of Listeria monocytogenes to stress conditions encountered in food and food processing environments. *Frontiers in microbiology* **9,** 2700 (2018).

50. Desai, A. N., Anyoha, A., Madoff, L. C. & Lassmann, B. Changing epidemiology of Listeria monocytogenes outbreaks, sporadic cases, and recalls globally: A review of ProMED reports from 1996 to 2018. *International Journal of Infectious Diseases* **84,** 48–53 (2019).

51. Tilney, L. G. & Portnoy, D. A. Actin filaments and the growth, movement, and spread of the intracellular bacterial parasite, Listeria monocytogenes. *The Journal of cell biology* **109,** 1597–1608.

52. Chaturongakul, S., Raengpradub, S., Wiedmann, M. & Boor, K. J. Modulation of stress and virulence in Listeria monocytogenes. *Trends in microbiology* **16,** 388–396 (2008).

53. Toledo-Arana, A., Dussurget, O., Nikitas, G., Sesto, N., Guet-Revillet, H., Balestrino, D., Loh, E., Gripenland, J., Tiensuu, T., Vaitkevicius, K., *et al.* The Listeria transcriptional landscape from saprophytism to virulence. *Nature* **459,** 950–956 (2009).

54. Chatterjee, I., Schmitt, S., Batzilla, C. F., Engelmann, S., Keller, A., Ring, M. W., Kautenburger, R., Ziebuhr, W., Hecker, M., Preissner, K. T., Bischoff, M., Proctor, R. A., Beck, H. P., Lenhof, H. P., Somerville, G. A. & Herrmann, M. Staphylococcus aureus ClpC ATPase is a late growth phase effector of metabolism and persistence. *Proteomics* **9,** 1152–76 (2009).

55. Hu, Y., Oliver, H. F., Raengpradub, S., Palmer, M. E., Orsi, R. H., Wiedmann, M. & Boor, K. J. Transcriptomic and phenotypic analyses suggest a network between the transcriptional regulators HrcA and σB in Listeria monocytogenes. *Appl. Environ. Microbiol.* **73,** 7981–7991 (2007).

56. Kazmierczak, M. J., Mithoe, S. C., Boor, K. J. & Wiedmann, M. Listeria monocytogenes σ^B regulates stress response and virulence functions. *Journal of bacteriology* **185,** 5722–5734 (2003).

57. De las Heras, A., Cain, R. J., Bielecka, M. K. & Vazquez-Boland, J. A. Regulation of Listeria virulence: PrfA master and commander. *Current opinion in microbiology* **14,** 118–127 (2011).

58. Nair, S., Derré, I., Msadek, T., Gaillot, O. & Berche, P. CtsR controls class III heat shock gene expression in the human pathogen Listeria monocytogenes. *Molecular microbiology* **35,** 800–811 (2000).

59. Michel, B. After 30 years of study, the bacterial SOS response still surprises us. *PLoS biology* **3,** 1174–1176 (2005).

60. Van der Veen, S., Hain, T., Wouters, J. A., Hossain, H., de Vos, W. M., Abee, T., Chakraborty, T. & Wells-Bennik, M. H. The heat-shock response of Listeria monocytogenes comprises genes involved in heat shock, cell division, cell wall synthesis, and the SOS response. *Microbiology* **153,** 3593–3607 (2007).

61. Sokolovic, Z., Fuchs, A. & Goebel, W. Synthesis of species-specific stress proteins by virulent strains of Listeria monocytogenes. *Infection and immunity* **58,** 3582–3587 (1990).

62. Agoston, R., Soni, K., Jesudhasan, P. R., Russell, W. K., Mohácsi-Farkas, C. & Pillai, S. D. Differential expression of proteins in Listeria monocytogenes under thermotolerance-inducing, heat shock, and prolonged heat shock conditions. *Foodborne pathogens and disease* **6,** 1133–1140 (2009).

63. Hébraud, M. & Guzzo, J. The main cold shock protein of Listeria monocytogenes belongs to the family of ferritin-like proteins. *FEMS Microbiology Letters* **190,** 29–34 (2000).

64. Van der Veen, S., van Schalkwijk, S., Molenaar, D., De Vos, W. M., Abee, T. & Wells-Bennik, M. H. The SOS response of Listeria monocytogenes is involved in stress resistance and mutagenesis. *Microbiology* **156,** 374–384 (2010).

65. Cortes, B. W., Naditz, A. L., Anast, J. M. & Schmitz-Esser, S. Transcriptome sequencing of Listeria monocytogenes reveals major gene expression changes in response to lactic acid stress exposure but a less pronounced response to oxidative stress. *Frontiers in Microbiology* **10,** 3110 (2019).

66. Soni, K. A., Nannapaneni, R. & Tasara, T. The contribution of transcriptomic and proteomic analysis in elucidating stress adaptation responses of Listeria monocytogenes. *Foodborne pathogens and disease* **8,** 843–852 (2011).

67. Bergholz, T. M., Bowen, B., Wiedmann, M. & Boor, K. J. Listeria monocytogenes shows temperature-dependent and-independent responses to salt stress, including responses that induce cross-protection against other stresses. *Appl. Environ. Microbiol.* **78,** 2602–2612 (2012).

68. Bowman, J. P., Hages, E., Nilsson, R. E., Kocharunchitt, C. & Ross, T. Investigation of the Listeria monocytogenes Scott A acid tolerance response and associated physiological and phenotypic features via whole proteome analysis. *Journal of proteome research* **11,** 2409–2426 (2012).

69. Giotis, E. S., Muthaiyan, A., Natesan, S., Wilkinson, B. J., Blair, I. S. & McDowell, D. A. Transcriptome analysis of alkali shock and alkali adaptation in Listeria monocytogenes 10403S. *Foodborne pathogens and disease* **7,** 1147–1157 (2010).

70. Cacace, G., Mazzeo, M. F., Sorrentino, A., Spada, V., Malorni, A. & Siciliano, R. A. Proteomics for the elucidation of cold adaptation mechanisms in Listeria monocytogenes. *Journal of Proteomics* **73,** 2021–2030 (2010).

71. Hu, Y., Raengpradub, S., Schwab, U., Loss, C., Orsi, R. H., Wiedmann, M. & Boor, K. J. Phenotypic and transcriptomic analyses demonstrate interactions between the transcriptional regulators CtsR and Sigma B in Listeria monocytogenes. *Appl. Environ. Microbiol.* **73,** 7967–7980 (2007).

72. Katayama-Fujimura, Y., Gottesman, S. & Maurizi, M. R. A multiple-component, ATP-dependent protease from Escherichia coli. *J Biol Chem* **262,** 4477–85 (1987).

73. Maglica, Z., Kolygo, K. & Weber-Ban, E. Optimal efficiency of ClpAP and ClpXP chaperone-proteases is achieved by architectural symmetry. *Structure* **17,** 508–16 (2009).

74. Sauer, R. T. & Baker, T. A. AAA+ proteases: ATP-fueled machines of protein destruction. *Annu Rev Biochem* **80,** 587–612 (2011).

75. Wang, J., Hartling, J. A. & Flanagan, J. M. The structure of ClpP at 2.3 A resolution suggests a model for ATP-dependent proteolysis. *Cell* **91,** 447–56 (1997).

76. Thompson, H. J., Wilson, A., Lu, J., Singh, M., Jiang, C., Upadhyaya, P., el-Bayoumy, K. & Ip, C. Comparison of the effects of an organic and an inorganic form of selenium on a mammary carcinoma cell line. *Carcinogenesis* **15,** 183–6 (1994).

77. Li, D. H., Chung, Y. S., Gloyd, M., Joseph, E., Ghirlando, R., Wright, G. D., Cheng, Y. Q., Maurizi, M. R., Guarne, A. & Ortega, J. Acyldepsipeptide antibiotics induce the formation of a structured axial channel in ClpP: A model for the ClpX/ClpA-bound state of ClpP. *Chem Biol* **17,** 959–69 (2010).

78. Böttcher, T. & Sieber, S. Beta-lactones as privileged structures for the active-site labeling of versatile bacterial enzyme classes. *Angew Chem Int Ed Engl* **47,** 4600–3 (2008).

79. Gersch, M., Kolb, R., Alte, F., Groll, M. & Sieber, S. A. Disruption of oligomerization and dehydroalanine formation as mechanisms for ClpP protease inhibition. *J Am Chem Soc* **136,** 1360–6 (2014).

80. Pahl, A., Lakemeyer, M., Vielberg, M. T., Hackl, M. W., Vomacka, J., Korotkov, V. S., Stein, M. L., Fetzer, C., Lorenz-Baath, K., Richter, K., Waldmann, H., Groll, M. & Sieber, S. A. Reversible Inhibitors Arrest ClpP in a Defined Conformational State that Can Be Revoked by ClpX Association. *Angew Chem Int Ed Engl* **54,** 15892–6 (2015).

81. Schmitz, K. R., Carney, D. W., Sello, J. K. & Sauer, R. T. Crystal structure of Mycobacterium tuberculosis ClpP1P2 suggests a model for peptidase activation by AAA+ partner binding and substrate delivery. *Proc Natl Acad Sci U S A* **111,** E4587–95 (2014).

82. Schmitz, K. R. & Sauer, R. T. Substrate delivery by the AAA+ ClpX and ClpC1 unfoldases activates the mycobacterial ClpP1P2 peptidase. *Mol Microbiol* **93,** 617–28 (2014).

83. Leodolter, J., Warweg, J. & Weber-Ban, E. The Mycobacterium tuberculosis ClpP1P2 Protease Interacts Asymmetrically with Its ATPase Partners ClpX and ClpC1. *PLOS ONE* **10,** 1–21 (2015).

84. Szyk, A. & Maurizi, M. R. Crystal structure at 1.9A of E. coli ClpP with a peptide covalently bound at the active site. *J Struct Biol* **156,** 165–74 (2006).

85. Gersch, M., Stahl, M., Poreba, M., Dahmen, M., Dziedzic, A., Drag, M. & Sieber, S. A. Barrel-shaped ClpP Proteases Display Attenuated Cleavage Specificities. *ACS Chem Biol* **11,** 389–99 (2016).

86. Kato, D., Boatright, K. M., Berger, A. B., Nazif, T., Blum, G., Ryan, C., Chehade, K. A., Salvesen, G. S. & Bogyo, M. Activity-based probes that target diverse cysteine protease families. *Nat Chem Biol* **1,** 33–8 (2005).

87. Kim, Y. I., Burton, R. E., Burton, B. M., Sauer, R. T. & Baker, T. A. Dynamics of substrate denaturation and translocation by the ClpXP degradation machine. *Mol Cell* **5,** 639–48 (2000).

88. Joshi, S. A., Hersch, G. L., Baker, T. A. & Sauer, R. T. Communication between ClpX and ClpP during substrate processing and degradation. *Nature Structural &Amp; Molecular Biology* **11,** 404 (2004).

89. Krojer, T., Sawa, J., Schäfer, E., Saibil, H. R., Ehrmann, M. & Clausen, T. Structural basis for the regulated protease and chaperone function of DegP. *Nature* **453,** 885–890 (2008).

90. Lee, B. G., Park, E. Y., Lee, K. E., Jeon, H., Sung, K. H., Paulsen, H., Rubsamen-Schaeff, H., Brotz-Oesterhelt, H. & Song, H. K. Structures of ClpP in complex with acyldepsipeptide antibiotics reveal its activation mechanism. *Nat Struct Mol Biol* **17,** 471–8 (2010).

91. Gersch, M., Famulla, K., Dahmen, M., Gobl, C., Malik, I., Richter, K., Korotkov, V. S., Sass, P., Rubsamen-Schaeff, H., Madl, T., Brotz-Oesterhelt, H. & Sieber, S. A. AAA+ chaperones and acyldepsipeptides activate the ClpP protease via conformational control. *Nat Commun* **6,** 6320 (2015).

92. Carney, D. W., Compton, C. L., Schmitz, K. R., Stevens, J. P., Sauer, R. T. & Sello, J. K. A Simple Fragment of Cyclic Acyldepsipeptides Is Necessary and Sufficient for ClpP Activation and Antibacterial Activity. *Chembiochem* **15,** 2216–20 (2014).

93. Kanemori, M., Nishihara, K., Yanagi, H. & Yura, T. Synergistic roles of HslVU and other ATP-dependent proteases in controlling in vivo turnover of sigma32 and abnormal proteins in Escherichia coli. *Journal of Bacteriology* **179,** 7219–7225 (1997).

94. Gersch, M., Hackl, M. W., Dubiella, C., Dobrinevski, A., Groll, M. & Sieber, S. A. A mass spectrometry platform for a streamlined investigation of proteasome integrity, posttranslational modifications, and inhibitor binding. *Chem Biol* **22,** 404–11 (2015).

95. Balogh, D., Dahmen, M., Stahl, M., Poreba, M., Gersch, M., Drag, M. & Sieber, S. A. Insights into ClpXP proteolysis: heterooligomerization and partial deactivation enhance chaperone affinity and substrate turnover in Listeria monocytogenes. *Chemical Science* **8,** 1592–1600 (2017).

96. Beuron, F., Maurizi, M. R., Belnap, D. M., Kocsis, E., Booy, F. P., Kessel, M. & Steven, A. C. At sixes and sevens: characterization of the symmetry mismatch of the ClpAP chaperone-assisted protease. *J Struct Biol* **123,** 248–59 (1998).

97. Grimaud, R., Kessel, M., Beuron, F., Steven, A. C. & Maurizi, M. R. Enzymatic and structural similarities between the Escherichia coli ATP-dependent proteases, ClpXP and ClpAP. *J Biol Chem* **273,** 12476–81 (1998).

98. Banecki, B., Wawrzynow, A., Puzewicz, J., Georgopoulos, C. & Zylicz, M. Structure-function analysis of the zinc-binding region of the ClpX molecular chaperone. *Journal of Biological Chemistry* **276,** 18843–18848 (2001).

99. Bewley, M. C., Graziano, V., Griffin, K. & Flanagan, J. M. The asymmetry in the mature amino-terminus of ClpP facilitates a local symmetry match in ClpAP and ClpXP complexes. *J Struct Biol* **153,** 113–28 (2006).

100. Kirstein, J., Hoffmann, A., Lilie, H., Schmidt, R., Rübsamen-Waigmann, H., Brötz-Oesterhelt, H., Mogk, A. & Turgay, K. The antibiotic ADEP reprogrammes ClpP, switching it from a regulated to an uncontrolled protease. *EMBO molecular medicine* **1,** 37–49 (2009).

101. Alexopoulos, J., Ahsan, B., Homchaudhuri, L., Husain, N., Cheng, Y. Q. & Ortega, J. Structural determinants stabilizing the axial channel of ClpP for substrate translocation. *Mol Microbiol* **90,** 167–80 (2013).

102. Amor, A. J., Schmitz, K. R., Sello, J. K., Baker, T. A. & Sauer, R. T. Highly Dynamic Interactions Maintain Kinetic Stability of the ClpXP Protease During the ATP-Fueled Mechanical Cycle. *ACS Chemical Biology* **11,** 1552–1560 (2016).

103. Hersch, G. L., Burton, R. E., Bolon, D. N., Baker, T. A. & Sauer, R. T. Asymmetric interactions of ATP with the AAA+ ClpX6 unfoldase: allosteric control of a protein machine. *Cell* **121,** 1017–27 (2005).

104. Wagner, T., Merino, F., Stabrin, M., Moriya, T., Antoni, C., Apelbaum, A., Hagel, P., Sitsel, O., Raisch, T., Prumbaum, D., *et al.* SPHIRE-crYOLO is a fast and accurate fully automated particle picker for cryo-EM. *Communications biology* **2,** 1–13 (2019).

105. Moriya, T., Saur, M., Stabrin, M., Merino, F., Voicu, H., Huang, Z., Penczek, P. A., Raunser, S. & Gatsogiannis, C. High-resolution single particle analysis from electron cryo-microscopy images using SPHIRE. *JoVE (Journal of Visualized Experiments),* e55448 (2017).

106. Donaldson, L. W., Wojtyra, U. & Houry, W. A. Solution Structure of the Dimeric Zinc Binding Domain of the Chaperone ClpX. *Journal of Biological Chemistry* **278,** 48991–48996 (2003).

107. Trabuco, L. G., Villa, E., Mitra, K., Frank, J. & Schulten, K. Flexible fitting of atomic structures into electron microscopy maps using molecular dynamics. *Structure* **16,** 673–683 (2008).

108. Fux, A., Korotkov, V. S., Schneider, M., Antes, I. & Sieber, S. A. Chemical cross-linking enables drafting ClpXP proximity maps and taking snapshots of in situ interaction networks. *Cell chemical biology* **26,** 48–59 (2019).

109. Glynn, S. E., Martin, A., Nager, A. R., Baker, T. A. & Sauer, R. T. Structures of Asymmetric ClpX Hexamers Reveal Nucleotide-Dependent Motions in a AAA+ Protein-Unfolding Machine. *Cell* **139,** 744–756 (2009).

110. Gates, S. N., Yokom, A. L., Lin, J., Jackrel, M. E., Rizo, A. N., Kendsersky, N. M., Buell, C. E., Sweeny, E. A., Mack, K. L., Chuang, E., *et al.* Ratchet-like polypeptide translocation mechanism of the AAA+ disaggregase Hsp104. *Science* **357,** 273–279 (2017).

111. Lo, Y.-H., Sobhany, M., Hsu, A. L., Ford, B. L., Krahn, J. M., Borgnia, M. J. & Stanley, R. E. Cryo-EM structure of the essential ribosome assembly AAA-ATPase Rix7. *Nature communications* **10,** 1–12 (2019).

112. Ripstein, Z. A., Huang, R., Augustyniak, R., Kay, L. E. & Rubinstein, J. L. Structure of a AAA+ unfoldase in the process of unfolding substrate. *eLife* **6,** e25754 (2017).

113. Stinson, B. M., Nager, A. R., Glynn, S. E., Schmitz, K. R., Baker, T. A. & Sauer, R. T. Nucleotide Binding and Conformational Switching in the Hexameric Ring of a AAA+ Machine. *Cell* **153,** 628–639 (2013).

114. Gatsogiannis, C., Merino, F., Roderer, D., Balchin, D., Schubert, E., Kuhlee, A., Hayer-Hartl, M. & Raunser, S. Tc toxin activation requires unfolding and refolding of a β-propeller. *Nature* **563,** 209–213 (2018).

115. De la Peña, A. H., Goodall, E. A., Gates, S. N., Lander, G. C. & Martin, A. Substrate-engaged 26S proteasome structures reveal mechanisms for ATP-hydrolysis–driven translocation. *Science* **362,** eaav0725 (2018).

116. Majumder, P., Rudack, T., Beck, F., Danev, R., Pfeifer, G., Nagy, I. & Baumeister, W. Cryo-EM structures of the archaeal PAN-proteasome reveal an around-the-ring ATPase cycle. *Proceedings of the National Academy of Sciences* **116,** 534–539 (2019).

117. Jennings, L. D., Bohon, J., Chance, M. R. & Licht, S. The ClpP N-Terminus Coordinates Substrate Access with Protease Active Site Reactivity. *Biochemistry* **47,** 11031–11040 (2008).

118. Geiger, S. R., Bottcher, T., Sieber, S. A. & Cramer, P. A conformational switch underlies ClpP protease function. *Angew Chem Int Ed Engl* **50,** 5749–52 (2011).

119. Kimber, M. S., Yu, A. Y. H., Borg, M., Leung, E., Chan, H. S. & Houry, W. A. Structural and theoretical studies indicate that the cylindrical protease ClpP samples extended and compact conformations. *Structure* **18,** 798–808 (2010).

120. Ye, F., Zhang, J., Liu, H., Hilgenfeld, R., Zhang, R., Kong, X., Li, L., Lu, J., Zhang, X., Li, D., Jiang, H., Yang, C. G. & Luo, C. Helix unfolding/refolding characterizes the functional dynamics of Staphylococcus aureus Clp protease. *J Biol Chem* **288,** 17643–53 (2013).

121. Zhang, J., Ye, F., Lan, L., Jiang, H., Luo, C. & Yang, C. G. Structural switching of Staphylococcus aureus Clp protease: a key to understanding protease dynamics. *J Biol Chem* **286,** 37590–601 (2011).

122. Ni, T., Ye, F., Liu, X., Zhang, J., Liu, H., Li, J., Zhang, Y., Sun, Y., Wang, M., Luo, C., *et al.* Characterization of gain-of-function mutant provides new insights into ClpP structure. *ACS chemical biology* **11,** 1964–1972 (2016).

123. Stahl, M. & Sieber, S. A. An amino acid domino effect orchestrates ClpP's conformational states. *Current opinion in chemical biology* **40,** 102–110 (2017).

124. Eisele, M. R., Reed, R. G., Rudack, T., Schweitzer, A., Beck, F., Nagy, I., Pfeifer, G., Plitzko, J. M., Baumeister, W., Tomko Jr, R. J., *et al.* Expanded coverage of the 26S proteasome conformational landscape reveals mechanisms of peptidase gating. *Cell reports* **24,** 1301–1315 (2018).

125. Smith, D. M., Chang, S.-C., Park, S., Finley, D., Cheng, Y. & Goldberg, A. L. Docking of the proteasomal ATPases' carboxyl termini in the 20S proteasome's α ring opens the gate for substrate entry. *Molecular cell* **27,** 731–744 (2007).

126. Wehmer, M., Rudack, T., Beck, F., Aufderheide, A., Pfeifer, G., Plitzko, J. M., Förster, F., Schulten, K., Baumeister, W. & Sakata, E. Structural insights into the functional cycle of the ATPase module of the 26S proteasome. *Proceedings of the National Academy of Sciences* **114,** 1305–1310 (2017).

127. Deville, C., Franke, K., Mogk, A., Bukau, B. & Saibil, H. R. Two-step activation mechanism of the ClpB disaggregase for sequential substrate threading by the main ATPase motor. *Cell reports* **27,** 3433–3446 (2019).

128. Liu, H. & Naismith, J. H. An efficient one-step site-directed deletion, insertion, single and multiple-site plasmid mutagenesis protocol. *BMC biotechnology* **8,** 91 (2008).

129. Englander, S. W. & Kallenbach, N. R. Hydrogen exchange and structural dynamics of proteins and nucleic acids. *Quarterly reviews of biophysics* **16,** 521–655 (1983).

130. Wales, T. E. & Engen, J. R. Hydrogen exchange mass spectrometry for the analysis of protein dynamics. *Mass spectrometry reviews* **25,** 158–170 (2006).

131. Pettersen, E. F., Goddard, T. D., Huang, C. C., Couch, G. S., Greenblatt, D. M., Meng, E. C. & Ferrin, T. E. UCSF Chimera–a visualization system for exploratory research and analysis. *J Comput Chem* **25,** 1605–12 (2004).

132. Gatsogiannis, C., Merino, F., Prumbaum, D., Roderer, D., Leidreiter, F., Meusch, D. & Raunser, S. Membrane insertion of a Tc toxin in near-atomic detail. *Nature structural & molecular biology* **23,** 884 (2016).

133. Grant, T. & Grigorieff, N. Measuring the optimal exposure for single particle cryo-EM using a 2.6 Å reconstruction of rotavirus VP6. *Elife* **4,** e06980 (2015).

134. Penczek, P. A., Fang, J., Li, X., Cheng, Y., Loerke, J. & Spahn, C. M. CTER—Rapid estimation of CTF parameters with error assessment. *Ultramicroscopy* **140,** 9–19 (2014).

135. Tang, G., Peng, L., Baldwin, P. R., Mann, D. S., Jiang, W., Rees, I. & Ludtke, S. J. EMAN2: an extensible image processing suite for electron microscopy. *Journal of structural biology* **157,** 38–46 (2007).

136. Terwilliger, T. C., Sobolev, O. V., Afonine, P. V. & Adams, P. D. Automated map sharpening by maximization of detail and connectivity. *Acta Crystallographica Section D: Structural Biology* **74,** 545–559 (2018).

137. Biasini, M., Bienert, S., Waterhouse, A., Arnold, K., Studer, G., Schmidt, T., Kiefer, F., Cassarino, T. G., Bertoni, M., Bordoli, L., *et al.* SWISS-MODEL: modelling protein tertiary and quaternary structure using evolutionary information. *Nucleic acids research* **42,** W252–W258 (2014).

138. Frenz, B., Walls, A. C., Egelman, E. H., Veesler, D. & DiMaio, F. RosettaES: a sampling strategy enabling automated interpretation of difficult cryo-EM maps. *Nature methods* **14,** 797–800 (2017).

139. Emsley, P., Lohkamp, B., Scott, W. G. & Cowtan, K. Features and development of Coot. *Acta Crystallogr D Biol Crystallogr* **66,** 486–501 (2010).

140. Singharoy, A., Teo, I., McGreevy, R., Stone, J. E., Zhao, J. & Schulten, K. Molecular dynamics-based refinement and validation for sub-5 Å cryo-electron microscopy maps. *eLife* **5,** e16105 (2016).

141. Humphrey, W., Dalke, A., Schulten, K., *et al.* VMD: visual molecular dynamics. *Journal of molecular graphics* **14,** 33–38 (1996).

142. Phillips, J. C., Braun, R., Wang, W., Gumbart, J., Tajkhorshid, E., Villa, E., Chipot, C., Skeel, R. D., Kale, L. & Schulten, K. Scalable molecular dynamics with NAMD. *Journal of computational chemistry* **26,** 1781–1802 (2005).

143. Huang, J., Rauscher, S., Nawrocki, G., Ran, T., Feig, M., de Groot, B. L., Grubmüller, H. & MacKerell, A. D. CHARMM36m: an improved force field for folded and intrinsically disordered proteins. *Nature methods* **14,** 71–73 (2017).

144. Chen, V. B., Arendall, W. B., Headd, J. J., Keedy, D. A., Immormino, R. M., Kapral, G. J., Murray, L. W., Richardson, J. S. & Richardson, D. C. MolProbity: all-atom structure validation for macromolecular crystallography. *Acta Crystallographica Section D: Biological Crystallography* **66,** 12–21 (2010).

145. Barad, B. A., Echols, N., Wang, R. Y.-R., Cheng, Y., DiMaio, F., Adams, P. D. & Fraser, J. S. EMRinger: side chain-directed model and map validation for 3D cryo-electron microscopy. *Nature methods* **12,** 943–946 (2015).

146. Ashkenazy, H., Erez, E., Martz, E., Pupko, T. & Ben-Tal, N. ConSurf 2010: calculating evolutionary conservation in sequence and structure of proteins and nucleic acids. *Nucleic acids research* **38,** W529–W533 (2010).

147. Masood, T. B., Sandhya, S., Chandra, N. & Natarajan, V. CHEXVIS: a tool for molecular channel extraction and visualization. *BMC bioinformatics* **16,** 119 (2015).

148. Goddard, T. D., Huang, C. C., Meng, E. C., Pettersen, E. F., Couch, G. S., Morris, J. H. & Ferrin, T. E. UCSF ChimeraX: Meeting modern challenges in visualization and analysis. *Protein Science* **27,** 14–25 (2018).

149. Gahan, C., O'Driscoll, B. & Hill, C. Acid adaptation of Listeria monocytogenes can enhance survival in acidic foods and during milk fermentation. *Appl. Environ. Microbiol.* **62,** 3128–3132 (1996).

150. Elsholz, A. K. W., Michalik, S., Zühlke, D., Hecker, M. & Gerth, U. CtsR, the Gram-positive master regulator of protein quality control, feels the heat. *The EMBO Journal* **29,** 3621–3629 (2010).

151. Kamp, H. D. & Higgins, D. E. A protein thermometer controls temperature-dependent transcription of flagellar motility genes in Listeria monocytogenes. *PLoS pathogens* **7** (2011).

152. Johansson, J., Mandin, P., Renzoni, A., Chiaruttini, C., Springer, M. & Cossart, P. An RNA thermosensor controls expression of virulence genes in Listeria monocytogenes. *Cell* **110,** 551–561 (2002).

153. Miller, C., Thomsen, L. E., Gaggero, C., Mosseri, R., Ingmer, H. & Cohen, S. N. SOS response induction by ß-lactams and bacterial defense against antibiotic lethality. *Science* **305,** 1629–1631 (2004).

154. Cirz, R. T., Jones, M. B., Gingles, N. A., Minogue, T. D., Jarrahi, B., Peterson, S. N. & Romesberg, F. E. Complete and SOS-mediated response of Staphylococcus aureus to the antibiotic ciprofloxacin. *Journal of bacteriology* **189,** 531–539 (2007).

155. Cooper, B., Islam, N., Xu, Y., Beard, H. S., Garrett, W. M., Gu, G. & Nou, X. Quantitative proteomic analysis of staphylococcus aureus treated with punicalagin, a natural antibiotic from pomegranate that disrupts iron homeostasis and induces SOS. *Proteomics* **18,** 1700461 (2018).

156. Goerlich, O., Quillardet, P. & Hofnung, M. Induction of the SOS response by hydrogen peroxide in various Escherichia coli mutants with altered protection against oxidative DNA damage. *Journal of bacteriology* **171,** 6141–6147 (1989).

157. Cohn, M. T., Kjelgaard, P., Frees, D., Penadés, J. R. & Ingmer, H. Clp-dependent proteolysis of the LexA N-terminal domain in Staphylococcus aureus. *Microbiology* **157,** 677–684 (2011).

158. Little, J. W. & Gellert, M. The SOS regulatory system: control of its state by the level of RecA protease. *Journal of molecular biology* **167,** 791–808 (1983).

159. Neher, S. B., Flynn, J. M., Sauer, R. T. & Baker, T. A. Latent ClpX-recognition signals ensure LexA destruction after DNA damage. *Genes Dev* **17,** 1084–9 (2003).

160. Kawai, Y., Moriya, S. & Ogasawara, N. Identification of a protein, YneA, responsible for cell division suppression during the SOS response in Bacillus subtilis. *Molecular microbiology* **47,** 1113–1122 (2003).

161. Gatsogiannis, C., Balogh, D., Merino, F., Sieber, S. A. & Raunser, S. Cryo-EM structure of the ClpXP protein degradation machinery. *Nature Structural & Molecular Biology* **26,** 946–954 (2019).

162. Schölz, C., Lyon, D., Refsgaard, J. C., Jensen, L. J., Choudhary, C. & Weinert, B. T. Avoiding abundance bias in the functional annotation of posttranslationally modified proteins. *Nature methods* **12,** 1003 (2015).

163. Van Der Veen, S., Abee, T., De Vos, W. M. & Wells-Bennik, M. H. Genome-wide screen for Listeria monocytogenes genes important for growth at high temperatures. *FEMS microbiology letters* **295,** 195–203 (2009).

164. Guillon, B., Bulteau, A.-L., Wattenhofer-Donzé, M., Schmucker, S., Friguet, B., Puccio, H., Drapier, J.-C. & Bouton, C. Frataxin deficiency causes upregulation of mitochondrial Lon and ClpP proteases and severe loss of mitochondrial Fe-S proteins. *The FEBS journal* **276,** 1036–1047 (2009).

165. Farrand, A. J., Friedman, D. B., Reniere, M. L., Ingmer, H., Frees, D. & Skaar, E. P. Proteomic analyses of iron-responsive, Clp-dependent changes in Staphylococcus aureus. *Pathogens and disease* **73,** ftv004 (2015).

166. Michel, A., Agerer, F., Hauck, C. R., Herrmann, M., Ullrich, J., Hacker, J. & Ohlsen, K. Global regulatory impact of ClpP protease of Staphylococcus aureus on regulons involved in virulence, oxidative stress response, autolysis, and DNA repair. *J Bacteriol* **188,** 5783–96 (2006).

167. Feng, J., Michalik, S., Varming, A. N., Andersen, J. H., Albrecht, D., Jelsbak, L., Krieger, S., Ohlsen, K., Hecker, M., Gerth, U., *et al.* Trapping and proteomic identification of cellular substrates of the ClpP protease in Staphylococcus aureus. *Journal of proteome research* **12,** 547–558 (2013).

168. Mei, Z., Wang, F., Qi, Y., Zhou, Z., Hu, Q., Li, H., Wu, J. & Shi, Y. Molecular determinants of MecA as a degradation tag for the ClpCP protease. *Journal of Biological Chemistry* **284,** 34366–34375 (2009).

169. Lakemeyer, M., Bertosin, E., Möller, F., Balogh, D., Strasser, R., Dietz, H. & Sieber, S. A. Tailored Peptide Phenyl Esters Block ClpXP Proteolysis by an Unusual Breakdown into a Heptamer-Hexamer Assembly. *Angewandte Chemie International Edition* **58,** 7127–7132 (2019).

170. Felix, J., Weinhäupl, K., Chipot, C., Dehez, F., Hessel, A., Gauto, D. F., Morlot, C., Abian, O., Gutsche, I., Velazquez-Campoy, A., *et al.* Mechanism of the allosteric activation of the ClpP protease machinery by substrates and active-site inhibitors. *Science advances* **5,** eaaw3818 (2019).

Part III

Appendix

A. Publications

Parts of this thesis have been published in peer-reviewed journals as listed below:

Insights into ClpXP proteolysis: heterooligomerization and partial deactivation enhance chaperone affinity and substrate turnover in *Listeria monocytogenes*
Dóra Balogh*, Maria Dahmen*, Matthias Stahl, Marcin Poręba, Malte Gersch, Marcin Drag and Stephan A. Sieber
Chemical Science, **2017**, 8, pp 1592-1600

Cryo-EM structure of the ClpXP protein degradation machinery
Christos Gatsogiannis*, Dóra Balogh*, Felipe Merino, Stephan A. Sieber and Stefan Raunser
Nature Structural & Molecular Biology, **2019**, 26, pp 946-954

*equal contribution

Research topics that are not covered in this thesis:

My individual contributions are described under the respective projects.

Selective Activation of Human Caseinolytic Protease P (ClpP)
Matthias Stahl, Vadim S. Korotkov, Dóra Balogh, Leonhard M. Kick, Malte Gersch, Axel Pahl, Pavel Kielkowski, Klaus Richter, Sabine Schneider, Stephan A. Sieber
Angewandte Chemie International Edition, **2018**, 57, pp 14602-14607

Performing biochemical assays, expression of proteins and discussion of the results.

Tailored Peptide Phenyl Esters Block ClpXP Proteolysis by an Unusual Breakdown into a Heptamer–Hexamer Assembly
Markus Lakemeyer, Eva Bertosin, Friederike Möller, Dóra Balogh, Ralf Strasser, Hendrik Dietz, Stephan A. Sieber
Angewandte Chemie International Edition, **2019**, 58, pp 7127-7132

Expression of proteins for SwitchSENSE experiments and discussion of the results.

B. Conferences

Parts of this thesis have been presented at conferences:

SFB1035 PhD & Postdoc Retreat
1st – 3rd April 2017, Spitzingsee, Germany
oral presentation

Bioorganic Chemistry Gordon Research Conference
11th – th June 2017, Andover, NH, USA
poster presentation

SFB1035 Annual Meeting
20th – 21st July 2017, Garching, Germany
poster presentation

35th Winter School on Proteinases and Their Inhibitors
28th February – 4th March 2018, Tiers, Italy
oral presentation

SFB1035 PhD & Postdoc Retreat
13th – 15th May 2019, Roggenburg, Germany
oral presentation